Bauhaus-Universität Weimar

Quality Assessment of Dynamic Soil-Structure Interaction Models Using Energy Measures

DOCTORAL THESIS

submitted in satisfaction of the requirements for the degree of
Doctor of Science in Civil Engineering

of the Bauhaus-Universität Weimar
Faculty of Civil Engineering

submitted by

Mourad Nasser
from Latakia, Syria

Mentor: Prof. Dr.-Ing. habil. Carsten Könke
Prof. Dr.-Ing. Frank Wuttke
Prof. Dr. George D. Manolis

Defense date: 30 November 2012

ACKNOWLEDGEMENTS

The present work was developed in the years 2008 to 2012 while I was working as a research associate with the Research Training Group 1462 – "Evaluation of Coupled Numerical Partial Models in Structural Engineering" at the Bauhaus-Universität Weimar and accepted by the university's department of civil engineering as a dissertation. I would like to take this opportunity to express my gratitude to the German Research Foundation DFG for its financial support.

This research project would not have been possible without the support of many people. It is a pleasure to convey my gratitude to them all in my humble acknowledgement. I gratefully acknowledge Prof. Dr.-Ing. habil. Carsten Könke for his supervision, advice and guidance, as well as the constructive discussions within the framework of our research group. These discussions inspired me to realize this research work. I would also like to extend my gratitude to Prof. Dr.-Ing. Frank Wuttke for his encouragement, assistance and advice, especially in the very early stage of this research. Thanks to his support, I had a good start in my research work. I owe my deepest gratitude to Prof. Dr. George D. Manolis. Through the guidance, encouragement and support that he provided in many ways, I had a very beneficial and pleasant stay in Thessaloniki. I am indebted to him more than he knows. I would also like to convey my special appreciation to Prof. Dr. Anastasios G. Sextos without whose knowledge and invaluable assistance this study would not have been successful. I gratefully acknowledge the advice and assistance of Dr.-Ing. Thomas Most. His truly scientific intuition has made him a constant fountain of ideas. He has especially inspired me and many of my colleagues in our research group. Many thanks go in particular to Prof. Dr.-Ing. habil. Frank Werner and to Dr. rer. nat. Tom Lahmer for their valuable advice in the scientific discussions, as well as to Prof. Dr.-Ing. habil. Tom Schanz for being the first person to receive me as a member of the research group. Special thanks to my friends Toni Fröbel, Mathias Leipold and Idna Wudtke who have supported me in every possible way. Not forgetting my friends at the Aristotle University in Thessaloniki, I also thank Athanasios Markou, Katsanos Evangelos and Olympia Taskari. Finally, I wish to express my love and gratitude to my family and friends in Latakia. Thank you for your love and fortitude, which gave me the strength to accomplish this work.

ABSTRACT

In this research work, an energy approach is employed for assessing quality in dynamic soil-structure interaction (SSI) models, and energy measures are introduced and investigated as general indicators of structural response. Dynamic SSI models with various abstraction levels are then investigated according to different coupling scenarios for soil and structure models. The hypothesis of increasing model uncertainty with decreasing complexity is investigated and a mathematical framework is provided for the treatment of model uncertainty. This framework is applied to a case study involving alternative models for incorporating dynamic SSI effects. In the evaluation process, energy measures are used within the framework of the *adjustment factor* approach in order to quantitatively assess the uncertainty associated with SSI models. Two primary types of uncertainty are considered, namely the uncertainty in the model framework and the uncertainty in the model input parameters. Investigations on model framework uncertainty show that the more complex three-dimensional FE model has the best quality of the models investigated, whereas the Wolf SSI model produces the lowest model uncertainty of the simpler models. The fixed-base model produces the highest estimated uncertainty and accordingly the worst quality of all models investigated. These results confirm the hypothesis of increasing model uncertainty with decreasing complexity only when the assessment is based on the ratio of structural hysteretic energy to input energy as a response indicator.

TABLE OF CONTENTS

SYMBOLS AND ABBREVIATIONS

The following list defines the principal symbols used in this work. Other symbols are defined in context.

General parameters and symbols

A_0	Polar moment of inertia for foundation on halfspace
a_0	Dimensionless frequency
c	Internal damping of single degree-of-freedom structure
c_p	Velocity of compression wave
c_s, V_s	Velocity of shear wave
E	Young's modulus of elasticity
E_a	Absorbed energy in structure
E_d	Damping energy dissipated in structure
E_h	Irrecoverable hysteretic energy in structure
E_i	Total earthquake input energy
E_k	Kinetic energy in structure
E_s	Recoverable elastic strain energy in structure
F_y	Yield force
f	Frequency in Hz
G	Lamé's constant, also known as shear modulus
H	Total height of structure from base to roof
h	Effective height of structure
I	Moment of inertia
K, C	Frequency-independent coefficients of translational spring and dashpot for foundation on halfspace
K_ω, C_ω	Frequency-dependent coefficients of translational spring and dashpot for foundation on halfspace

K_ϑ, C_ϑ	Frequency-independent coefficients of rotational spring and dashpot for foundation on halfspace
k	Lateral stiffness of single degree-of-freedom structure
$\bar{k}_u$, $\bar{k}_\theta$	Complex-valued dynamic foundation impedance for translation and rocking deformations
M_ϑ	Polar mass moment of inertia of for the internal degree of freedom ϑ corresponding to the rotational cone
m	Mass of structure
N_{eq}	Equivalent number of yield excursions
P_0	Amplitude of harmonic excitation
r	Restoring force
r_y	Yield strength
t	Variable for time-dependent functions
u	Displacement of structure relative to its base
u_f	Horizontal displacement of foundation relative to free-field
u_g	Free-field ground displacement
u_{max}	Maximum deformation of structure
u_{mon}	Ultimate deformation capacity of structure under a monotonically increasing lateral deformation
u_t	Total displacement of structure
u_y	Yield displacement
x, y, z	Cartesian coordinate system
γ	Shear strain
ε	Normal strain
$\{\varepsilon\}$	Strain vector
η	Structural strength ratio
θ	Base rocking of foundation slab

λ	Lamé's constant
λ_w	Wavelength
μ	Displacement ductility of structure
μ_{mon}	Monotonic ductility capacity of structure
ν	Poisson's ratio
ξ	Viscous damping ratio of single degree-of-freedom structure
ρ	Mass density
σ	Normal stress
$\{\sigma\}$	Stress vector
τ	Shear stress
ϕ	Mode shape of structure
ω	Angular frequency
ω_n	Natural frequency of structure

Parameters and symbols of stochastic methods

Corr, ρ	Coefficient of correlation
Cov	Covariance function
$E(\cdot)$	Mean value of $\cdot$
E_a^*	Additive adjustment factor
F	Cumulative distribution function
p	Probability density function
$P_{\mathcal{M}_i}$	Probability of model $\mathcal{M}_i$
$\mathbf{R}$	Permutation matrix for Latin hypercube sampling
$\mathbf{R_x}$	Correlation matrix
$\mathbf{S}$	Simulation matrix for Latin hypercube sampling
$\mathbf{T}$	Sampling matrix for Latin hypercube sampling
$V(\cdot)$	Variance value of $\cdot$
X	Single random variable
$\mathbf{X}$	Random variable vector

$Y^{\mathcal{M}_i}$	Response of reference model $\mathcal{M}_i$
Y_{pred}	Predicted system response
$Y^{\mathcal{M}_i^*}$	Total response of model $\mathcal{M}_i^*$
y^*	Prediction of the response elicited by reference model
$y^{\mathcal{M}_i}$	Deterministic prediction of the response by model $\mathcal{M}_i$
$\epsilon_{\triangle}^{\mathcal{M}_i}$	Model framework uncertainty
$\epsilon^{\mathcal{M}_{ref}}$	Error associated with reference model response
μ	Mean value
σ	Standard deviation
$\mathbf{\Sigma_x}$	Covariance matrix

Abbreviations used

2D	Two-dimensional finite element model
3D	Three-dimensional finite element model
BEM	Boundary Element Method
DI_{PA}	Park and Ang Damage Index (1985)
DOF	Degrees of Freedom
F	Fixed-base
FEM	Finite Element Method
G	Gazetas model
MDOF	Multiple Degree of Freedom
PGA	Peak Ground Acceleration
PGV	Peak Ground Velocity
PSV	Pseudo-Spectral Velocity
SDOF	Single Degree of Freedom
SSI	Soil-Structure Interaction
W	Wolf model

LIST OF FIGURES

LIST OF TABLES

Chapter 1

INTRODUCTION

1.1 Statement of the Problem

Interest in the behavior of engineering systems in fixed, or in most cases several alternative scenarios, indicates how important is the use of a model as a common tool in structural engineering. However, the problem that usually arises is how to select the best possible model from the pool of those available in order to correctly estimate the design force quantities. In general, engineering systems involve complex influencing factors, which also interact with each other. This is why it is difficult to describe the real system mathematically in a way that takes all relevant inherent mechanisms into account in order to predict its behavior in the real world. Within this context, models are constructed and used as an approximation of the reality. Since we are approximating reality, a great deal of care should be given to selecting the most appropriate model from the set of models available, by taking the different types of uncertainty underlying the model into account.

Past earthquakes have shown that assigning the correct type of dynamic soil-structure interaction (SSI) can be decisive for the stability of structures and serve as protection against damage and collapse. The assumption of fixed support for a structure founded on soft soil ignores the interaction effects that result from the scattering of waves when they reach the foundation surface and the energy radiated from the structure during its vibration. These interaction effects

lead to dynamic responses that may differ considerably in amplitude and frequency content from the responses obtained when a fixed support is assumed. Thus, the need for reliable SSI models has increased in recent years. Much of the research of the last three decades has focused on SSI studies following seminal publications summarizing work that was conducted in this area in the 1960s and 1970s (Johnson, 1981). However, structural engineers are often faced with the task of selecting an appropriate model from a set of several models with variable complexities in order to deal with the problem at hand. The models proposed in the literature that deal with the SSI problem range from the simplified, multiple-degree-of-freedom (MDOF) lumped-parameter models with masses, springs and dashpots to sophisticated three-dimensional finite element (FE) or even hybrid models that include specialized techniques such as boundary elements (BE) for the soil half-space (Chopra, 2007). Simplified models provide an undemanding framework for structural design, but may be inadequate because of assumptions and idealizations that are not consistent with the actual response of complex, asymmetric buildings (Naiem, 2001; Nasser et al., 2010). On the other hand, discrete parameter models are more general in principle and incorporate many details, However the computational effort increases considerably when a very large number of degrees of freedom are required to model this type of sophistication, which culminates with the implementation of nonlinear constitutive models for tracing post-elastic behavior. Such large scale models inevitably give rise to uncertainties regarding the selection of values for the input parameters. Thus, appropriate modeling techniques for a given structural system should be selected and also include all the factors that will most likely influence the structural response, especially in the presence of environmentally-induced loads such as earthquakes (FEMA, 2005).

1.2 Objectives and Approaches

A coupled soil-structure system can experience resonance due to the broad range of excitation frequencies. Consequently, completely different displacement responses might be produced under different excitations. Decisions regarding SSI models that lead to more conservative design models cannot be made independently of the excitation frequency. A reliable, conceptually clear criterion is needed in order to assess the quality of the different SSI models independently of

the particular ground motion and hysteretic rules used. Defining such a criterion is considered a crucial factor in order to judge the quality of a model consistently.

The energy approach can serve as a powerful tool for the purpose of model assessment, since it is based on a clear physical concept. The constructed energy response time histories can provide valuable insight into the behavior of a structure during an earthquake. The energy criterion states that the structure will be damaged if it is required to dissipate energy that is larger than its capacity. Of the different components of earthquake energy, the hysteretic energy that structures dissipate is associated with inelastic behavior and consequently with the damage of structures. Although the increasing duration of the excitation leads to increased input and hysteretic energies, it does not influence the ratio of hysteretic energy to input energy (Rahnama and Manuel, 1996).

Uncertainties are associated with every modeling process. They are inherent and usually cannot be reduced. Uncertain model response is generally associated with both the input variables involved and prior hypotheses of model configuration. The objective of the research discussed in this dissertation is to propose a generic and hierarchical methodology for assessing the quality of dynamic SSI models. The hypothesis of increasing model uncertainty with decreasing complexity is investigated and a mathematical framework is provided for the treatment of model uncertainty and applied to a case study involving alternative models for incorporating dynamic SSI effects. The uncertainty in modeling is characterized as an attribute of model complexity. It is defined in terms of the error of the model output and then assessed quantitatively. The proposed evaluation methodology based on energy measures provides a tool to support structural engineers in making informed decisions in the selection of one particular SSI model over another, despite the general uncertainties associated with them. This can help reduce the numerical simulation effort and unnecessary costs created by more complex models.

Dynamic SSI models with various abstraction levels are investigated in this work according to different coupling scenarios for soil and structure models. The modeling of the structure seems to be rather straightforward. Furthermore, the energy dissipated by MDOF systems can be estimated using equivalent single-degree-of-freedom (SDOF) systems (McKevitt et al., 1980). Thus, more emphasis is given to the soil model since it is more uncertain. In addition to the

fixed-base model investigated, the effects of SSI are considered using both simplified and more sophisticated models. As a simplified SSI model, the lumped-parameter system based on springs and dashpots is implemented in the time domain. At the other extreme, a three-dimensional finite element model for the soil-foundation-structure system is implemented. Additional two-dimensional models are also employed in order to investigate the effects of absorbing boundaries, which are usually used in such three-dimensional finite element models to prevent the reflection of waves from the boundaries of the models. Energy measures, as well as other structural response indicators, are derived and employed within the framework of the proposed evaluation methodology in this work.

1.3 Organization of the Dissertation

This dissertation is divided into five chapters, which cover the different research fields investigated in this research work. After the introduction given in Chapter 1, the three main chapters presented include an introduction and summary for each chapter.

Chapter 1 states the objective of the assessment for dynamic SSI models, describes the problem and indicates how the assessment can be developed further.

Chapter 2 addresses the interaction mechanisms between soil, foundation and structure that can be taken into account by using two different modeling methods, i.e., the direct and substructure methods. Dynamic SSI models with different abstraction levels are introduced. Subsequently, the adopted models are implemented by way of a numerical example, which illustrates how SSI effects alter the structural response solely because of the choice of models in the analysis of the dynamic behavior of a structure.

Chapter 3 investigates the dynamic SSI models introduced and implemented in Chapter 2 using energy measures as general indicators of the elastic and inelastic structural responses. The different terms of energy imparted to a structure are computed using the energy approach, which is based on a physically clear concept. A forced dynamic analysis of structure is performed using two basic types of base motion, namely sinusoidal and pulse ground excitations. As a primary application, the energies of elastic structural response are computed analytically

without incorporating dynamic SSI effects. Subsequently, the investigation is extended to the inelastic response of a fixed-base structure, as well as a coupled soil structure system.

Chapter 4 proposes a methodology for assessing the quality of the dynamic SSI models investigated in Chapters 2 and 3. The evaluation is based on the underlying uncertainty, which is classified into aleatory and epistemic uncertainty. This will be shown to play an essential role in the application of the theoretical formulations in this chapter. Uncertainty in the input parameters is taken into account by means of the sampling strategy described in this chapter in order to determine the total model uncertainty of dynamic SSI models.

Chapter 5 presents the concluding remarks on the proposed evaluation methodology and discusses the results obtained in this research work. An outline for future work is also included in this chapter.

Chapter 2

DYNAMIC SOIL-STRUCTURE INTERACTION

2.1 Introduction

Structural engineers generally assume that structures subjected to dynamic loading are fixed at their bases. This assumption ignores the important effects of the dynamic interaction between structure and soil if the structure is not founded on rock or if the supporting soil does not have high stiffness in comparison to the superstructure. Consequently, accounting for the actual support conditions may decrease the overall stiffness of a structure and lead to a more flexible structure. Damping of the supporting soil, as well as its periods of vibration in relation to that of the structure are also important aspects that affect the overall structural response, whereas the increase in the natural period may cause a significant change in the seismic response of the structure. Therefore, it is important to incorporate the dynamic soil-structure interaction (SSI) effects in the analysis of the dynamic behavior of structures.

In this chapter, the interaction mechanisms between soil, foundation and structure are described in section 2.3, which can be considered using two different modeling methods (subsection 2.5). Four SSI models are described in section 2.6 and section 2.7 presents a numerical example illustrating how SSI effects alter the structural response by using the adopted models in the

analysis of the dynamic behavior of a structure. The quality of the adopted SSI models are assessed later on using the evaluation methodology introduced in Chapter 4.

2.2 Previous Studies

Much of the research of the last three decades has focused on SSI studies following seminal publications summarizing work that was conducted in this area in the 1960s and 1970s (Johnson, 1981). Methods of different levels of complexity are available for engineers. The models proposed in the literature range from the simplified, MDOF lumped-parameter models with masses, springs and dashpots to sophisticated three-dimensional finite element or even hybrid models that include specialized techniques such as boundary elements for the soil half-space (Chopra, 2007). Procedures that take the SSI in the seismic analysis of buildings into account are introduced by Dutta and Roy (2002) with a comprehensive review of the literature. A thorough discussion of the methods of dynamic SSI analysis is presented by Wolf (1985) and the concepts and results regarding some important aspects of dynamic SSI are discussed in Wolf and Song (2002).

The impedance functions approach is widely used by structural engineers. Significant papers that deal with this approach have been published by Wong and Luco (1985) and Crouse et al. (1990). Methods on the dynamic analysis of foundations that follow the foundation stiffness approach were initiated in the past by Hsieh (1962) and Lysmer (1965) and then extended by Richart and Whitman (1967) and Richart et al. (1970). This approach is widely used by structural engineers, where soil behavior is taken into account by simple mechanical elements, such as springs, masses and dashpots with frequency dependent or frequency independent stiffness and damping coefficients. The latter was determined by a procedure of curve fitting (Wolf, 1994) and the conceptual background for deriving the coefficients was provided by Veletsos (1974). Dobry and Gazetas (1986) and Dobry et al. (1986) pointed out that coefficients of long footings lying on saturated clay are more strongly dependent on the frequency of dynamic loading. Based on experimental verification and an extensive survey of the literature, in addition to the results obtained by using the boundary element method (BEM), Gazetas (1991) proposed closed-form expressions to compute the stiffness and damping coefficients for arbitrary shaped

footings resting on homogeneous elastic half-space, whereas Tassoulas and Kausel (1984) and Veletsos and Tang (1987) developed coefficients for annular footings. Gazetas (1991) is considered as a benchmark literature in the field of dynamic SSI. The macro-element concept provides a simplifying approach for dealing with the SSI problem. This approach is based on the concept of generalized stress and strain variables (Nova and Montrasio, 1991; Prager, 1955). According to this approach, the foundation and the near field soil are replaced with a plastic hinge, whereas the linear far field is described by a system of spring and dashpot. Only a single point represents the interaction between the near and the far fields. Nova and Di Prisco (2003) have introduced several applications of the macro-element and a similar simplifying and practical approach that also incorporates the capacity spectrum method is developed in Schanz et al. (2008).

More sophisticated models using the finite element method (FEM) are also used to solve the problem of SSI. Modeling the near field using the FEM requires implementing artificial boundaries that characterize the behavior of the unbounded soil media. Different modeling approaches can be applied in order to absorb outgoing waves from the soil-structure system (Lysmer and Kuhlemeyer, 1969; Liao and Wong, 1984). However, Kausel (1988) pointed out that most of the available artificial boundaries are mathematically equivalent. The so-called scaled boundary finite element method was proposed in Wolf and Schanz (2004) as an efficient method to solve problems that involve stress discontinuities (Deeks and Wolf, 2002). Another suggestion found in the literature is to use the BEM for modeling the unbounded soil media combined with the FEM to model the structure (Dobry and Gazetas, 1986; Dobry et al., 1986; Wolf, 1985). In these types of models, special care should be given to the compatibility conditions at the interface between coupled finite elements and boundary elements. Alternatively, the infinite element concept can serve to model the unbounded soil medium (Ungless, 1973; Bettess, 1977). In this method, the behavior of the unbounded medium is obtained by means of the displacement shape function and the geometrical decay function (Bettess, 1980; Medina and Penzien, 1982). Otherwise, the infinite element is mapped into a finite element (Zhao and Valliappan, 1993). Chuhan et al. (1999) introduced a model coupled of finite elements, boundary elements, infinite elements and infinite boundary elements that incorporates the interaction between the structure and the nonlinear layered soil.

A two-step dynamic procedure, called the domain reduction method, was originally developed by Bielak et al. (2003) and Yoshimura et al. (2003) and extended by Jeremić (2010) to be used for the dynamic analysis of soil-foundation-structure systems. This method allows the large computational domain to be reduced to a more convenient size.

2.3 Effects of Dynamic Soil-Structure Interaction

Ignoring dynamic soil-structure interaction effects can be practical and convenient only when performing an analysis for flexible systems on rock or very stiff soil. For structures on soil, two interaction mechanisms between soil, foundation and structure can be recognized, namely inertial interaction and kinematic interaction (Kramer, 1996; Stewart et al., 1998).

2.3.1 Inertial interaction

The inertial forces generated by the vibrating structure are transmitted to the foundation and supporting soil, which leads to increased translations and rotations at the base level of the structure. As a result, the structure becomes more flexible as the vibration period increases.

This type of interaction can be analyzed as illustrated in Figure 2.1 employing a single-degree-of-freedom structure of mass m, lateral stiffness k, internal damping c and height h on a flexible foundation represented by frequency-dependent translational and rotational springs $\bar{k}_u$ and $\bar{k}_\theta$. θ refers to base rocking of the foundation slab, u_g is the free-field ground displacement, u_f is the horizontal displacement of the foundation relative to free-field and u is the displacement of the structure relative to its base.

2.3.2 Kinematic interaction

Since foundation stiffness and supporting soil stiffness are different, the motion experienced by the foundation will deviate from that of the free-field soil. This is caused by the so-called base slab averaging and embedment effects (Stewart et al., 1998) illustrated in Figure 2.2. The base slab averaging effect can be observed from the reduced foundation motion in relation to the

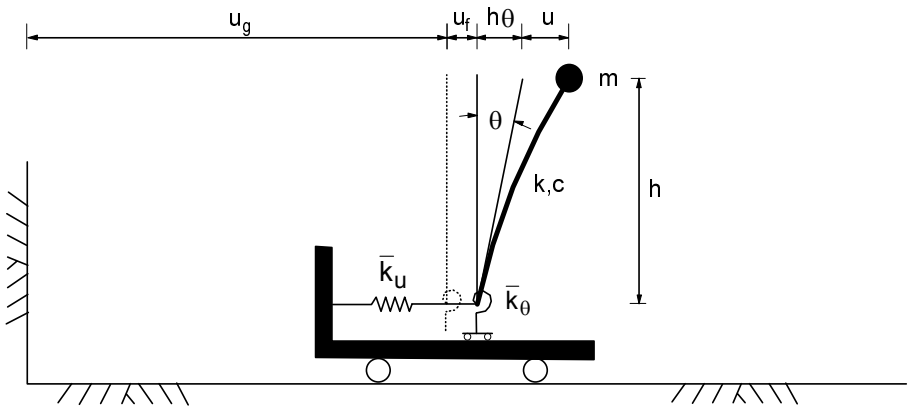

Figure 2.1: Simplified model for analysis of inertial interaction (Stewart et al., 1998)

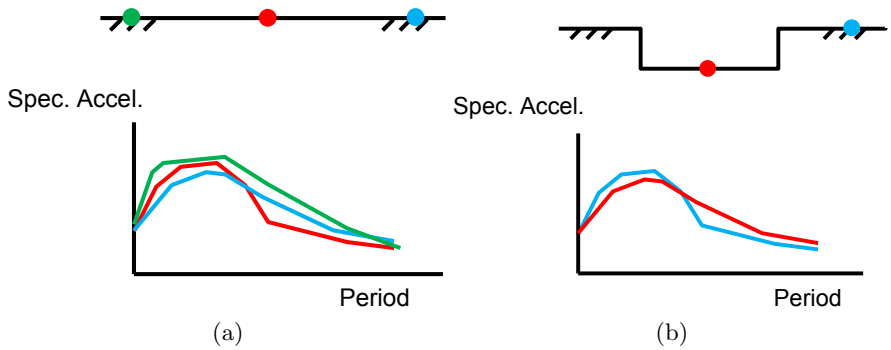

Figure 2.2: Mechanisms contributing to kinematic interaction: (a) Base-slab averaging effects, (b) Embedment effects

free-field motion, and the embedment effects are explained by the reduction of ground motion associated with the increasing depth in a soil deposit. Accordingly, kinematic interaction plays a more significant role for structures with embedded foundations (Mylonakis et al., 2006).

2.3.3 Base isolation system

In this subsection, a brief description of typical lead rubber bearing (LRB) systems comprising a lead core and laminated rubber layers is provided (Manolis et al., 2011). More specifically, LRBs are fabricated from low damping (unfilled) elastomers with shear modulii in the range of $0.8 - 1.2 N/mm^2$ and lead core diameters ranging between 15% and 30% of the bonded bearing diameter. The elastomer part provides the isolation and recentering mechanism, while the lead

core dissipates energy and the inner steel shims provide load capacity and confinement of the lead core. A maximum shear strain value for the LRB is generally between 125% to 200% and the yield stress of the lead core depends on the temperature; after one load cycle it is around $12.5MPa$, and after three cycles it drops to about $10.5MPa$.

The nonlinear governing equations for an LRB undergoing time-dependent loading are as follows:

$$\begin{aligned} F_L(t) &= C_L\dot{\omega(t)} + \alpha_l K_L \omega(t) + (1-\alpha_l)K_L z(t), \\ \dot{z} &= A\dot{\omega} - \beta_l|\dot{\omega}||z|^{n-1}z - \gamma_l\dot{\omega}|z|^n \end{aligned} \tag{2.1}$$

In the above, $\omega(t)$ is the lateral displacement and $F_L(t)$ is the restoring horizontal force in the LRB, while $z(t)$ is an additional displacement parameter controlling the hysteretic part of the restoring force. All of the parameters, i.e., $K_L, C_L, \alpha_l, A, \beta_l, \gamma_l, n$, stem from the LRB material and mechanical properties. For example, a non-degrading smooth system model would have values of $\alpha_l = 1/21, A = 1, \beta_l = \gamma_l = 0.5, n = 1$.

Although it is possible to use linearization to produce equivalent stiffness and damping coefficients in the relation between $z(t)$ and $\omega(t)$, which is subsequently converted to an SDOF-type equation, this requires use of a full-fledged stochastic analysis (Baber and Wen, 1979). The alternative is to break down the second of Eq. 2.1 into four differential equations, each divided by $\dot{\omega}$, and valid in the following specific response regions:

$$\begin{aligned} \frac{dz}{d\omega} &= A - (\beta_l + \gamma_l)z^n && z \geq 0, \dot{\omega} \geq 0 \\ \frac{dz}{d\omega} &= A - (\gamma_l - \beta_l)z^n && z \geq 0, \dot{\omega} < 0 \\ \frac{dz}{d\omega} &= A + (-1)^{n+1}(\beta_l + \gamma_l)z^n && z < 0, \dot{\omega} < 0 \\ \frac{dz}{d\omega} &= A + (-1)^{n+1}(\gamma_l - \beta_l)z^n && z < 0, \dot{\omega} \geq 0 \end{aligned} \tag{2.2}$$

Note that the differentials $dz/d\omega$ and $d\dot{z}/d\dot{\omega}$ are exactly the same and that if $n = 1$, the four differential equations can be easily solved in their respective domains. It is obvious that a frequency domain approach will not work for this type of nonlinear model; instead, a time-stepping algorithm with Newton-Raphson type iterations within a given step is necessary. Approaches

along these lines were recently followed by Papakonstantinou et al. (2008), who modified the standard beam finite element to include additional degrees of freedom to handle the evolution of the Bouc-Wen equations with kinematic hardening.

Here, Eq. 2.1 is approximated through the use of a fractional derivative constitutive law (Atanakovic and Spasic, 2004) that can be viewed as the limit for linearized models to capture the nonlinear response. In essence, a relation between the stress and strain rates is introduced in the uniaxial tension/compression of the LRB material, which is expressed macroscopically as a relation between the restoring force and lateral displacement in the form

$$F_L(t) + \tau_F F_L^{(a)}(t) = K_L \left[\omega(t) + \tau_W \omega^{(a)}(t)\right], \qquad (\cdot)^{(a)} = d^a(\cdot)/dt^a \tag{2.3}$$

In the above, the derivative order is $0 < a < 1$ and the two material constants that have units of time to the power a as shown in Eq. 2.3 must obey the constraint $\Delta\tau = (\tau_W - \tau_F) > 0$. Obviously, these model parameters can only be determined by careful calibration with the experimental results. It should be noted here that when the fractional derivative order a is unity, the three-parameter model of linear viscoelasticity, which combines the Kelvin solid with the Maxwell fluid, is recovered. Now, the advantage of fractional derivative formulations is that their Fourier transform exists (Luchko et al., 2008) and can be integrated within the structural model.

2.4 Waves in the Elastic Half-Space

The soil medium in all the SSI models investigated in this work is assumed to remain linearly elastic with linear hysteretic material damping during the dynamic excitation. Performing a nonlinear analysis of soil for numerous samples for two-dimensional and three-dimensional FE soil-structure systems is very expensive computationally. However, performing such an analysis may be justified for important structures.

After the energy is released by the earthquake source inside the earth's crust, it radiates in the form of elastic waves. These earthquake waves are generally described by body waves and surface waves. With regard to body waves, we distinguish between two types of waves

that propagate within the earth, known as P-waves, which are also referred to as primary waves or compressional waves; and S-waves, which are also called secondary waves or shear waves.. These two types of waves describe the behavior of the material particles. Tension and compression deformations are characterized by P-waves, whereas shear deformations in vertical and horizontal planes are described by S-waves.

This section describes the wave equations for infinite, homogeneous, elastic media and gives a brief introduction of compression and shear waves. The basic equations of elastodynamics (Richart et al., 1970) assuming isotropic, homogeneous and linear elastic material properties for the soil, are summarized below. In a linear elastic continuum, the fundamental equations of the theory of elasticity are the conditions of the stresses, strains and displacements that describe the constitutive relationships, as well as the conditions of equilibrium and compatibility. The components of a stress vector for an elemental volume of a loaded body is given by

$$\{\sigma\}^T = [\sigma_{xx} \quad \sigma_{yy} \quad \sigma_{zz} \quad \tau_{xy} \quad \tau_{yz} \quad \tau_{zx}] \tag{2.4}$$

and the strain components related to the six stress components given in Eq. 2.4 are

$$\{\varepsilon\}^T = [\varepsilon_{xx} \quad \varepsilon_{yy} \quad \varepsilon_{zz} \quad \gamma_{xy} \quad \gamma_{yz} \quad \gamma_{zx}] \tag{2.5}$$

Let u, v and w denote the components of the displacement vector in a Cartesian coordinate system x, y, z. Assuming that the displacement gradients are small compared to one, then the general strain components are given as

$$\begin{aligned} \varepsilon_{xx} &= \frac{\partial u}{\partial x} & \varepsilon_{yy} &= \frac{\partial v}{\partial y} & \varepsilon_{zz} &= \frac{\partial w}{\partial z} \\ \gamma_{xy} &= \frac{1}{2}\left(\frac{\partial u}{\partial y} + \frac{\partial v}{\partial x}\right) & \gamma_{yz} &= \frac{1}{2}\left(\frac{\partial v}{\partial z} + \frac{\partial w}{\partial y}\right) & \gamma_{zx} &= \frac{1}{2}\left(\frac{\partial w}{\partial x} + \frac{\partial u}{\partial z}\right) \end{aligned} \tag{2.6}$$

For isotropic material, the stresses can be expressed as the strains resulting from the following expressions

$$\begin{aligned} \sigma_{xx} &= \lambda\Delta + 2G\varepsilon_{xx} & \tau_{xy} &= 2G\varepsilon_{xy} \\ \sigma_{yy} &= \lambda\Delta + 2G\varepsilon_{yy} & \tau_{yz} &= 2G\varepsilon_{yz} \\ \sigma_{zz} &= \lambda\Delta + 2G\varepsilon_{zz} & \tau_{zx} &= 2G\varepsilon_{zx} \end{aligned} \tag{2.7}$$

where G and λ are the Lamé constants related to the modulus of elasticity E and Poisson's ratio ν by

$$\lambda = \frac{\nu E}{(1+\nu)(1-2\nu)}, \qquad G = \frac{E}{2(1+\nu)} \tag{2.8}$$

and Δ is the volume strain defined as the sum of the normal strains in the three coordinate directions

$$\Delta = \varepsilon_{xx} + \varepsilon_{yy} + \varepsilon_{zz} \tag{2.9}$$

The equations of motion in terms of stresses and inertia are given by

$$\begin{aligned} \frac{\partial \sigma_{xx}}{\partial x} + \frac{\partial \tau_{xy}}{\partial y} + \frac{\partial \tau_{xz}}{\partial z} &= \rho \frac{\partial^2 u}{\partial t^2} \\ \frac{\partial \tau_{yx}}{\partial x} + \frac{\partial \sigma_{yy}}{\partial y} + \frac{\partial \tau_{yz}}{\partial z} &= \rho \frac{\partial^2 v}{\partial t^2} \\ \frac{\partial \tau_{zx}}{\partial x} + \frac{\partial \tau_{zy}}{\partial y} + \frac{\partial \sigma_{zz}}{\partial z} &= \rho \frac{\partial^2 w}{\partial t^2} \end{aligned} \tag{2.10}$$

where ρ is the density of the material and t is the time. The basic equations of elastodynamics can then be obtained from Eqs. 2.6, 2.7 and 2.10 as

$$\rho \frac{\partial^2 u}{\partial t^2} = (\lambda + G) \frac{\partial \Delta}{\partial x} + G \nabla^2 u \tag{2.11}$$

$$\rho \frac{\partial^2 v}{\partial t^2} = (\lambda + G) \frac{\partial \Delta}{\partial y} + G \nabla^2 v \tag{2.12}$$

$$\rho \frac{\partial^2 w}{\partial t^2} = (\lambda + G) \frac{\partial \Delta}{\partial z} + G \nabla^2 w \tag{2.13}$$

with

$$\nabla^2 = \frac{\partial^2}{\partial x^2} + \frac{\partial^2}{\partial y^2} + \frac{\partial^2}{\partial z^2} \tag{2.14}$$

2.4.1 Compression waves

By differentiating the equations of motion 2.11, 2.12 and 2.13 with respect to x, y and z, respectively, and then adding the result, a special solution of the basic equations can be obtained as follows

$$\frac{\partial^2 \Delta}{\partial t^2} = \frac{(\lambda + 2G)}{\rho} \nabla^2 \Delta \tag{2.15}$$

This is the classical form of the wave equation known as compression waves or the P-waves equation. It implies that the wave is propagated through the medium with the velocity c_p defined as

$$c_p = \sqrt{\frac{\lambda + 2G}{\rho}} = \sqrt{\frac{E(1-\nu)}{\rho(1+\nu)(1-2\nu)}} \tag{2.16}$$

2.4.2 Shear waves

By differentiating Eq. 2.12 with respect to z, and Eq. 2.13 with respect to y, and then subtracting the result, another special solution of the basic equations can be obtained, as shown below

$$\frac{\partial^2 \omega_x}{\partial t^2} = \frac{G}{\rho} \nabla^2 \omega_x \tag{2.17}$$

where ω_x is the rotation about the x-axis. Two more similar equations can be obtained from processing the remaining combinations which gives

$$\frac{\partial^2 \omega_y}{\partial t^2} = \frac{G}{\rho} \nabla^2 \omega_y \tag{2.18}$$

$$\frac{\partial^2 \omega_z}{\partial t^2} = \frac{G}{\rho} \nabla^2 \omega_z \tag{2.19}$$

Eqs. 2.17, 2.18 and 2.19 represent the so-called shear waves or S-waves equations which propagate with the velocity c_s defined as

$$c_s = \sqrt{\frac{G}{\rho}} = \sqrt{\frac{E}{2\rho(1+\nu)}} \tag{2.20}$$

2.5 Direct Method and Substructure Method

In dynamic SSI, it is essential that unbounded soil is appropriately considered in the model being analyzed. The two classical procedures used to incorporate dynamic SSI in the analysis are referred to as the direct and substructure methods.

In the direct method, the entire system, including soil, foundation and structure, is analyzed in one single step. The unbounded soil is replaced in this method with artificial boundary, which

characterizes the behavior of the far-field soil media. Nonlinear analysis of the behavior of the system can be performed using the FEM for modeling all of the system components. However, the computational effort is very expensive in this case due to the large number of degrees of freedom in the soil region and especially for nonlinear soil behavior. Therefore, such models are rarely used in practice. For a more efficient and direct SSI analysis, an equivalent linearity of soil can be assumed as done by Lysmer et al. (1975) and McKenna and Fenves (2001).

In the substructure method, the system is generally divided into two subsystems, which can be analyzed separately: a superstructure that may include a portion of the supporting soil, and a substructure that includes the unbounded soil medium. In the case of embedded structures, three subsystems connected with common nodes can be created for analyzing the problem as described in Figure 2.3 (Lysmer et al., 1999). Both soil and structure are assumed to exhibit linear behavior in the substructure method since the principle of superposition is followed here.

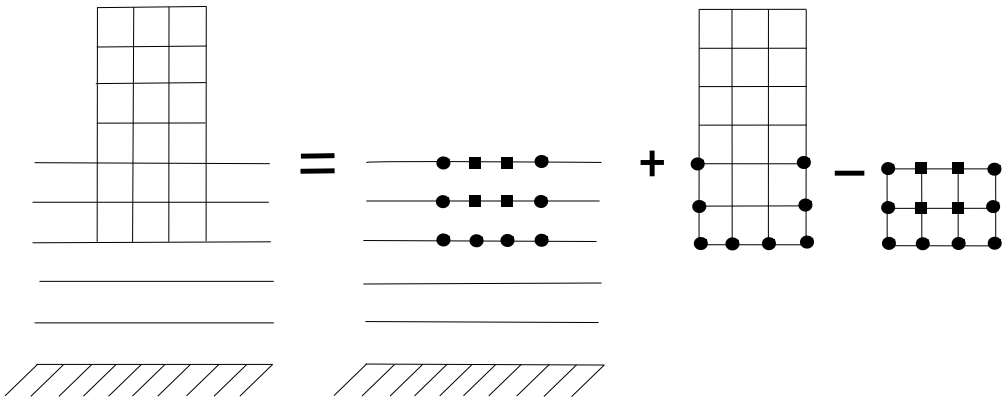

Figure 2.3: Substructuring system adapted after (Lysmer et al., 1999): (a) Total system, (b) Free-field site, (c) Structure, (d) Excavated soil volume

2.6 Soil-Structure Interaction Models Used

In this section, four different soil-structure interaction models are described. The quality of these adopted models will be assessed later on using the evaluation methodology proposed

in Chapter 4. The models are adopted in such a way so as to represent both simplified and more complex models that are commonly used by structural engineers in practice. The adopted models are two simpler models (Wolf and Gazetas models) and two more complex finite element (FE) models that are usually considered to be more representative of the real system than the simpler models.

2.6.1 Simple physical Wolf models

The simple physical models shown in Figure 2.4 were developed by Wolf (1994) for foundation on surface of homogeneous linear-elastic half-space. These models are based on assumed displacement patterns instead of rigorous elasticity solutions. Wolf provides simple physical models, which he developed as follows:

- *Cone models*: Truncated semi-infinite cones for translational and rotational components of motion based on the rod theory with the corresponding one-dimensional displacement.
- *Discrete element models*: Spring-dashpot-mass models representing the unbounded soil. All coefficients of these models are frequency independent.
- *Prescribed wave patterns in the horizontal plane*: One-dimensional body and surface waves on the free surface and cylindrical waves.

Table 2.1 summarizes the properties of the cones and the discrete element models representing a rigid massless foundation with area A_0 and polar moment of inertia I_0 on surface of homogeneous half-space with Poisson's ratio ν, density ρ, shear-wave velocity c_s and dilatation wave velocity c_p. The truncated semi-infinite cone has an equivalent radius r_0, apex height z_0 and wave velocity c as shown in Figure 2.4 (a). In Figure 2.4 (b) represents the spring-dashpot system which is dynamically equivalent to the translational cone. The spring-dashpot system is illustrated in Figure 2.4 (c) with and without the polar mass moment of inertia M_ϑ for the internal degree of freedom ϑ corresponding to the rotational cone.

The coefficients are assigned based on the static analysis, therefore they are all frequency independent. The dynamic stiffness coefficient is interpreted as a spring and dashpot with

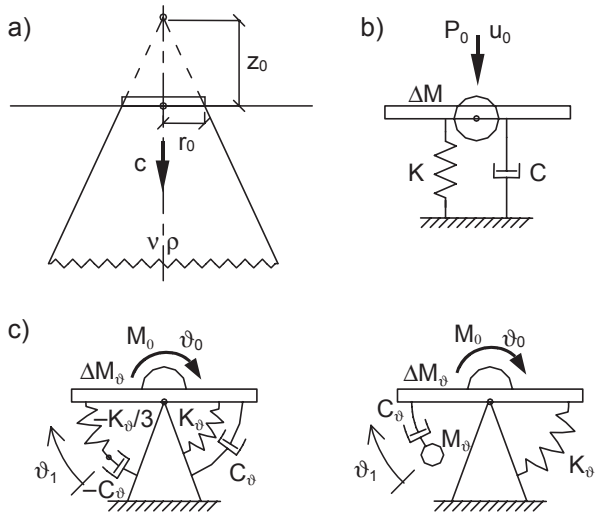

Figure 2.4: Cone model and corresponding lumped-parameter models for foundation on surface of homogeneous half-space (Wolf and Deeks, 2004): a) Truncated semi-infinite cone, b) Spring-dashpot-mass model for translational degree of freedom, c) Spring-dashpot-mass model for rotational degree of freedom

frequency-dependent coefficients as

$$K_\omega = Kk(a_0); \qquad C_\omega = \frac{r_0}{c_s} Kc(a_0) \tag{2.21}$$

where $k(a_0)$ is the dimensionless spring coefficient, $c(a_0)$ is the dimensionless damping coefficient and a_0 is the dimensionless frequency, which is defined as

$$a_0 = \frac{\omega r_0}{c_s} \tag{2.22}$$

Figure 2.5 illustrates the resulting dimensionless spring and damping coefficients as functions of the dimensionless frequency a_0 for Poisson's ratio $\nu = 0.2$ for disk on homogeneous half-space in horizontal motion computed after Wolf (1994). Similar curves have also been derived for vertical, rocking and torsional motions.

Table 2.1: Parameters for modeling foundation on surface of homogeneous half-space (Wolf and Deeks, 2004)

Motion	**Horizontal**	**Vertical**		**Rocking**		**Torsional**
Equivalent radius r_0	$\sqrt{\frac{A_0}{\pi}}$	$\sqrt{\frac{A_0}{\pi}}$		$\sqrt[4]{\frac{4I_0}{\pi}}$		$\sqrt[4]{\frac{2I_0}{\pi}}$
Aspect ratio $\frac{z_0}{r_0}$	$\frac{\pi}{8}(2-\nu)$	$\frac{\pi}{4}(1-\nu)\left(\frac{c}{c_s}\right)^2$		$\frac{9\pi}{32}(1-\nu)\left(\frac{c}{c_s}\right)^2$		$\frac{9\pi}{32}$
Poisson's ratio ν	all ν	$\nu \le \frac{1}{3}$	$\frac{1}{3} < \nu \le \frac{1}{2}$	$\nu \le \frac{1}{3}$	$\frac{1}{3} < \nu \le \frac{1}{2}$	all ν
Wave velocity c	c_s	c_p	$2c_s$	c_p	$2c_s$	c_s
Trapped mass ΔM ΔM_ϑ	0	0	$2.4\left(\nu-\frac{1}{3}\right)\rho A_0 r_0$	0	$1.2\left(\nu-\frac{1}{3}\right)\rho I_0 r_0$	0
Lumped-parameter model		$K = \rho c^2 A_0/z_0$ $C = \rho c A_0$		$K_\vartheta = 3\rho c^2 I_0/z_0$ $C_\vartheta = \rho c I_0$ $M_\vartheta = \rho I_0 z_0$		

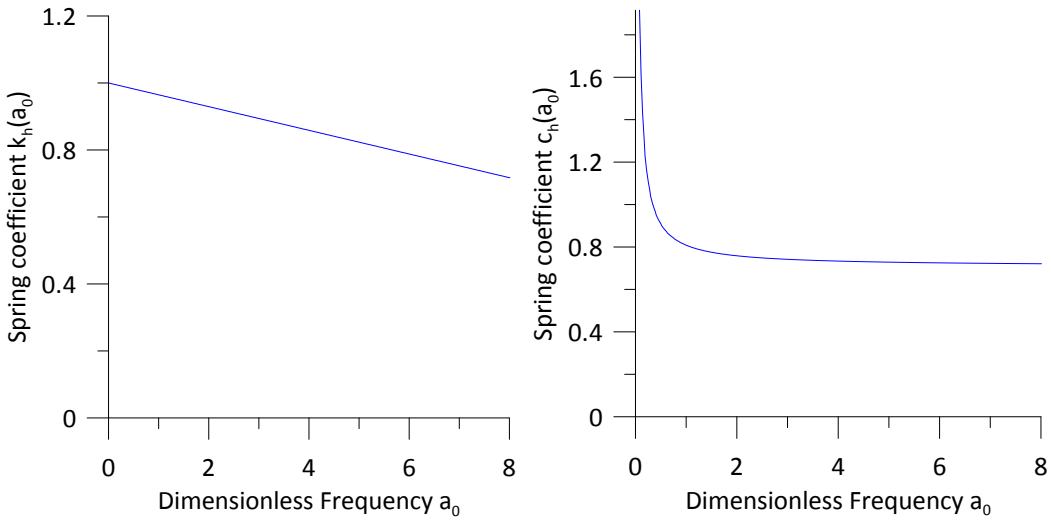

Figure 2.5: Dynamic stiffness coefficient of disk on homogeneous half-space in horizontal motion for Poisson's ratios $\nu = 0.2$ computed after (Wolf, 1994)

2.6.2 Gazetas dynamic springs and dashpots

As explained in subsection 2.3.1, D'Alembert forces associated with the acceleration of the superstructure during the excitation affect the complete soil-foundation-structure system leading to inertial soil-structure interaction. A commonly used procedure for taking the effects of this type of interaction into account is to compute the dynamic impedance functions (springs and dashpots) associated with each component of motion. The rigid foundation shown in Figure 2.6

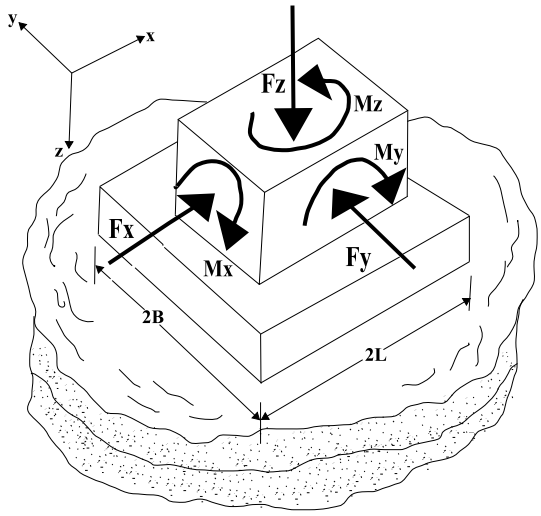

Figure 2.6: Rigid foundation block with its six degrees of freedom

has six degrees of freedom associated with the components of motion: three translational and three rotational. Gazetas (1991) presented a general method for computing each of these six displacements and rotations. He concluded that soil in the case of a vertically oscillating foundation can be replaced with a system of spring and dashpot. He then extended his definition of dynamic impedance for vertical excitation to each of the remaining five modes of vibration and developed corresponding closed-form expressions and graphs for dynamic spring and dashpot coefficients. Figure 2.7 illustrates the spring k and dashpot c associated with the vertical degree of freedom for an embedded foundation subjected to a harmonic vertical force $P(t) = P_0\, e^{i\omega t}$ with the amplitude P_0 and frequency ω.

Gazetas introduced formulas and graphs for foundations with different shapes on the surface

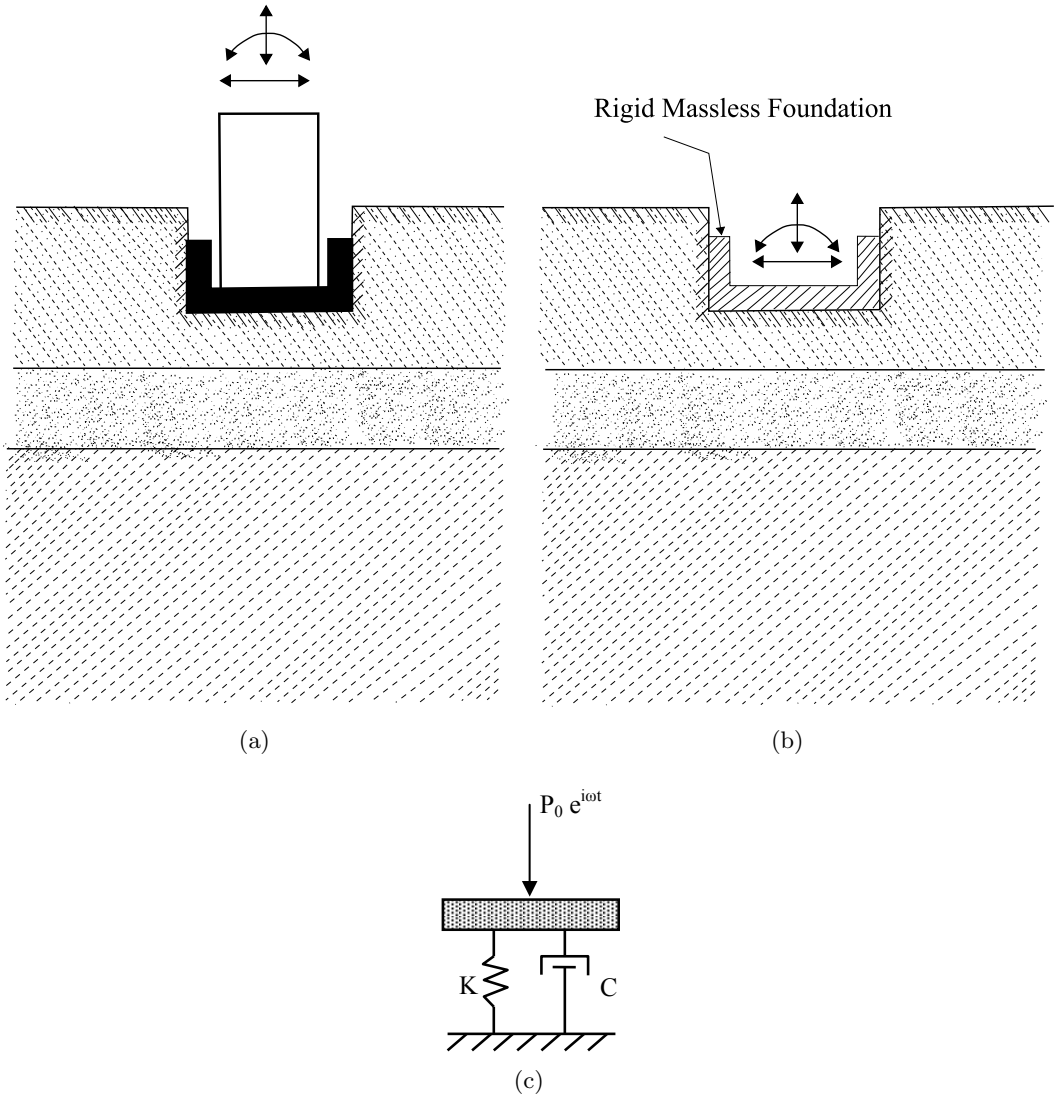

Figure 2.7: A foundation-structure system on layered soil (a), the associated rigid and massless foundation (b) and physical interpretation of dynamic spring and dashpot in vertical mode of vibration (c) adapted after (Gazetas, 1991) and (Mylonakis et al., 2006)

of or embedded in half-space that can be homogeneous or inhomogeneous. Tables 2.2 and 2.3 illustrate the formulas for computing the dynamic coefficients for foundations of any solid shape lying on the surface of a homogeneous half-space. The graphs related the aforementioned tables are presented in Figure 2.8, illustrating the relation between the dimensionless frequency a_0 on the one side and the dynamic stiffness coefficients k and radiation damping coefficients $\bar{c}$ on the other side for foundation with 2L length and 2B width of the foundation, respectively, V_s refers to the shear-wave velocity and ω represents the circular excitation frequency. Gazetas developed his formulas and graphs for different L/B ratios based on simple physical models calibrated against boundary element formulations and data from the literature, which he referenced in his paper.

2.6.3 Finite element modeling

Powerful computers are used to investigate and analyze systems with complex interactive behavior, such as the dynamic behavior of soil-foundation-structure systems using the FEM. In this method, the near field is modeled using a finite number of elements, whereas the far field is replaced with an artificial boundary, which characterizes the behavior of the unbounded soil media coupled to the near field through their common nodal points, which are also called interaction nodes, as shown in Figure 2.9.

The classical formulation of the dynamic soil-structure interaction problem using the FEM requires setting up geometrical boundary conditions. Different modelling approaches can be applied in order to absorb outgoing waves from the soil-structure system. Most of these approaches are based on the theory of wave propagation. The Lysmer boundaries (Lysmer and Kuhlemeyer, 1969), or the so-called viscous boundaries, described in this subsection, are applied to the three-dimensional FE soil model implemented in this work.

Finite element size

The numerical analysis is assumed to lead to more accurate results as the finite element size Δs approaches zero. The selection of the minimum value of Δs mainly depends on the sufficiency

Table 2.2: Static stiffness coefficients for arbitrary shaped foundations on homogeneous half-space surface (Mylonakis et al., 2006)

Vibration mode	Dynamic stiffness $\mathscr{K} = Kk(\omega)$	
	Static stiffness K	
	General shape (foundation–soil contact surface area $= A_b$ with equivalent rectangle $2L \times 2B$; $L > B$)	Square $L = B$
Vertical, z	$K_z = \frac{2GL}{1-\nu}(0.73 + 1.54\chi^{0.75})$ with $\chi = \frac{A_b}{4L^2}$	$K_z = \frac{4.54GB}{1-\nu}$
Horizontal, y (lateral direction)	$K_y = \frac{2GL}{2-\nu}(2 + 2.5\chi^{0.85})$	$K_y = \frac{9GB}{2-\nu}$
Horizontal, x (longitudinal direction)	$K_x = K_y - \frac{0.2}{0.75-\nu} GL\left(1 - \frac{B}{L}\right)$	$K_x = K_y$
Rocking, rx (around x axis)	$K_{rx} = \frac{G}{1-\nu} / \underset{bx}{0.75} \left(\frac{L}{B}\right)^{0.25} \left(2.4 + 0.5\frac{B}{L}\right)$ with I_{bx} = area moment of inertia of foundation–soil contact surface around x axis	$K_{rx} = \frac{0.45GB^3}{1-\nu}$
Rocking, ry (around y axis)	$K_{ry} = \frac{G}{1-\nu} / \underset{by}{0.75}\left[3\left(\frac{L}{B}\right)^{0.15}\right]$ with I_{by} = area moment of inertia of foundation–soil contact surface around y axis	$K_{ry} = K_{rx}$
Torsional	$K_t = GJ_t^{0.75}\left[4 + 11\left(1 - \frac{B}{L}\right)^{10}\right]$ with $J_t = I_{bx} + I_{by}$ polar moment of inertia of foundation–soil contact surface	$K_t = 8.3GB^3$

Table 2.3: Dynamic stiffness and dashpot coefficients for arbitrary shaped foundations on homogeneous half-space surface (Mylonakis et al., 2006)

Vibration mode	Dynamic stiffness $\mathscr{K} = Kk(\omega)$	Radiation dashpot coefficient C
	Dynamic stiffness coefficient k (General shape; $0 \leqslant a_0 \leqslant 2$)	(General shapes)
Vertical, z	$k_z = k_z\left(\frac{L}{B}, v, a_0\right)$ plotted in Graph a	$C_z = (\rho V_{\mathrm{La}} A_{\mathrm{b}})\bar{c}_z$ $\bar{c}_z = \bar{c}_z\left(\frac{L}{B}, a_0\right)$ plotted in Graph c
Horizontal, y (lateral direction)	$k_y = k_y\left(\frac{L}{B}, a_0\right)$ plotted in Graph b	$C_y = (\rho V_{\mathrm{s}} A_{\mathrm{b}})\bar{c}_y$ $\bar{c}_y = \bar{c}_y\left(\frac{L}{B}, a_0\right)$ plotted in Graph d
Horizontal, x (longitudinal direction)	$k_x \simeq 1$	$C_x \simeq \rho V_{\mathrm{s}} A_{\mathrm{b}}$
Rocking, rx (around x axis)	$k_{\mathrm{r}x} = 1 - 0.20a_0$	$C_{\mathrm{r}x} = (\rho V_{\mathrm{La}} I_{bx})\bar{c}_{\mathrm{r}x}$ $\bar{c}_{\mathrm{r}x} = \bar{c}_{\mathrm{r}x}\left(\frac{L}{B}, a_0\right)$ plotted in Graph e
Rocking, ry (around y axis)	$\begin{cases} v < 0.45; \\ k_{\mathrm{r}y} \simeq 1 - 0.30a_0 \\ v \simeq 0.5: \\ k_{\mathrm{r}y} \simeq 1 - 0.25a_0\left(\frac{L}{B}\right)^{0.30} \end{cases}$	$C_{\mathrm{r}y} = (\rho V_{\mathrm{La}} I_{by})\bar{c}_{\mathrm{r}y}$ $\bar{c}_{\mathrm{r}y} = \bar{c}_{\mathrm{r}y}\left(\frac{L}{B}, a_0\right)$ plotted in Graph f
Torsional	$k_{\mathrm{t}} \simeq 1 - 0.14a_0$	$C_t = (\rho V_{\mathrm{s}} J_t)\bar{c}_t$ $\bar{c}_t = \bar{c}_t\left(\frac{L}{B}, a_0\right)$ plotted in Graph g

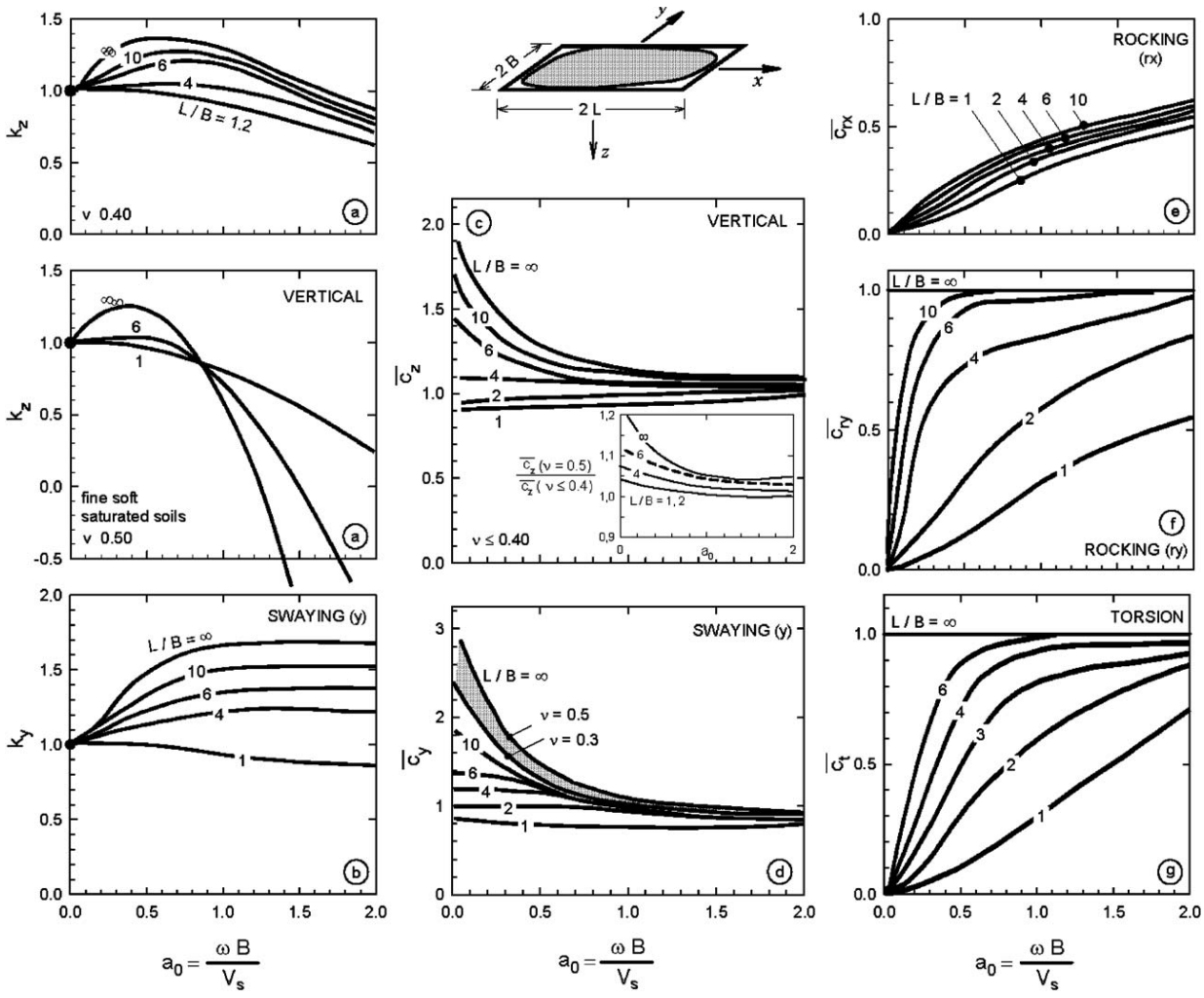

Figure 2.8: Graphs accompanying Table 2.2 (Mylonakis et al., 2006)

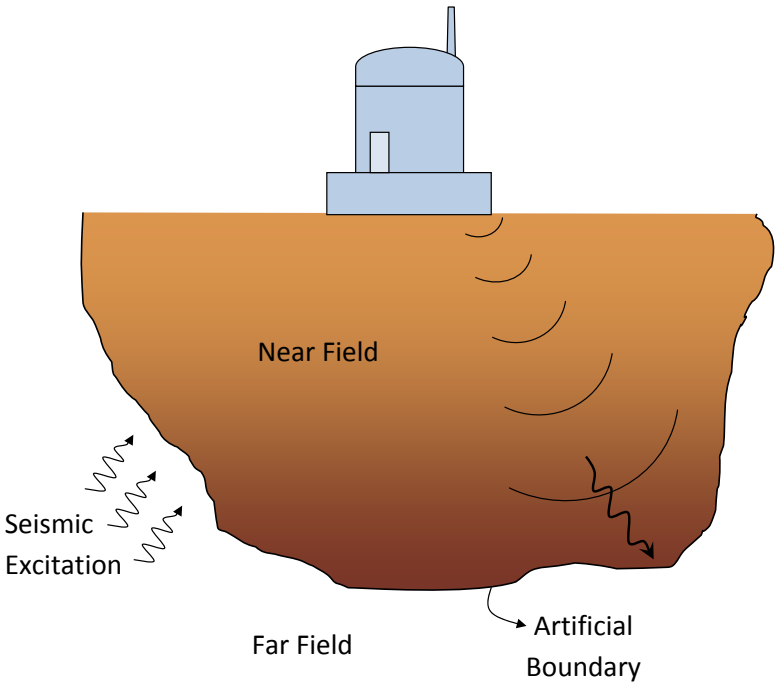

Figure 2.9: Modeling soil-structure system using FEM with applied artificial boundary

of the computational resources available, and its maximum value has to be chosen so that the peaks of the propagated wave can be captured without filtering out any relevant frequencies (Bathe and Wilson, 1976; Lysmer et al., 1974). Therefore, determination of the maximum value is based on the wavelength λ_w. Typically, ten nodes per shortest wavelength are required. Accordingly, Δs is given as

$$\Delta s \leq \frac{\lambda_{w,min}}{10} \tag{2.23}$$

where the shortest wavelength can be obtained based on the shear wave velocity c_s in the element and the highest frequency f_{max} of the applied load as

$$\lambda_{w,min} = \frac{c_s}{f_{max}} \tag{2.24}$$

Absorbing Lysmer boundaries

The modeling of domain boundaries representing the infinite soil media is essential in the analysis of dynamic soil-structure interaction. Such boundaries are needed in order to reduce

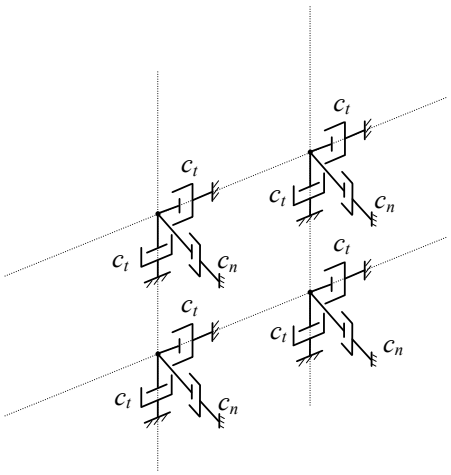

Figure 2.10: Dashpots connected to each degree of freedom of a boundary node representing absorbing boundaries

the computational resources and time required to perform the dynamic analysis.

Absorbing Lysmer boundaries (Lysmer and Kuhlemeyer, 1969), or the so-called viscous boundaries, consist of viscous dampers that are applied to all degrees of freedom of the boundary nodes of elastic soil media, as shown in Figure 2.10, in order to absorb outgoing waves from the soil-structure system. Lysmer and Kuhlemeyer (1969) expressed the boundary conditions as

$$\sigma = a\rho c_p \dot{u} \tag{2.25}$$

$$\tau = b\rho c_s \dot{v} \tag{2.26}$$

where σ and τ represent the normal stress and shear stress on the boundaries, respectively. a and b are dimensionless parameters, which are equal to one for plane waves impinging the artificial boundary at right angles. ρ is the mass of density, and c_p and c_s represent compressional wave velocity and shear wave velocity, respectively. $\dot{u}$ and $\dot{v}$ are the normal and tangential velocities, respectively.

Assuming that the waves impinge at a right angle on the artificial boundary and lumping the distributed dampers described by Eqs. 2.25 and 2.26 (Wolf, 1988), the coefficients of dampers

in each node in the two-dimensional case can be defined as

$$c_n = L\rho c_p \tag{2.27}$$

$$c_t = L\rho c_s \tag{2.28}$$

where c_n and c_t are the coefficients of dampers in longitudinal and tangential directions, respectively. L is the applicable length. In the three-dimensional case, L denotes the applicable area and Eq. 2.28 is applicable in the other tangential direction.

2.7 Numerical Application

In this section, structural response is investigated taking into account dynamic SSI effects by implementing the adopted models described in section 2.6. The first step is to derive the displacement response time histories for the different models. In Chapter 3, the energy response time histories are derived. With regard to the soil medium, its response is assumed to be damped linear elastic, whereas the structural response is inelastic as presented in subsection 2.7.2.

The structural response is investigated using a horizontal sinusoidal base acceleration with an amplitude of 2 m/s^2 and a period of 0.5 s (see Figure 2.11) applied to the nodes at the base of the two- and three-dimensional FE models. Accordingly, the base of the structure in both of the aforementioned models is subjected to an amplified excitation resulting from the upward one-dimensional propagating shear wave. In the simpler models, the soil model is replaced in the Wolf and Gazetas models with springs and dashpots representing the soil media. Therefore, the free-field motion should be computed. The motion shown in Figure 2.12 is produced by the propagation of the harmonic base excitation applied to the base of the two-dimensional FE soil model. Accordingly, the input motion applied at the base of the structure using the Wolf and Gazetas models was recorded in a prior free-field analysis of the two-dimensional FE soil model. Free-field acceleration time histories are also obtained by a vertically propagating plane wave due to the applied harmonic excitation using the program Cyclic 1D (Elgamal et al., 2010). These time histories are used for the verification of the free-field motion obtained from the FE soil models. Additionally, the structural response is also investigated without incorporating the

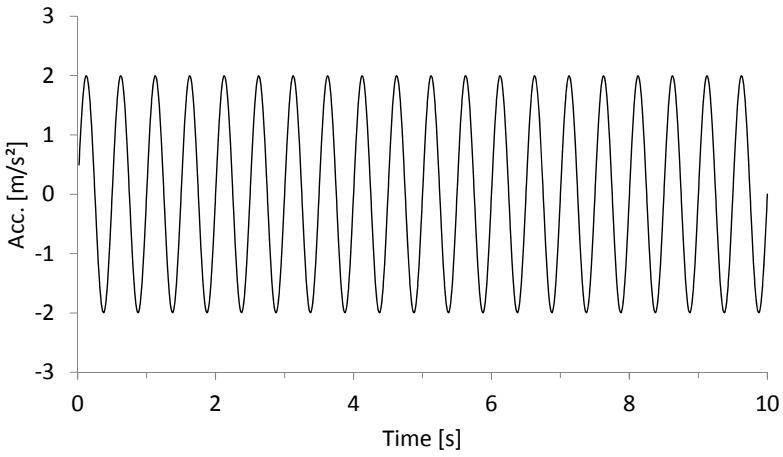

Figure 2.11: Harmonic ground excitation (f = 2Hz) applied to the nodes at the base of the two- and three-dimensional FE models

dynamic SSI effects. This is done by applying the free-field ground motion directly to the fixed base of the structure.

The foundation input motion is not computed for the simpler models. Consequently, kinematic interaction effects (subsection 2.3.2) are not taken into account when using the Wolf and Gazetas models. The ignored kinematic interaction is considered as a type of uncertainty in modeling. Accordingly, it is characterized as an attribute of model complexity, which is discussed in Chapter 4. However, it is not expected to have any significant kinematic interaction effects, which would influence the structure being studied since it is supported by a shallow foundation with relatively small dimensions.

2.7.1 Model descriptions

A step-by-step inelastic time history analysis using Hilber-Hughes-Taylor method is performed for an undamped single-degree-of-freedom (SDOF) system equivalent to a three-story moment resistant RC frame structure with a mass of $17.63t$ and a fundamental period equal to $0.5s$ for the fixed-base case, and subjected to the aforementioned harmonic base acceleration. The structure in this example has a displacement ductility ratio $\mu = 2$ and a strength ratio $\eta = 1.5$. Its surface foundation lies over a homogeneous damped elastic half-space and has a length $L_f = 6m$ and a width $B_f = 4m$ with a modulus of elasticity $E_f = 2.99 \times 10^{10}\ N/m^2$. The

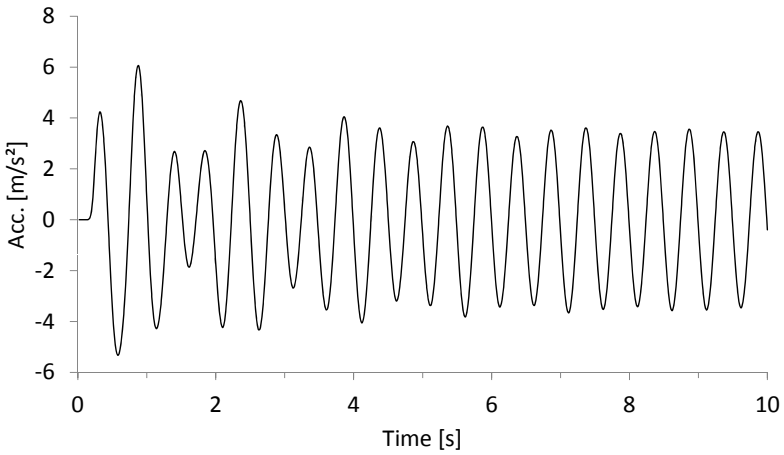

Figure 2.12: Amplified excitation produced by the propagation of the harmonic base excitation applied to the base of the two-dimensional FE soil model

foundation is assumed to be rigid in the analysis of the structure coupled to the Wolf and Gazetas models. In order to reduce the computational resources required to solve the dynamic soil-structure interaction problem, a two-dimensional FE model can be used as a simplification of the full three-dimensional model. The nodes in this model have vertical and one horizontal in-plane degrees of freedom. The out-of-plane degree of freedom is restricted. However, the two-dimensional FE model used in this work cannot be considered as a simplification of the three-dimensional model. It has a relatively large width in order to prevent the reflection of the propagating waves from the model's boundaries as explained in subsection 2.6.3. Consequently, no absorbing boundaries are applied to its boundary nodes. This allows the efficiency of the absorbing boundaries applied to the three-dimensional FE soil model to be proofed.

Table 2.4 illustrates the values used for the soil variables: Mass density ρ, Poisson's ratio ν, shear-wave velocity c_s, shear modulus G and soil damping ratio D. The geometry for the two- and three-dimensional FE models are shown in Figures 2.13 and 2.14, respectively. Each eight-node solid element is a cube with a length of one meter. For computational efficiency each of the 3D-FE soil model dimensions is limited to $20m$.

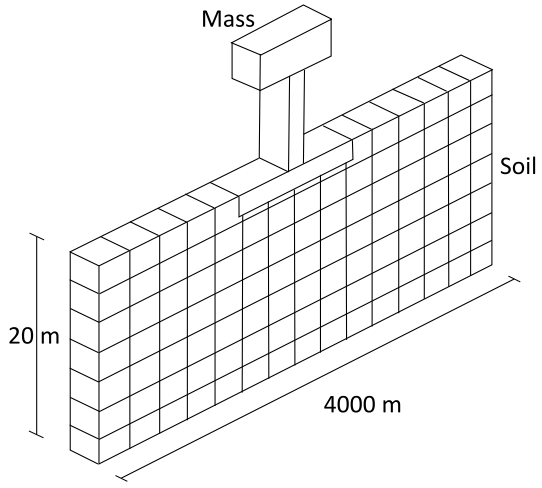

Figure 2.13: The two-dimensional finite element soil-structure interaction model

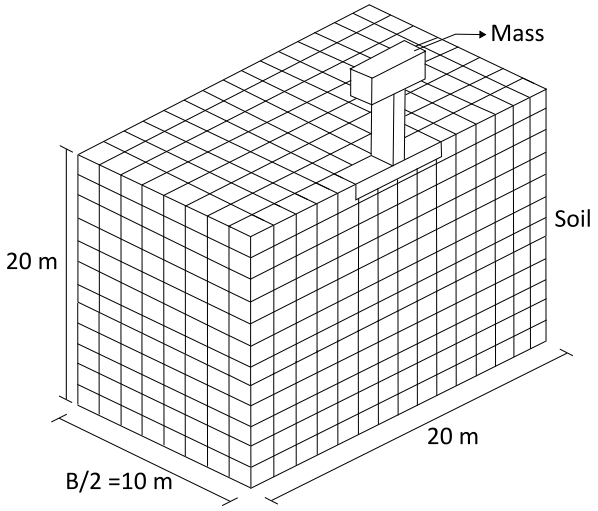

Figure 2.14: The three-dimensional finite element soil-structure interaction model

Table 2.4: Input parameters for soil variables

ρ [kg/m^3]	ν	c_s [m/s]	G [N/m^2]	D [%]
1800	0.2	100	18×10^6	5

2.7.2 Hysteretic rules

Many hysteretic models have been developed based on experimental results in order to describe the hereditary nature of the restoring force in inelastic systems under dynamic loading because this force cannot be defined as a function of the instantaneous displacement and velocity. In this subsection, the Takeda and Bouc-Wen hysteretic models are introduced. These hysteretic models are adopted for performing the inelastic time history analysis for the fixed-base structure, as well as for the structure coupled to different soil models.

The Takeda model (Takeda et al., 1970) is one of the most used models in the nonlinear analysis of reinforced concrete structures. It consists of sixteen rules for determining a trilinear primary curve as shown in Figure 2.15. These rules, which are based on many experimental data, govern the stiffness characteristics at unloading, reloading, cracking and yielding in successive cycles.

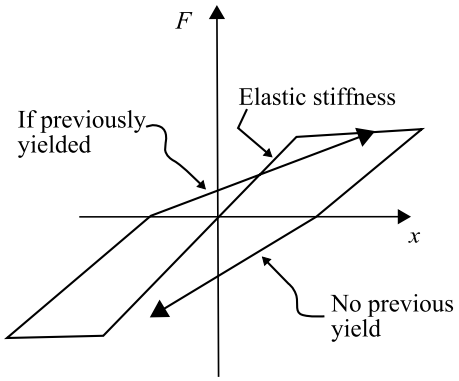

Figure 2.15: Takeda hysteretic model

The Bouc-Wen hysteretic model shown in Figure 2.16 was originally introduced by Bouc (1967) and later generalized by Wen (1976). This model is represented by a nonlinear differential equation, which indicates the restoring force completely without additional rules or conditions.

The Bouc-Wen model can be used to describe the hysteretic behavior of the restoring force of inelastic structures, as well as to express nonlinear isolation systems. The model can characterize a wide range of hardening or softening hysteresis by adjusting its parameters, which also determines the shape of the hysteretic cycle as smoothly varying or nearly bilinear.

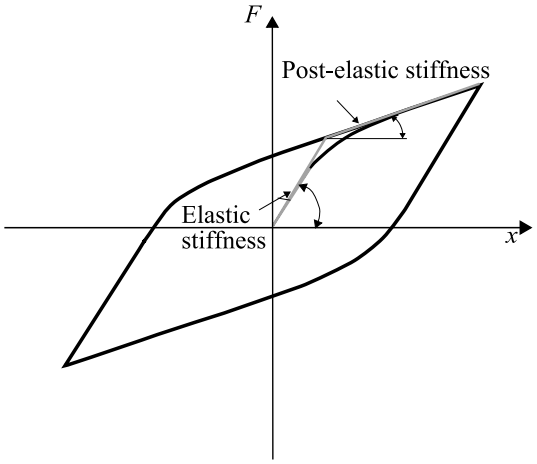

Figure 2.16: Hysteresis definition sketch of a single-degree-of-freedom Bouc-Wen model

2.7.3 Analysis results

The results of the modal analysis performed for each of the five models are illustrated in Table 2.5. The results show elongation expected in the natural period of the structure due to the flexibility of the supporting soil when it is coupled with different soil models in comparison to the response of the fixed-base structure.

Table 2.5: Natural periods of the structure coupled to the soil models

Model	Fixed-base	Wolf	Gazetas	2D FE	3D FE
Period [s]	0.5	0.622	0.588	0.8	0.765

The resulting relative displacement time histories at the top of the nonlinear fixed-base structure, as well as the coupled soil-structure models are recorded and plotted in Figure 2.17 for

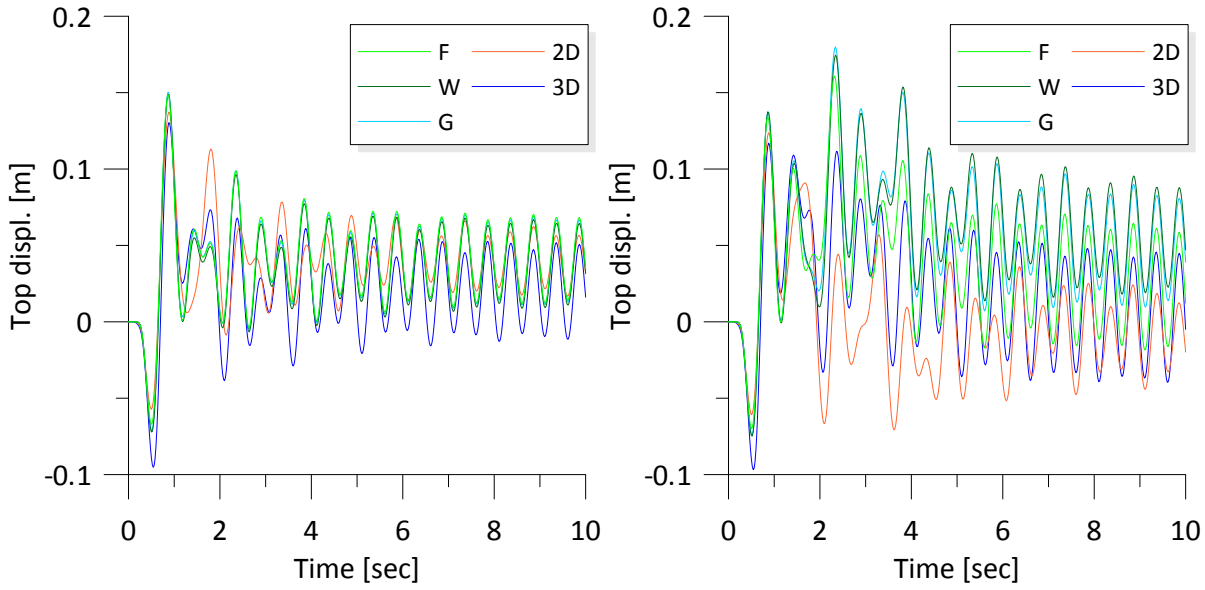

Figure 2.17: Relative displacement time histories for SSI models subjected to harmonic ground excitation (f = 2Hz) using: (a) Takeda hysteresis, (b) Bouc-Wen hysteresis

both the Takeda and Bouc-Wen hysteretic models. The time history responses resulting from the five models are demonstrated on the same plot to provide perspective. Similar behavior can be observed for both hysteretic rules at the beginning of the structural response. Once the structure reaches its inelastic stage, the hysteretic models are activated. Accordingly, the different maximum values of the displacement response are obtained. However, the fixed-base model, as well as the two simpler soil-structure interaction models produce higher values of displacement response compared to the more complex models. This can be explained by the resulting vibration periods presented in Table 2.5 since the excitation frequency is equal to the natural frequency of the fixed-base model and approaches the natural periods of the simpler models.

2.8 Summary

In this chapter, dynamic SSI effects are investigated using models with different abstraction levels. A comparison of the resulting structural periods of vibration in addition to the displace-

ment response time histories constructed for the coupled models to the results obtained from the fixed-base structure confirms the important role of dynamic SSI. The different periods of vibration obtained for the models investigated imply that the coupled systems can experience resonance due to the different ranges of excitation frequency. Modification in the displacement responses seems to be minimal when using the simpler SSI models compared to the fixed-base structure. This is especially true when following the rules of the Takeda hysteretic model. Changes in the structural response become more significant when more complex models are used. However, the results obtained do not provide any information about the quality of the models investigated. The excitations of different frequencies can lead to completely different displacement responses. Decisions regarding SSI models that lead to more conservative design models cannot be made independently from the exciton frequency. Hence, a reliable response indicator is needed in order to assess the quality of the different SSI models independently from the particular ground motion and hysteretic rules used. This will be discussed in the following chapters.

Chapter 3

ENERGY AND DAMAGE MEASURES RELATING TO STRUCTURAL RESPONSE

3.1 Introduction

Energy-based seismic design methodology was originally developed by Housner (Housner, 1956). Later on, energy concepts became widely accepted as an alternative principle to conventional seismic design strategies (Zahrah and Hall, 1984; Akiyama, 1985; Park and Ang, 1985). The energy approach is based on a clear concept. It provides valuable insight into the behavior of a structure during an earthquake through the use of constructed response time histories. This approach implies that a structure can dissipate a certain amount of energy through inelastic deformations, which allows the energy demand during an earthquake to be determined. Accordingly, a structure will sustain damage if the energy demand is larger than the energy dissipation capacity of the structure.

In this chapter, the dynamic soil-structure interaction models described and implemented in Chapter 2 will be investigated further by using energy measures as an indicator of structural response. The two available energy approaches are described and compared in section 3.3.

As a preliminary application, in section 3.4, the energies of elastic structural response are computed analytically without incorporating dynamic SSI effects. Subsequently, in section 3.5 the investigation is extended to the inelastic response of a fixed-base structure, as well as a coupled soil-structure system with numerical application. The energy response resulting from the different models implemented will be used in assessing the quality of these models in Chapter 4.

3.2 Previous Studies

The pioneering work of Housner (1956) initiated using the energy approach in seismic design for energy-based studies using energy approach in seismic design. Housner showed that energy is transmitted from ground motion to structures in different terms by using an accelerogram of the El Centro 1940 earthquake for the design of a water tank. He pointed out that a portion of this transmitted energy is absorbed within a structure in terms of recoverable elastic strain energy and irrecoverable hysteretic energy when it undergoes a nonlinear inelastic response. A portion of the energy exciting the structure will be in the form of kinetic energy, whereas the rest of the energy dissipates in terms of damping energy. Housner introduced the input energy E_i per unit mass for the elastic and inelastic structural response as

$$\frac{E_i}{m} = \frac{1}{2}(PSV)^2 \tag{3.1}$$

where m is a structure's mass and PSV denotes the pseudospectral velocity.

In the absence of artificial damping devices, hysteresis energy is an important indicator of the damage sustained by a structure since damage is very much related to the energy demand and energy capacity of that structure. Accordingly, the elastic structural response is associated with zero hysteretic energy. McKevitt et al. (1980) computed hysteretic energy, input energy and the ratio of hysteretic energy to the input energy for structures with different properties using the accelerograms of four earthquakes. They pointed out that hysteretic energy can be predicted by the viscous damping ratio, period, hysteretic model and yield strength ratio. They also inferred that the energy dissipated by MDOF systems can be estimated using equivalent

SDOF systems.

Zahrah and Hall (1984) inferred that structural damage, as represented by the maximum deformation and the number of yield excursions, is related to the amount of energy passed to structure. They calculated the input energy per unit mass as

$$\frac{E_i}{m} = \int \ddot{u}_g \dot{u} dt \tag{3.2}$$

where $\ddot{u}_g$ is the ground acceleration and $\dot{u}$ is the relative velocity of the structure with respect to the ground.

The number of yield excursions is one of the important factors affecting the amount of damage that structures may suffer during an excitation. It refers to the number of times that a structure undergoes a yield phase. However, the number of yield excursions does not account for the amount of energy dissipated by the yielding in a structure. Zahrah and Hall (1984) proposed an equivalent number of yield excursions as an index of the severity of ground shaking, which is expressed as

$$N_{eq} = \frac{E_h}{A} \; ; \quad A = \omega^2 u_y^2 (\mu - 1) \tag{3.3}$$

where E_h is the total hysteretic energy; A is the area under the resistance-displacement curve for the structure when it is loaded monotonically until it reaches the same maximum displacement that it experiences during the excitation; and ω, u_y and $\mu > 0$ are the cyclic frequency, yield displacement and displacement ductility of the structure, respectively. Zahrah and Hall (1984) proposed N_{eq} as a useful index to assess the damage potential of a ground excitation since the amount of hysteretic energy that a structure dissipates during an earthquake excitation reflects the severity of the ground motion.

Akiyama (1985) computed the input energy per unit mass for elastic structures as

$$\frac{E_i}{m} = \frac{1}{2} (V_e)^2 \tag{3.4}$$

where V_e is an equivalent velocity, which is calculated as

$$V_e = 2.5 T_n \quad \text{for} \quad T_n \leq T_g; \qquad V_e = 2.5 T_g \quad \text{for} \quad T_n \geq T_g \tag{3.5}$$

where T_n is the period of the structure and T_g is the predominant period of the ground motion assigned for the different types of soil.

Based on a combination of dissipated hysteretic energy and maximum deformation response, Park and Ang (1985) proposed a damage index expressed as

$$D_{PA} = \frac{u_{max}}{u_{mon}} + \beta_d \frac{E_h}{r_y u_{mon}} \tag{3.6}$$

where u_{max} is the maximum deformation, u_{mon} is the ultimate deformation capacity of the structure under a monotonically increasing lateral deformation, $\beta_d \geq 0$ is a parameter based on the structural characteristics, E_h is the hysteretic energy and r_y is the yield strength. By substituting the displacement ductility $\mu = u_{max}/u_y$ and the monotonic ductility capacity $\mu_{mon} = u_{mon}/u_y$ in Eq. 3.6, the damage index can be rewritten as

$$DI_{PA} = \frac{\mu}{\mu_{mon}} + \beta_d \frac{E_h}{r_y u_y \mu_{mon}} \tag{3.7}$$

where u_y is the yield deformation. DI_{PA} has been comprehensively used in the literature for different applications due to its simplicity and extensive calibration against a great deal of the damage data on earthquakes.. Cosenza et al. (1993) found a good correlation between DI_{PA} and other damage indices proposed by Banon and Veneziano (1982) and Krawinkler and Zohrei (1983) for a value of β_d based on experimental results and equal to 0.15, whereas Kunnath et al. (1990) evaluated the damage sustained by structures under cyclic loads and found that DI_{PA} correlates well with the observed damage.

Uang and Bertero (1990) introduced two methods for computing the energy terms imparted to a structure based on absolute and relative formulations of the energy equation. Both methods are derived from the same equation of dynamic equilibrium for an SDOF system. However, the resulting energy terms have different physical interpretations. They defined the absolute input energy per unit mass as

$$\frac{E_i^a}{m} = \int (\ddot{u}_t) du_g \tag{3.8}$$

whereas the relative input energy per unit mass is computed as

$$\frac{E_i}{m} = -\int \ddot{u}_g du \tag{3.9}$$

where u is the relative displacement of the mass, $u_t = u_g + u$ is the total displacement of the mass and u_g is the ground displacement. Based on the physical interpretation of Eqs. 3.8 and 3.9, Uang and Bertero (1990) deduced that the absolute energy, rather than the relative energy approach, correctly represents the physics of this concern.

Chai et al. (1995) proposed a modified damage index for DI_{PA} in Eq. 3.6 as

$$D_{PA}^{C} = \frac{u_{max}}{u_{mon}} + \beta_c \frac{E_h - E_{h(mon)}}{r_y u_{mon}} \tag{3.10}$$

where β_c is related to β_d in Eq. 3.6 as

$$\beta_c = \frac{\mu_{mon}\beta_d}{\mu_{mon} + (1 - \mu_{mon})\,\beta_d} \tag{3.11}$$

and $E_{h(mon)}$ is the hysteretic energy dissipated by the system under monotonically increasing deformation. They showed that by using their proposed parameter β_c the results come very close to those obtained by using small values for β_d.

Bruneau and Wang (1996) constructed energy response time histories for rectangular and harmonic base excitations based on closed form energy expressions for an SDOF system. They inferred that the relative energy concept is more closely related to parameters of engineering interest.

Rahnama and Manuel (1996) computed input energy, hysteretic energy, and the ratio of the hysteretic energy to input energy for SDOF systems with periods ranging from 0.1 to 4.0 seconds using strong motion duration values of 5, 10, 15 and 20 seconds. They concluded that the excitation's duration does not influence the ratio of hysteretic energy to input energy, although the increasing durations lead to increased input and hysteretic energies. Moreover, they found that the ratio of hysteretic energy to input energy is a very stable demand parameter since it did not show a dependency on the duration of strong motion.

Based on the inelastic responses of systems to five sets of ground motion recorded at rock sites in California, Goel (1997) deduced that the input energy was approximately the same regardless of whether the system plan was symmetric or asymmetric, whereas the hysteretic energy dissipated by an asymmetric plan system is slightly smaller in comparison to a corresponding symmetric plan system.

Manfredi (2001) proposed a method for obtaining the hysteretic and input energies based on the evaluation of an equivalent number of cycles correlated to the characteristics of an earthquake using the seismic index I_D, which he defined as

$$I_D = \frac{I_E}{\text{PGA} \cdot \text{PGV}} \tag{3.12}$$

where PGA and PGV are the peak ground acceleration and the peak ground velocity, respectively and I_E is given as

$$I_E = \int_0^{t_E} \ddot{u}_g^2 dt \tag{3.13}$$

where $\ddot{u}_g$ is the ground acceleration and t_E is the duration of an earthquake.

Finally, Khashaee et al. (2003) investigated the maximum ratio of hysteretic energy to input energy $(E_h/E_i)_m$, the ratio of the maximum hysteretic energy to the maximum input energy E_h/E_i, and the equivalent number of yield excursions N_{eq} for a set of twenty acceleration ground excitation records. They showed that the $(E_h/E_i)_m$ ratio reflects the damage potential associated with the largest yield excursion and the E_h/E_i and N_{eq} ratios reflect the damage potential associated with the total number of yield excursions and the cumulative inelastic deformation for the entire duration of the excitation. Khashaee (2004) proposed a damage index of between zero and one based on the ductility and ultimate ductility of the structure. He showed that the E_h/E_i ratio has a good correlation with his proposed damage index for 7-, 13-, and 20-story uniform buildings subjected to 160 accelerograms.

3.3 Energy Formulations

This section describes the different energy terms and their formulations as proposed by Uang and Bertero (1990). Consider the SDOF system in Figure 3.1. The response of the damped system subjected to a horizontal ground motion can be expressed by the following equation of motion

$$m\ddot{u}_t + c\dot{u} + r = 0 \tag{3.14}$$

where m is the system's mass, u is the relative displacement of the mass with respect to the ground, $u_t = u_g + u$ is the total displacement of the mass, u_g is the ground displacement, c is the viscous damping coefficient and r is the restoring force. Linear elastic systems are expressed as $r = ku$, where k represents the system's stiffness. The viscous damping coefficient c is assumed to be constant as is usually done in the nonlinear dynamic analysis of structures. Using the decomposition of the total displacement u_t of the system, Eq. 3.14 can be rewritten as

$$m\ddot{u} + c\dot{u} + r = -m\ddot{u}_g \tag{3.15}$$

3.3.1 Absolute energy approach

Uang and Bertero (1990) explained that, based on Eqs. 3.14 and 3.15, both systems in Figure 3.1 are considered to be equivalent. Accordingly, they distinguished between absolute and relative energy in a structure. The integration of Eq. 3.14 with respect to u gives

$$\int m\ddot{u}_t du + \int c\dot{u} du + \int r du = 0 \tag{3.16}$$

Considering that $u_t = u_g + u$, the first term of Eq. 3.16 can be rewritten as

$$\begin{aligned} \int m\ddot{u}_t du &= \int m\ddot{u}_t (du_t - du_g) \\ &= \int m\frac{d\dot{u}_t}{dt} du_t - \int m\ddot{u}_t du_g \\ &= \frac{m(\dot{u}_t)^2}{2} - \int m\ddot{u}_t du_g \end{aligned} \tag{3.17}$$

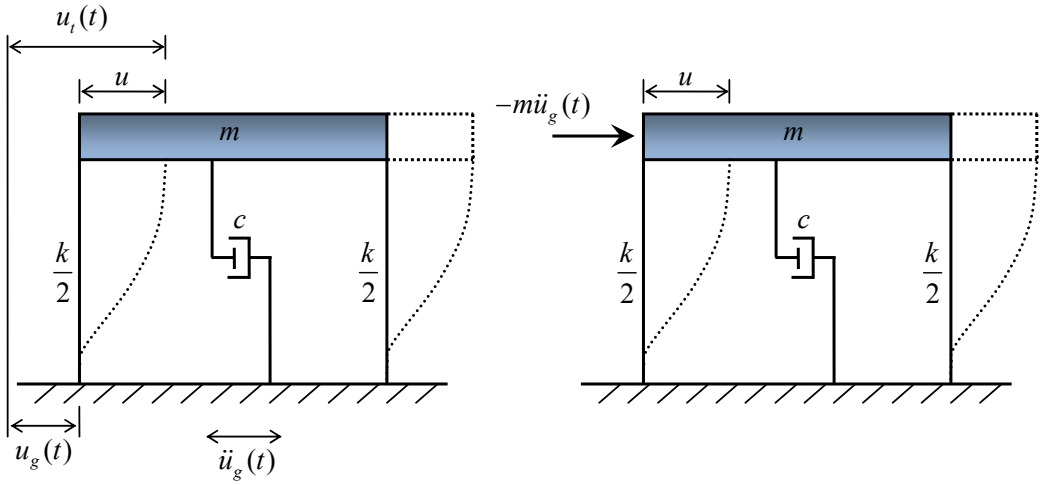

(a) (b)

Figure 3.1: Single degree-of-freedom system subjected to seismic ground motion: (a) Absolute response, (b) Relative response

Eq. 3.16 then becomes

$$\frac{m(\dot{u}_t)^2}{2} + \int c\dot{u}du + \int rdu = \int m\ddot{u}_t du_g \tag{3.18}$$

The absolute energy equation can be summarized as

$$E_k^a + E_d + E_a = E_i^a \tag{3.19}$$

where E_k^a refers to the *absolute* kinetic energy since the absolute velocity $\dot{u}_t$ is used for deriving it and is equal to

$$E_k^a = \frac{m(\dot{u}_t)^2}{2} \tag{3.20}$$

The second term in Eq. 3.19 refers to the energy dissipated by viscous damping (or damping energy) up to time t and equal to

$$E_d = \int c\dot{u}du = \int c\dot{u}^2 dt \tag{3.21}$$

and the third term in Eq. 3.19 is the absorbed energy, which is composed of the recoverable elastic strain energy E_s and the irrecoverable hysteretic energy E_h. Thus

$$E_a = E_s + E_h = \int r du \tag{3.22}$$

E_s is computed from

$$E_s = \frac{r^2}{2k} \tag{3.23}$$

and E_h is released once the system undergoes a nonlinear inelastic response. It is computed as the sum of the areas delimited by each loop drawn by the line of a force displacement relationship. The term on the right in Eq. 3.19 is defined as the *absolute* input energy

$$E_i^a = \int (m\ddot{u}_t) du_g \tag{3.24}$$

The definition as an *absolute* input energy is based on the use of the total acceleration $\ddot{u}_t$ in the calculation of the inertia force $m\ddot{u}_t$ applied to the structure. This force is equal to the restoring force r plus the damping force $c\dot{u}$ and represents the total force applied to the structure's foundation. Therefore E_i^a represents the work done by the total base shear $m\ddot{u}_t$ at the foundation on the foundation's displacement u_g.

3.3.2 Relative energy approach

Integrating Eq. 3.15 with respect to u gives

$$\int m\ddot{u} du + \int c\dot{u} du + \int r du = -\int m\ddot{u}_g du \tag{3.25}$$

In comparison to Eq. 3.18, the second term and the third term in Eq. 3.25, which refer to E_d and E_a, do stay the same. The relative energy equation can be summarized as

$$E_k + E_d + E_a = E_i \tag{3.26}$$

The first term in Eq. 3.26 refers to the *relative* kinetic energy since the relative structural velocity $\dot{u}$ is used in calculating it. E_k can be rewritten as

$$E_k = \int m\ddot{u}du = \int m\frac{d\dot{u}}{dt}du = \int md\dot{u}(\dot{u}) = \frac{m(\dot{u})^2}{2} \tag{3.27}$$

The term on the right in Eq. 3.26 is defined as the *relative* input energy

$$E_i = -\int m\ddot{u}_g du \tag{3.28}$$

which represents the work done by the equivalent static lateral force ($-m\ddot{u}_g$) on the fixed base system shown in Figure 3.1 (b). The full derivation of the energy formulations in this section are given in Uang and Bertero (1988).

3.3.3 Comparison of energy approaches

Energy approaches are based on the principle of energy balance as shown in Eqs. 3.19 and 3.26. In both of the absolute and the relative energy approaches, the sum of kinetic, damping and absorbed energies is always equal to the input energy. Damping and absorbed energy terms are uniquely defined, regardless of the energy approach used. The difference is in the input and kinetic energies. We take advantage of this balance principle in order to validate the numerical calculations in sections 3.4, 3.5.

Uang and Bertero (1988) deduced, based on the physical interpretation of the equations above, that the absolute energy approach rather than the relative energy approach correctly represents the physics of this subject matter. However, Bruneau and Wang (1996) pointed out that this inference has practical shortcomings, particularly regarding the definition of input and kinetic energies. They also noted that there are no crucial differences between both energy approaches since hysteretic energy, which reflects the cumulative inelastic cyclic response, is the most appropriate energy term in quantifying the structural capacity to dissipate energy during earthquakes. Based on this point of view, the relative energy approach will be followed in this work.

3.4 Energies of Elastic Structural Response

In this section, energy measures are introduced as a general indicator of elastic structural response, which will be adopted for investigating the SSI effects in section 3.5. The specific example used for this purpose is the Millikan library building located at the California Institute of Technology in Los Angeles (Bradford et al., 2004), which is modeled as a distributed parameter system that strikes a balance between the MDOF and FE models (Crocker, 2007). Kinetic and potential energies are derived for this structure without the presence of SSI effects at this stage, which show a marked dependence on the type of input (i.e., seismic motion), harmonic base excitation and wavelet pulses (Nasser and Manolis, 2011).

The distributed parameter model adopted to represent the Millikan library building assumes that the building behaves as a flexural beam (Chopra, 2007). Although dispersion effects due to abrupt changes in the structural configuration with regard to height are not considered here, these may be modeled by assuming a smooth variation of the structural stiffness and mass as functions of height (Graff, 1973). The solution of the equation governing the transverse vibration is then used for deriving the potential and kinetic energies for this linear elastic system, which serve as a measure for gauging its structural response.

3.4.1 The eigenvalue problem

Figure 3.2 depicts external forces acting on a cantilever beam of length L with flexural rigidity $EI(x)$ and mass $m(x)$. For free vibrations, the equation of motion can be written as

$$\left[EI\left(x\right)u''\right]'' + m\left(x\right)\ddot{u} = 0 \tag{3.29}$$

where the transverse displacement u is written in terms of the eigenvalues ϕ and the generalized coordinates q in the form $u(x,t) = \phi_n(x)q_n(t)$. It should be noted that repeated indices imply summation over the total number of modes $n = 1, 2,...$ deemed necessary for accurate results (usually a few modes, e.g., four are sufficient). Substituting in Eq. 3.29 and employing

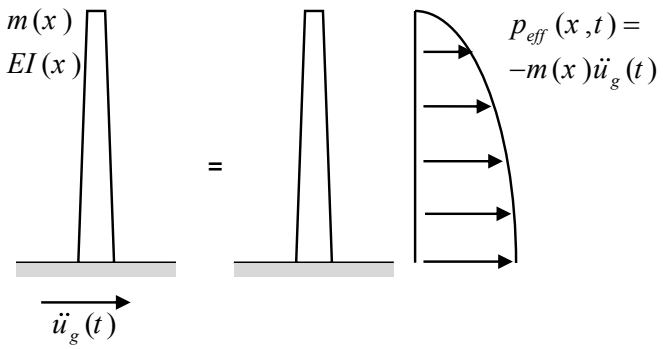

Figure 3.2: The cantilever beam with distributed mass

separation of variables yields

$$-\ddot{q}(t)/q(t) = \left[EI(x)\phi''(x)\right]''/\left[m(x)\phi(x)\right] \tag{3.30}$$

The subscript n is omitted for convenience and primes indicate the derivatives with respect to the x coordinate. If each side of the above equation is equal to a constant, i.e., the frequency ω^2, then we get two ordinary differential equations as

$$\ddot{q}(t) + \omega^2 q(t) = 0 \tag{3.31}$$

$$\left[EI(x)\phi''(x)\right]'' - \omega^2 m(x)\phi(x) = 0 \tag{3.32}$$

Eq. 3.31 indicates a harmonic vibration environment, while Eq. 3.32 is the augmented beam equation for dynamics. Assuming a uniform beam with a constant mass m and stiffness EI gives a homogeneous equation for the eigenvalue problem as

$$\phi^{IV}(x) - \beta^4\phi(x) = 0; \qquad \beta^4 = \omega^2 m/EI \tag{3.33}$$

which has the general solution

$$\phi(x) = C_1\sin\beta x + C_2\cos\beta x + C_3\sinh\beta x + C_4\cosh\beta x \tag{3.34}$$

The constants C_1 to C_4 are evaluated from the boundary conditions for a cantilever beam

$$u(0) = u'(0) = M(L) = Q(L) = 0 \tag{3.35}$$

where M and Q are the bending moment and shear force, respectively. A non-trivial solution yields the following transcendental equation

$$1 + \cos\beta L \cosh\beta L = 0 \tag{3.36}$$

The first four natural frequencies and their corresponding modal shapes (where $C = 1$) are

$$\omega_n = \left(\alpha_n / L^2\right)\sqrt{EI/m}; \quad \alpha_1 = 3.516; \quad \alpha_2 = 22.03; \quad \alpha_3 = 61.7; \quad \alpha_4 = 120.9 \tag{3.37}$$

$$\phi_n(x) = C\left[\cosh\beta_n x - \cos\beta_n x - \frac{\cosh\beta_n L + \cos\beta_n L}{\sinh\beta_n L + \sin\beta_n L}\left(\sinh\beta_n x - \sin\beta_n x\right)\right] \tag{3.38}$$

3.4.2 Modal analysis for forced dynamic response

In the presence of an external distributed force $p(x,t)$, the modal equations are integrated along the beam's length to produce the following governing equation for the forced undamped response

$$M_n \ddot{q_n}(t) + K_n q_n(t) = P_n(t) \tag{3.39}$$

The generalized mass, stiffness and loading parameters, respectively, are given below as

$$\begin{aligned} M_n = \int_0^L m(x)\left[\phi_n(x)\right]^2 dx; \quad K_n = \int_0^L \phi_n(x)\left[EI(x)\,\phi_n''(x)\right]'' dx, \\ P_n(t) = \int_0^L p(x,t)\,\phi_n(x)\,dx \end{aligned} \tag{3.40}$$

and the usual relation $K_n = \omega_n^2 M_n$ holds true for all modes $n = 1, 2, ...$ Also, it is possible to produce a symmetric integrand for the generalized stiffness expression given above by use of Leibnitz's rule of differentiation and the homogeneous boundary conditions given in Eq. 3.35.

In the case of a horizontal ground motion $\ddot{u}_g(t)$ applied at the base, the effective forces are

$$P_n(t) = -m\ddot{u}_g(t) \int_0^L \phi_n(x)\, dx \tag{3.41}$$

It is now possible to use Duhamel's integral as a closed-form solution of the equation of motion for the generalized coordinates as

$$q_n(t) = (1/M_n\omega_n) \int_o^t P(\tau) \sin[\omega_n(t-\tau)]\, d\tau \tag{3.42}$$

Finally, the total transverse beam displacement is obtained through modal superposition as

$$u(x,t) = \sum_{n=1}^{\infty} u_n(x,t) = \sum_{n=1}^{\infty} \phi_n(x)\, q_n(t) \tag{3.43}$$

3.4.3 Energy measures

Kinetic energy E_k and strain (or potential) energy E_s are defined as a modal sum for the distributed parameter system at any given time instance t as

$$E_k = \sum_{n=1}^{\infty} E_{k,n}, \quad E_{k,n} = \frac{1}{2} m \dot{q}_n^2(t) \int_0^L \phi_n^2(x)\, dx \tag{3.44}$$

$$E_s = \sum_{n=1}^{\infty} E_{s,n}, \quad E_{s,n} = \frac{1}{2} EI q_n^2(t) \int_0^L \left[\phi_n''(x)\right]^2 dx \tag{3.45}$$

The strain energy is equivalent to the elastic energy stored during the deformation process of the swinging structure. For free vibrations, the sum of these two energies at any time instant is constant. Otherwise, in the presence of external forces and damping effects, the work of the forces plus the dissipated energy must also be taken into account.

3.4.4 Numerical results

The Millikan Library (Figure 3.3) is a nine-story reinforced concrete building, which is $21m$ x $23m$ in plan and approximately $44m$ high. In addition to the moment frames in both the E-W

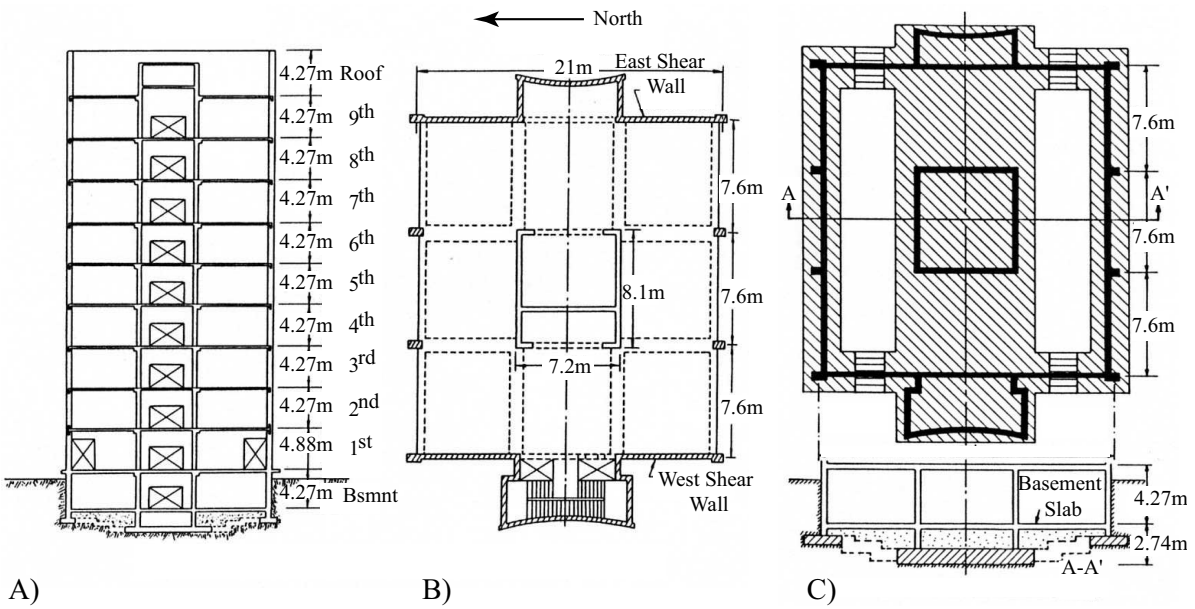

Figure 3.3: The Millikan Library (Favela, 2004): A) North-South cross section, B) Floor plan, C) Plan view and cross section of the foundation

and N-S directions, the Millikan Library also has shear walls that provide additional stiffness to the building as shown in the plan view in Figure 3.3 (B). More detailed information about the Millikan Library can be found in Foutch (1976), Luco et al. (1986) and Favela (2004).

The fundamental structural period of the building was computed using the free vibration methodology outlined above as $T_1 = 1.26s$ for the averaged material properties as shown in Figure 3.4. This was compared to a measured value of the fundamental period of the structure during the 1987 Whittier-Narrows earthquake, which was $1.07s$ in the E-W direction (Favela, 2004). Subsequently, a modal analysis using four vibration modes was performed for the forced dynamic response of this structure by introducing three basic types of base motion, namely a recorded earthquake signal, harmonic vibrations and pulse type wavelets. Simpson's rule was used to evaluate the Duhamel integral in Eq. 3.42. More specifically, the first excitation used is an acceleration time history record of a real earthquake applied at the base. The record for the 1987 Whittier-Narrows earthquake was introduced for this purpose (see Figure 3.5), which was an event whose epicenter was estimated at about $10km$ southeast of the Millikan library site. Figure 3.6 is a plot of both kinetic and potential energies that develop in the structure. It shows

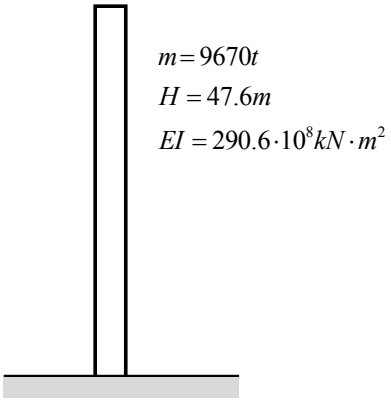

Figure 3.4: Mechanical model of the Millikan Library

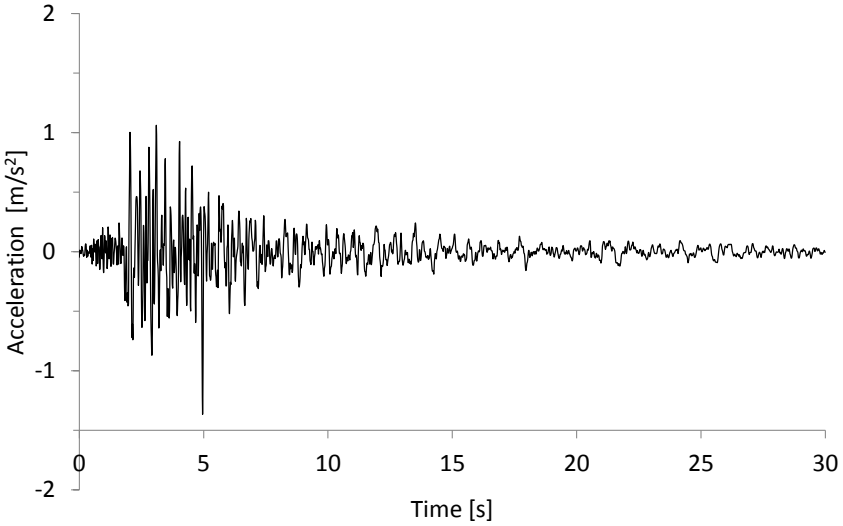

Figure 3.5: Acceleration time history of the 1987 Whittier-Narrows earthquake ($a_{max} = 1.37m/s^2$)

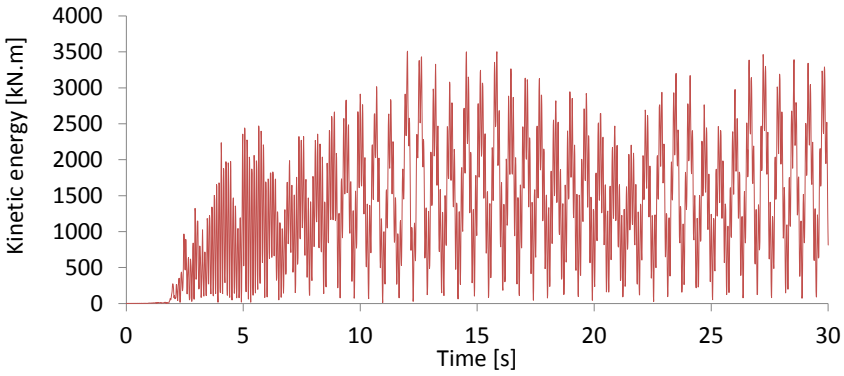

(a)

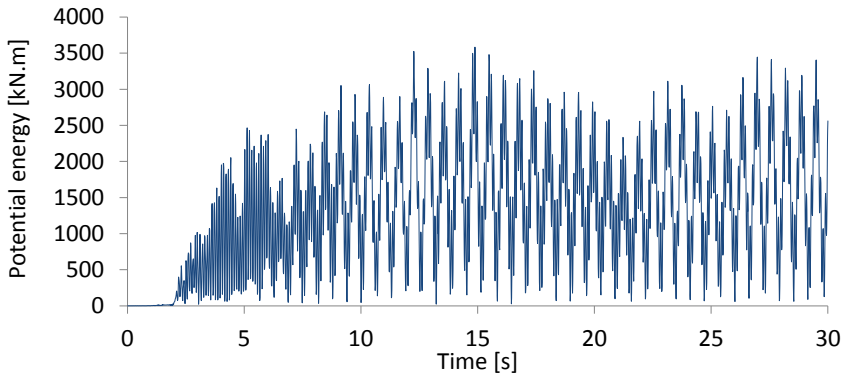

(b)

Figure 3.6: Variation of (a) kinetic and (b) potential energies in the Millikan library subjected to the 1987 Whittier-Narrows earthquake

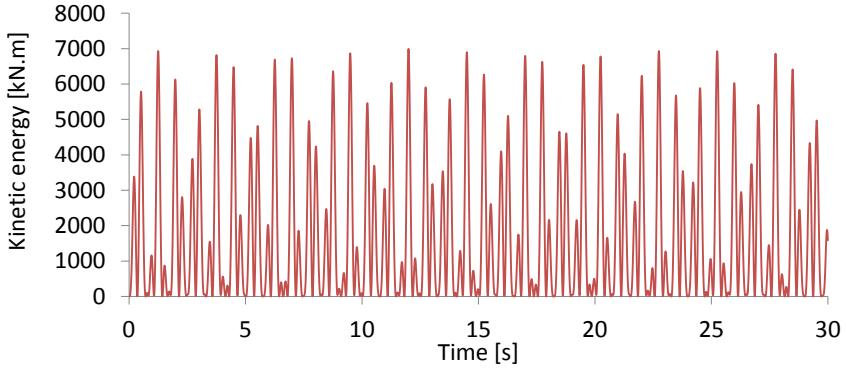

(a)

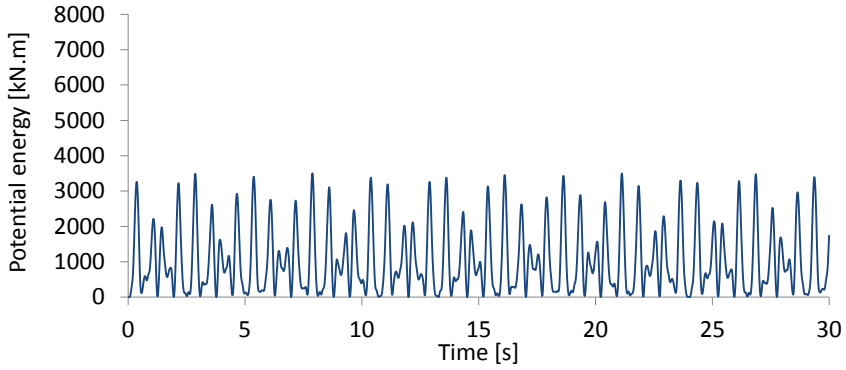

(b)

Figure 3.7: Variation of (a) kinetic and (b) potential energies in the Millikan library subjected to a harmonic base acceleration with an amplitude $1.37 m/s^2$ and a frequency of $2.0 Hz$

that the maximum kinetic energy occurs at $t = 12.02s$ and is equal to $E_k = 3509.02 kN \cdot m$. Also, the energy signal does not dampen away with time because of the absence of dissipation effects.

Next, the Millikan library's structural response was studied for an arbitrarily selected harmonic (sinusoidal) base acceleration with an amplitude of $1.37 m/s^2$ and a frequency of $2.0 Hz$.

The resulting kinetic and potential energies are plotted in Figure 3.7, which show a certain similarity with the 1987 Whittier-Narrows signal in that it also contains some nearly harmonic components over its duration that eventually fade away. It can be noticed that the maximum amplitude of the harmonic vibration is the same as that of the Whittier-Narrows 1987 earthquake for comparison purposes.

Finally, the third type of excitation is a group of fourteen Ricker wavelet pulses (Ryan, 1994), with four frequencies of $0.2, 0.4, 0.6$ and $0.8Hz$ and the remaining ten frequencies ranging from 1.0 to $10.0Hz$. The used excitation pulses are illustrated in Figures 3.8 to 3.11. Again, the wavelet amplitude in all cases is equal to $a_{max} = 1.37m/s^2$. This type of excitation allows a more careful study of the relation between the input signal frequency and the structural energy measures. Specifically, Figure 3.12 illustrates the time history energy response of structural systems to a pulse of $1.0Hz$, whereas Figure 3.13 shows the changes in the maximum energies when the structure is excited by a range of frequencies. The drop in the kinetic and potential energies can be observed as the frequency of the wavelets moves away from the dominant natural period of the Millikan library.

The interplay between the eigenproperties of the structure and the frequency content of the external signal is readily noticed in the time history plots, which is also confirmed in the frequency plots.

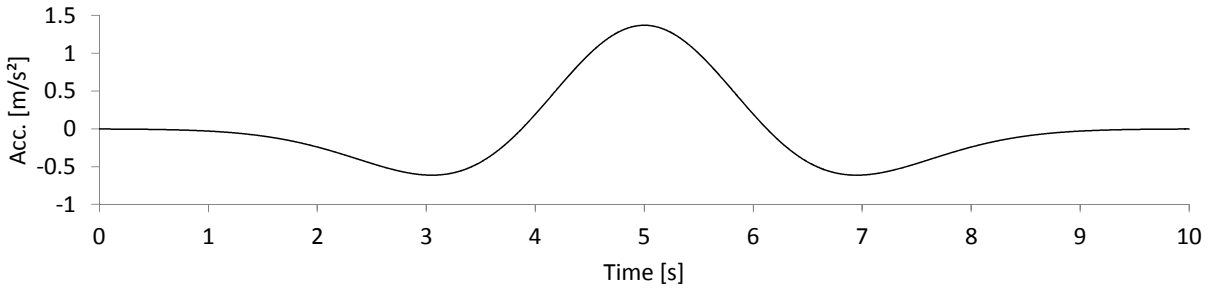

(a)

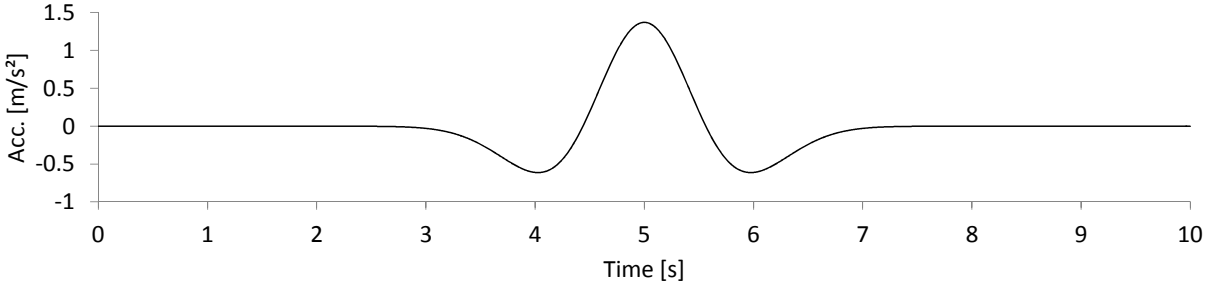

(b)

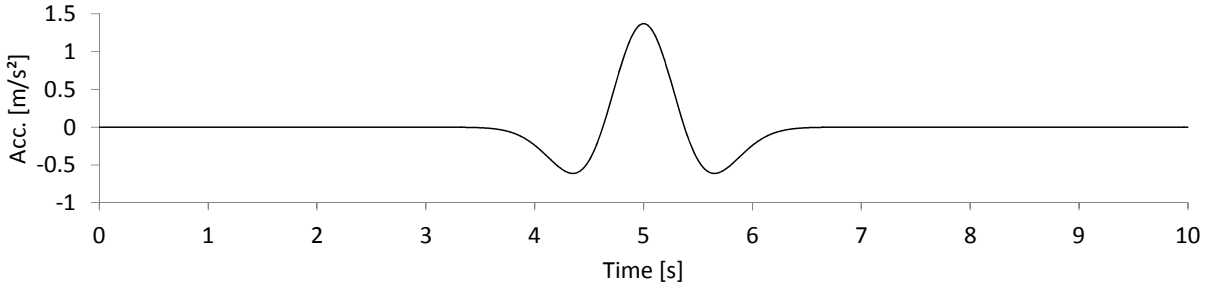

(c)

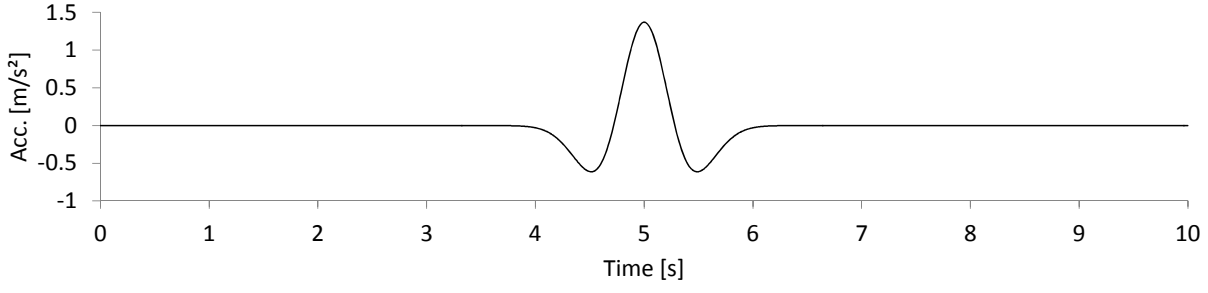

(d)

Figure 3.8: Ricker wavelet pulses with the amplitude $1.37m/s^2$ and the frequencies. (a) $f = 0.2Hz$, (b) $f = 0.4Hz$, (c) $f = 0.6Hz$, (d) $f = 0.8Hz$

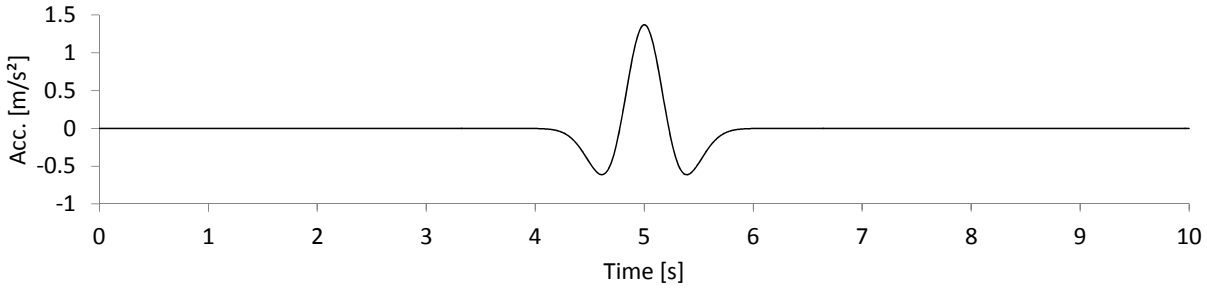

(a)

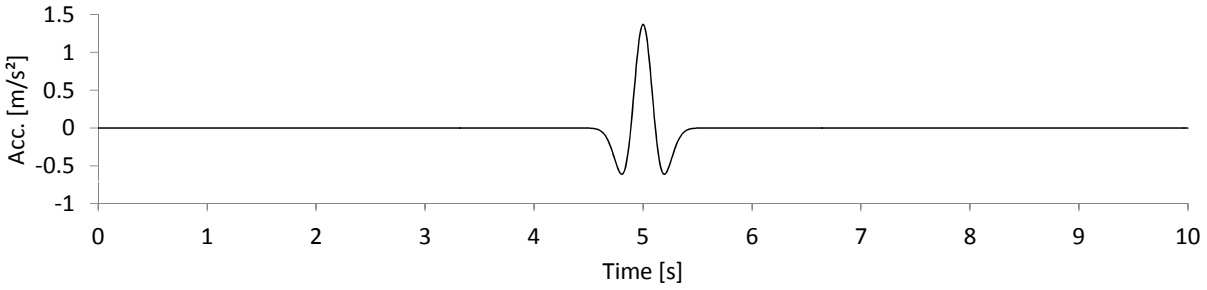

(b)

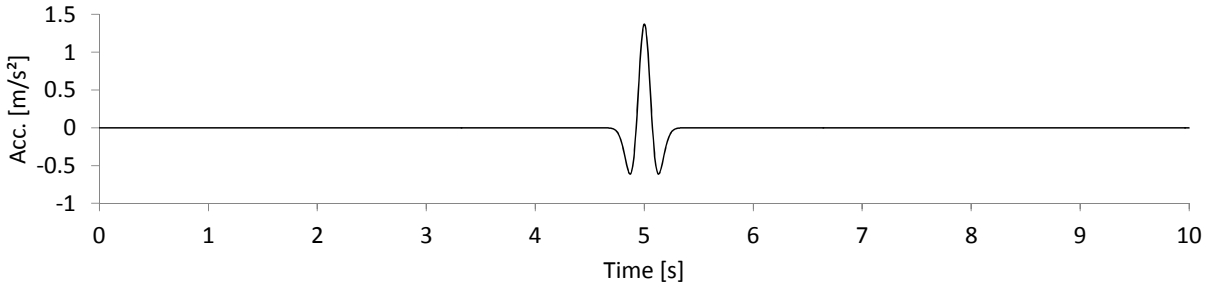

(c)

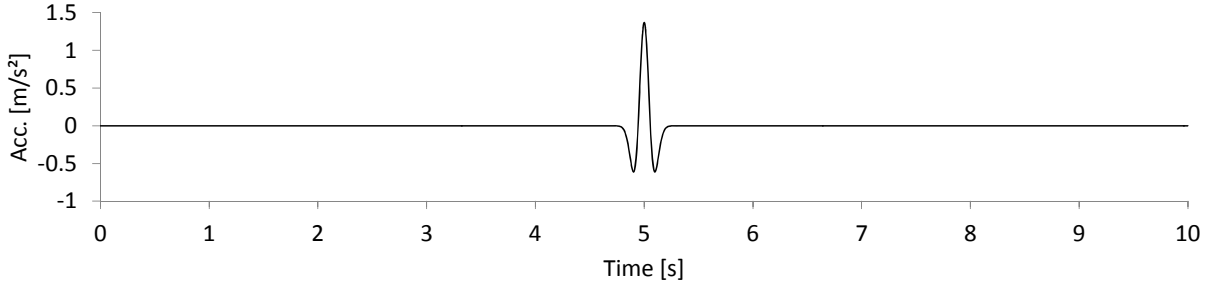

(d)

Figure 3.9: Ricker wavelet pulses with the amplitude $1.37m/s^2$ and the frequencies. (a) $f = 1Hz$, (b) $f = 2Hz$, (c) $f = 3Hz$, (d) $f = 4Hz$

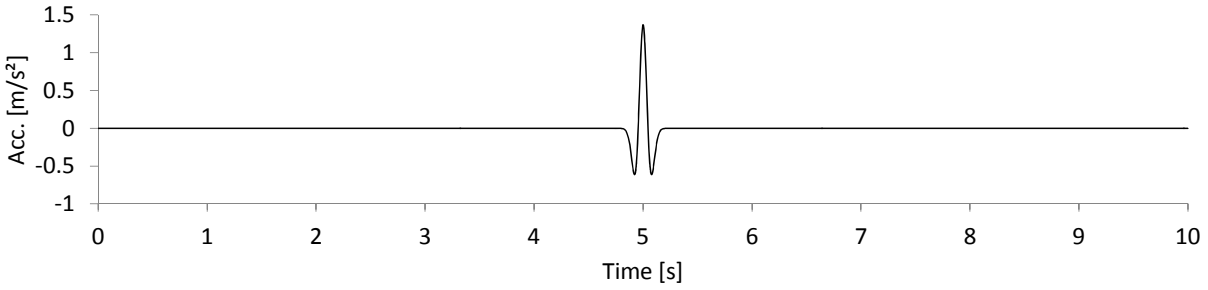

(a)

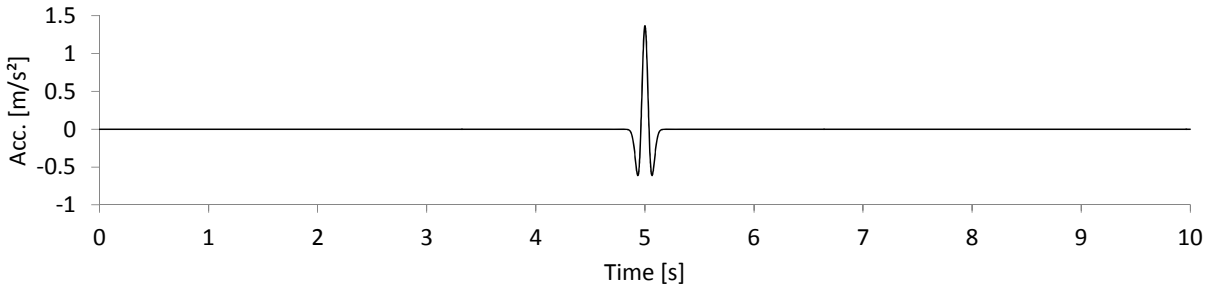

(b)

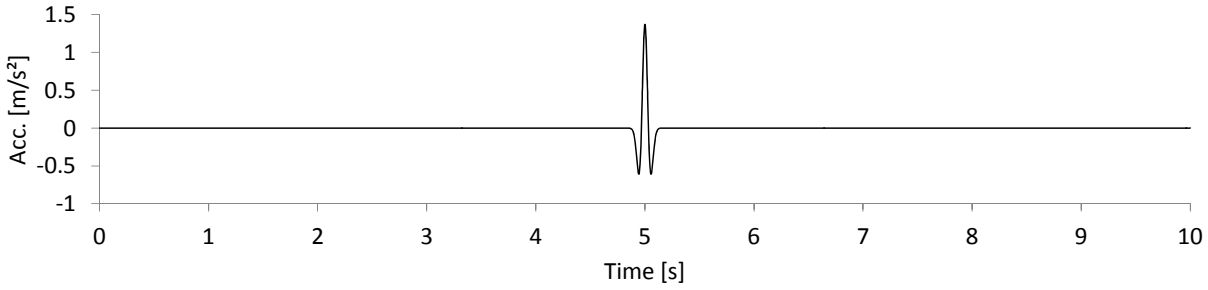

(c)

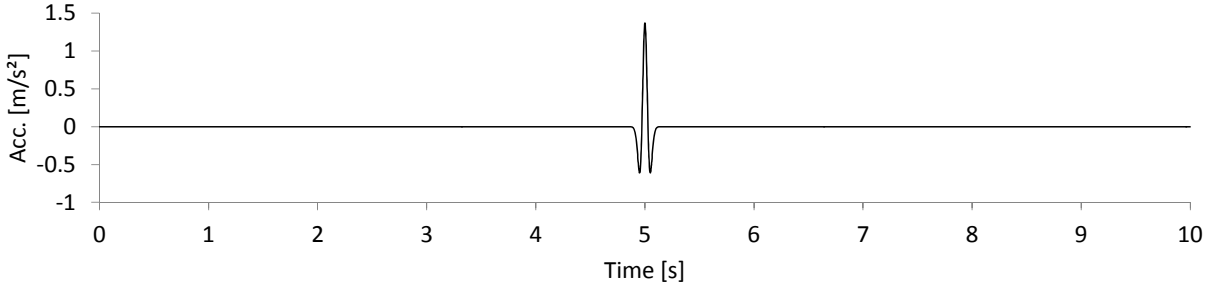

(d)

Figure 3.10: Ricker wavelet pulses with the amplitude $1.37m/s^2$ and the frequencies. (a) $f = 5Hz$, (b) $f = 6Hz$, (c) $f = 7Hz$, (d) $f = 8Hz$

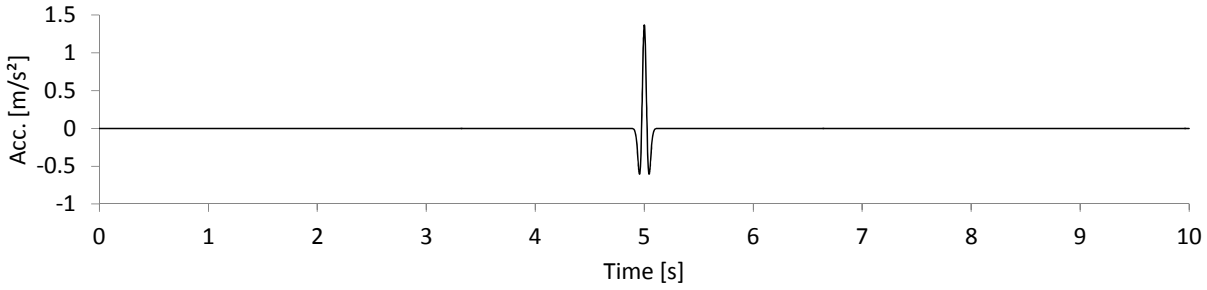

(a)

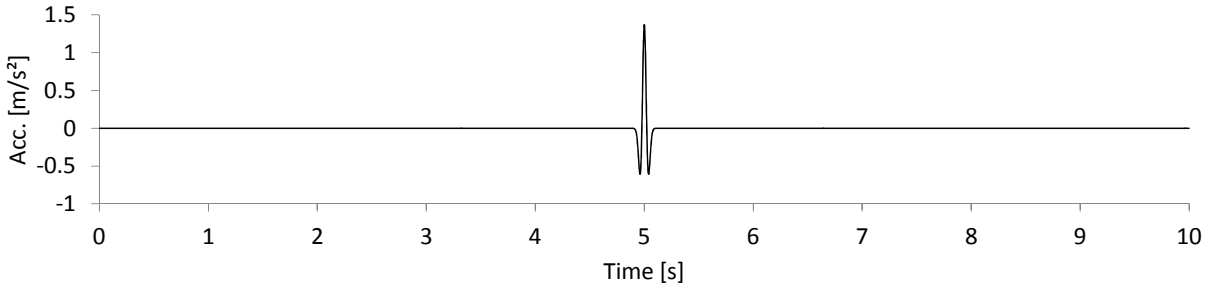

(b)

Figure 3.11: Ricker wavelet pulses with the amplitude $1.37m/s^2$ and the frequencies. (a) $f = 9Hz$, (b) $f = 10Hz$

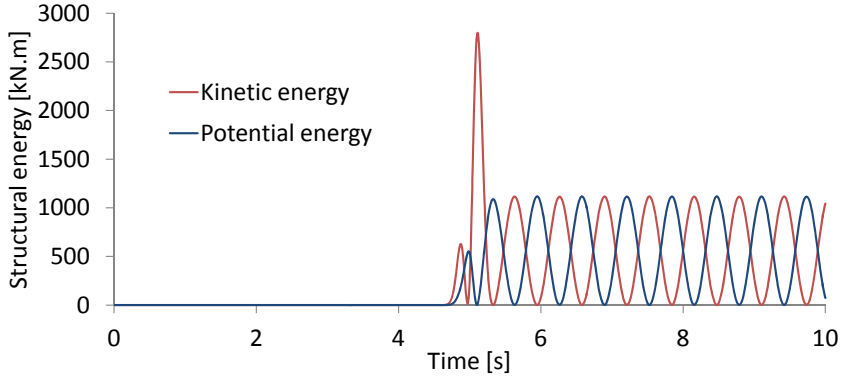

Figure 3.12: Variation of kinetic and potential energies in the Millikan library subjected to a pulse with an amplitude $1.37m/s^2$ and a frequency of $2.0Hz$

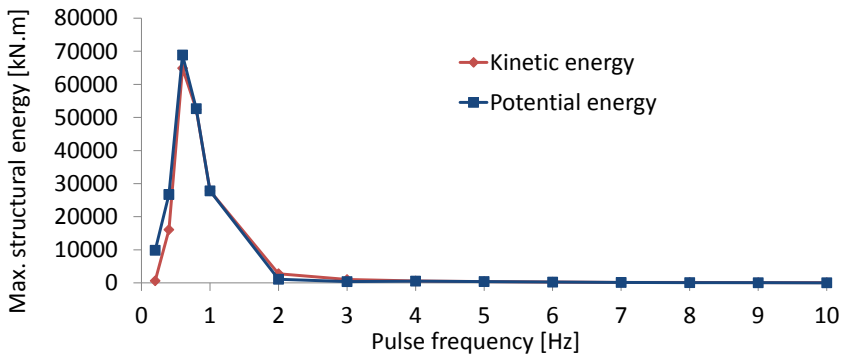

Figure 3.13: Variation of kinetic and potential energies in the Millikan library subjected to fourteen Ricker wavelet pulses of different frequency content

3.5 Energies of Inelastic Structural Response

In this section, energy measures are introduced as a general indicator of inelastic structural response. Energy terms imparted to the structure are derived from the relative energy approach described in subsection 3.3.2. Furthermore, dynamic SSI effects are also investigated in this section by coupling both partial models, i.e., the soil and structure models introduced in section 2.7.

Many researchers in the field of earthquake engineering have investigated structural response using pulses or the sine wavelets of various frequencies, intensities and durations, which conceptually describe a predictable earthquake signal. Investigating the structural response to basic types of dynamic base excitations allows the identification of some important elementary principles, which are not able to be easily identified from analysis results using typical dynamic earthquake excitations. Accordingly, a forced dynamic analysis of structure is performed in this section using two basic types of base motion, namely sinusoidal and pulse ground excitations. Subsequently, energy response time histories are constructed for the used ground excitation.

3.5.1 Dynamic equilibrium

For an SDOF system subjected to a ground excitation, the equation of motion can be written as

$$\ddot{u} + 2\omega\xi\dot{u} + \omega^2 u = -\ddot{u}_g \tag{3.46}$$

where ($\omega = \sqrt{k/m}$) is the natural circular frequency of the system and ($\xi = c/2m\omega$) is its viscous damping ratio. For an inelastic system response, Eq. 3.46 can be rewritten in a non-dimensional form (Mahin and Lin, 1983) as

$$\ddot{\mu} + 2\omega\xi\dot{\mu} + \omega^2\mu = -\frac{\omega^2}{\eta}\frac{\ddot{u}_g}{\ddot{u}_{gmax}} \tag{3.47}$$

where μ is the ductility ratio, which is equal to

$$\mu = \frac{u}{\delta_y} \tag{3.48}$$

η is the structural strength ratio, which is defined as

$$\eta = \frac{r_y}{m\ddot{u}_{gmax}} \tag{3.49}$$

and r_y and δ_y are the yield strength and yield displacement of the inelastic structure, respectively.

3.5.2 Energy response to sinusoidal excitation

In this subsection, the structural response to the harmonic base acceleration is investigated with an amplitude of $2m/s^2$ and a period of $0.5s$ and the responses to the Ricker wavelet pulses of different frequency content are examined in subsection 3.5.3. To illustrate the variations in the energy responses obtained when implementing different models, a step-by-step inelastic time history analysis is conducted for the system described in section 2.7 and subjected to the aforementioned sinusoidal base acceleration.

The resulting energy response time histories for the fixed-base structure, as well as for the coupled soil-structure models are presented in Figures 3.14 to 3.16 using the Bouc-Wen hysteresis model described in subsection 2.7.2. The time history responses of input energy, strain energy, kinetic energy and hysteretic energy are demonstrated on the same plot.

The cyclic inelastic structural response caused by the harmonic sinusoidal ground acceleration excitation becomes more stable after the first few cycles of excitation. It can be observed that

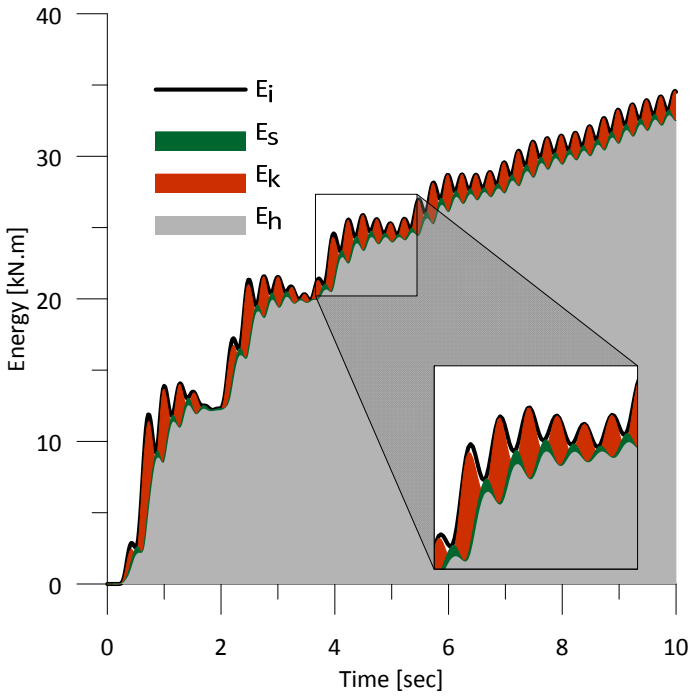

Figure 3.14: Time history energy responses for the fixed-base structure with Bouc-Wen hysteresis and subjected to harmonic ground excitation ($f = 2Hz$). E_i = input energy; E_s = strain energy; E_k = kinetic energy; E_h = hysteretic energy

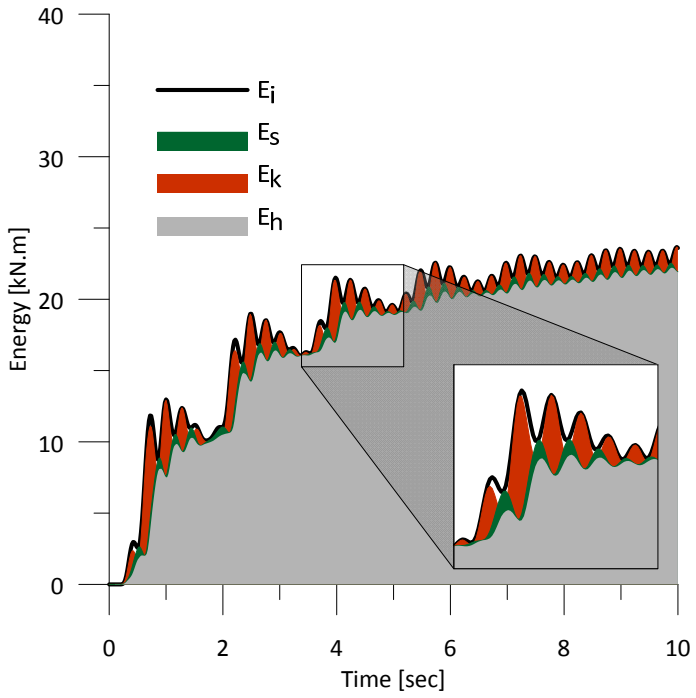

(a)

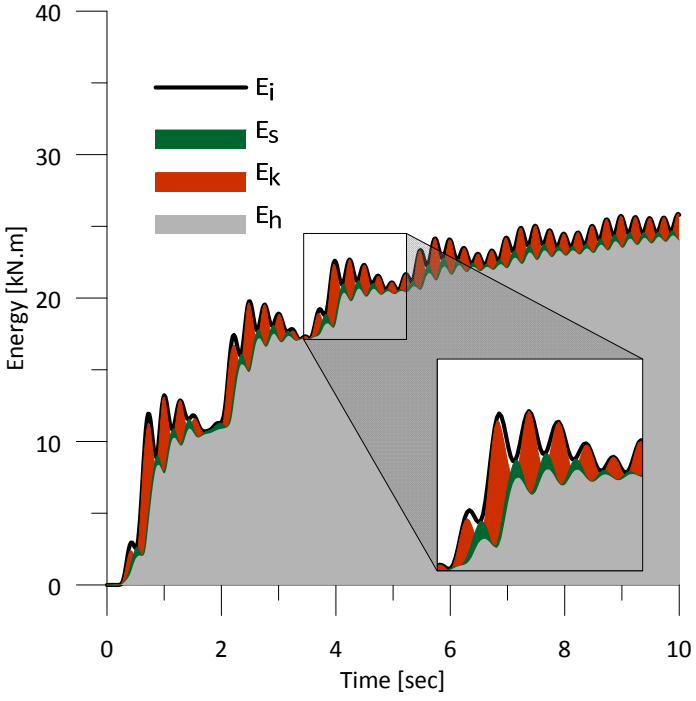

(b)

Figure 3.15: Energy response time histories for the structure with Bouc-Wen hysteresis and subjected to harmonic ground excitation ($f = 2Hz$) using: (a) Wolf lumped parameter models, (b) Gazetas dynamic springs. E_i = input energy; E_s = strain energy; E_k = kinetic energy; E_h = hysteretic energy

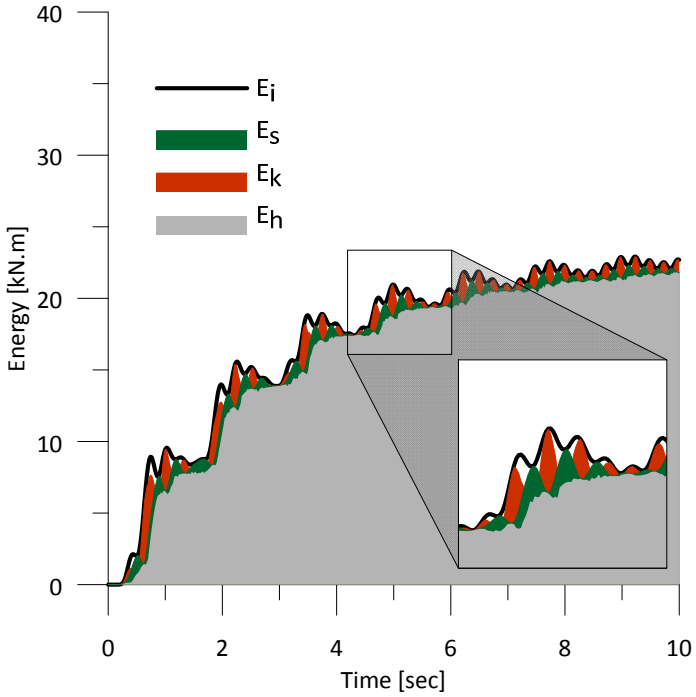

(a)

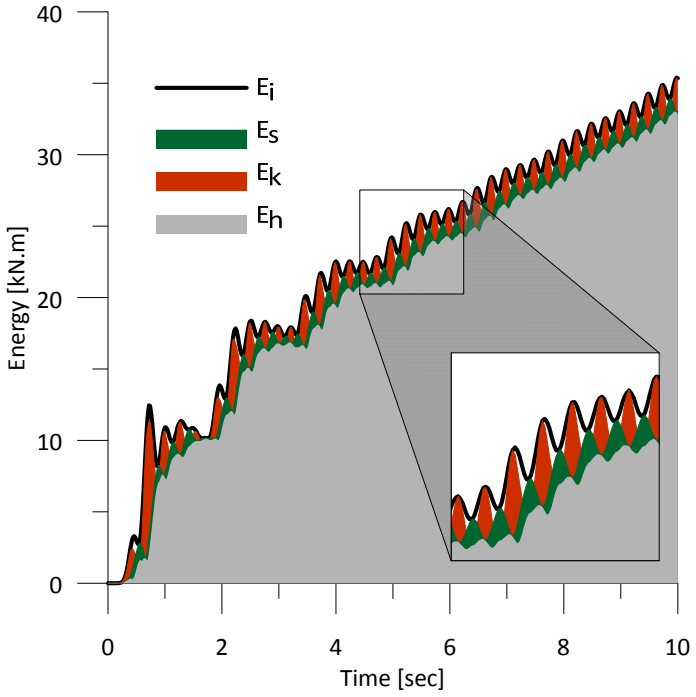

(b)

Figure 3.16: Energy response time histories for the structure with Bouc-Wen hysteresis and subjected to harmonic ground excitation ($f = 2Hz$) using: (a) Two-dimensional FE soil model, (b) Three-dimensional FE soil model. E_i = input energy; E_s = strain energy; E_k = kinetic energy; E_h = hysteretic energy

the kinetic energy and the strain energy fluctuate between the unbounded hysteretic energy and the input energy, while the resulting input energy keeps increasing as the hysteretic energy accumulates during the excitation. The strain energy is at a maximum when the structure reaches its maximum displacement and the kinetic energy is zero at the same point in time. Then the strain energy is zero when the structure crosses the next static equilibrium point and the kinetic energy is at a maximum at the same time.

Comparing the responses of the coupled soil-structure systems in Figure 3.15 to the response of the fixed-base structure in Figure 3.14, it can be seen that the coupled SSI models generally produce decreased energy responses. However, the resulting energies produced by the structure coupled with the three-dimensional FE soil model in Figure 3.15 (d) seem to be relatively large in comparison to the response of the rest of the SSI models. A probable reason for this higher response is the deficiency of the absorbing Lysmer boundaries (see subsection 2.6.3) used for the soil borders in the three-dimensional soil model. These viscous boundaries should transmit the energy of the waves reflected from the structure towards the model's boundaries. However, a full energy absorption of reflected waves cannot be assured (Kramer, 1996). The Lysmer boundaries can only completely absorb those waves that reach a boundary with an angle of incidence of under 90°. However, the angles of incidence on the boundary of a two or three-dimensional model can vary from about 0° to almost 180°.

Figures 3.17 and 3.18 show the structural responses using the Bouc-Wen and Takeda hysteretic models, respectively. The responses are represented by three indicators for each of the five models studied, i.e., the time history response of the cumulative hysteretic energy dissipated in a structure, which is a very important indicator of the cumulative damage sustained by it, and the time history response of the structural top displacement. Additionally, the Park-Ang damage index described in section 3.2 is also computed for each model.

The displacement response time histories are represented in Figure 3.17 (c) for the different models. It can be easily verified that the sum of the two successive steps in the time history response of hysteretic energy is equal to the area under the corresponding hysteresis loop. Since the system is undamped, the damping energy is zero and the input energy is the sum of the kinetic, hysteretic and strain energies and energy plots for the different models that maintain

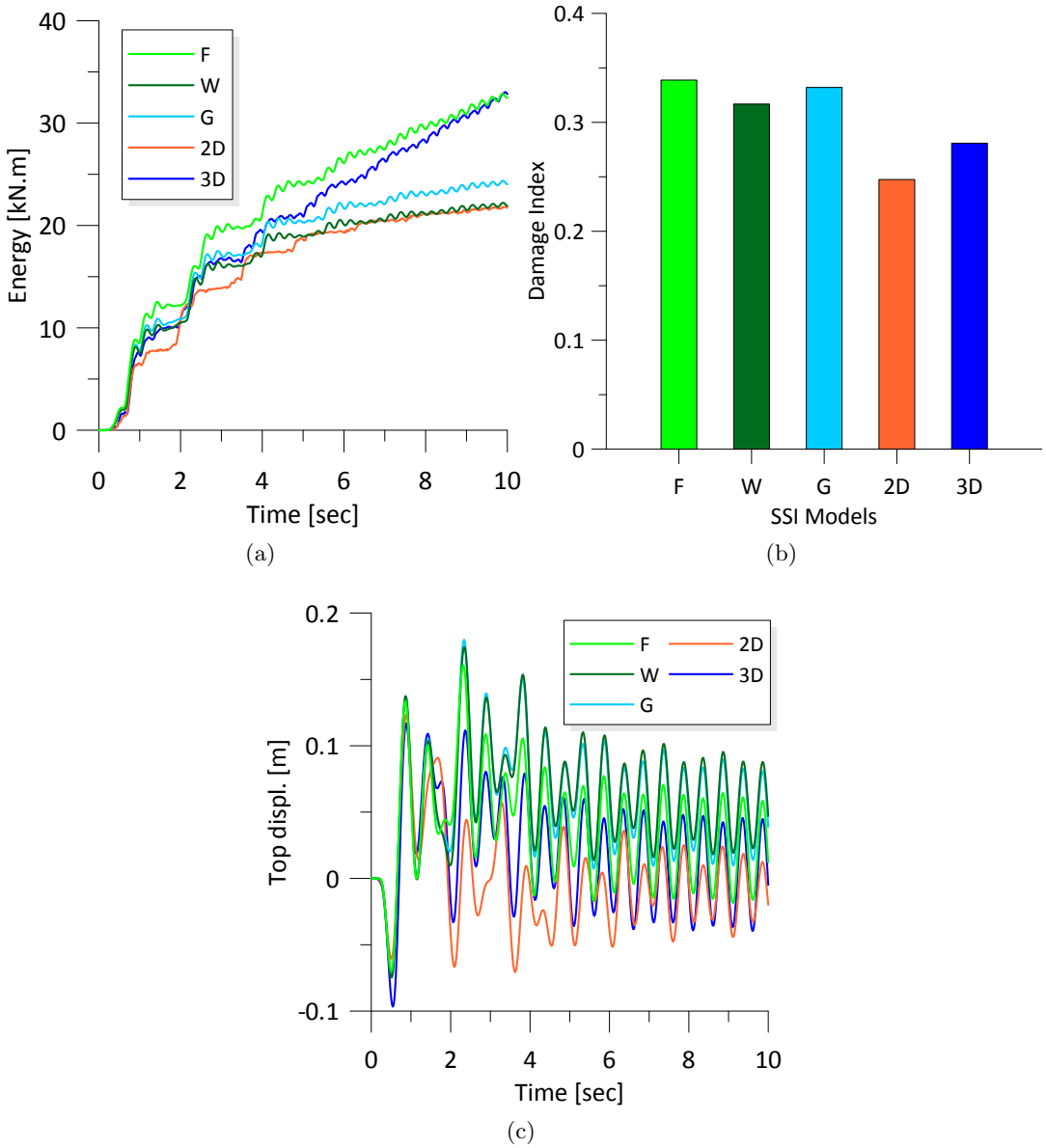

Figure 3.17: Structural hysteretic energy (a), the corresponding damage index (b) and structural top displacement (c) for the models with Bouc-Wen hysteresis and subjected to harmonic ground excitation ($f = 2Hz$). F = Fixed-base; W = Wolf model; G = Gazetas model; 2D = two-dimensional FE model; 3D = three-dimensional FE model

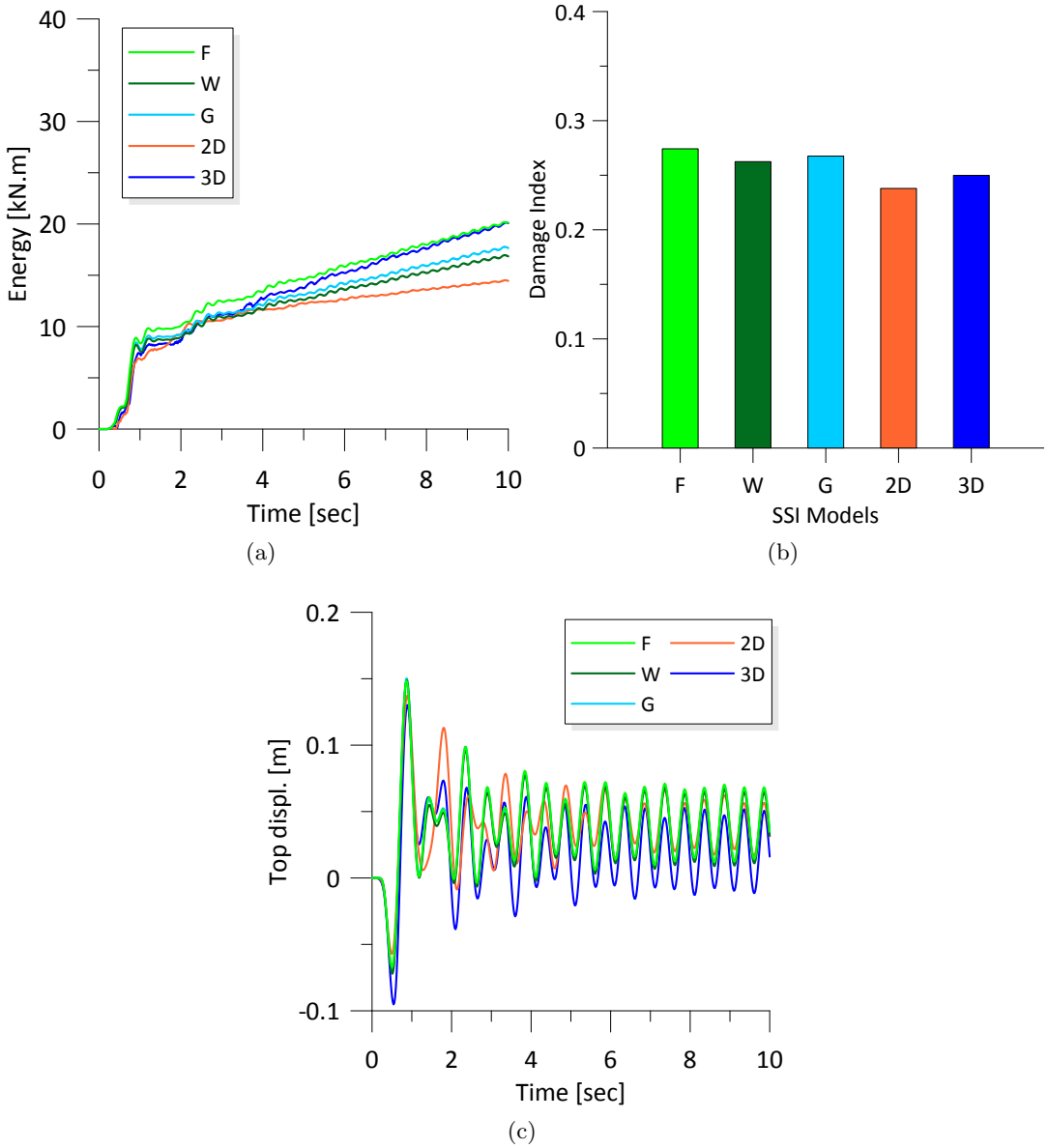

Figure 3.18: Structural hysteretic energy (a), the corresponding damage index (b) and structural top displacement (c) for the models with Takeda hysteresis and subjected to harmonic ground excitation ($f = 2Hz$). F = Fixed-base; W = Wolf model; G = Gazetas model; 2D = two-dimensional FE model; 3D = three-dimensional FE model

the principle of energy balance for the structure being studied.

Figure 3.17 (a) shows that the fixed-base model dissipates the largest amount of hysteretic energy in comparison to the other models investigated. On the other hand, the plots show that the energy response time histories with the lowest magnitudes interact in some ranges. An exact correspondence in the order of the models regarding the damage grade on one side and the amount of absorbed hysteretic energy on the other can be observed in the time range of zero to two seconds. However, it can be observed that more often than not, the response of the two-dimensional FE model delimits the lower bound of the energy response. The relation between the energy demand and damage can be observed in Figure 3.17 (a) and (b), where the highest magnitude of energy response produced by the fixed-base structure is associated with the highest damage grade. Alternatively, the lowest damage grade is observed for the two-dimensional FE model, which dissipates the lowest amount of hysteretic energy.

The previous observations also apply for the estimations in Figure 3.18 (b) where the Takeda hysteresis model is used. However, the grade of damage sustained by the different models is lower in comparison to Figure 3.17 (b) where Bouc-Wen hysteresis is used. This can be explained by the smaller amount of hysteretic energy that the Takeda model dissipates as shown in Figure 3.18 (a). A slight amplification in the time history response of top displacement can be seen in Figure 3.17 (c) when using the Bouc-Wen model compared to the Takeda model in Figure 3.18 (c).

3.5.3 Energy response to pulse excitations

In this subsection, the effects of excitation frequency on the energy response of the structure is investigated. The hysteretic energy responses to a group of six Ricker wavelet pulses (Ryan, 1994) of different frequency content are examined for the frequencies of $1.0, 1.2, 1.4, 1.6, 1.8$ and $2.0Hz$. The wavelet amplitude in all cases is equal to $a_{max} = 2.0m/s^2$. While the different energy terms imparted to the structure are investigated in subsection 3.5.2, the focus in this subsection is on the hysteretic energy response that stands for the cumulative nonlinear inelastic structural response. Consequently, hysteretic energy is considered as the most appropriate energy term to quantify the capacity of structures to dissipate energy during earthquakes.

The resulting hysteretic energy time histories for the fixed-base structure, as well as for the coupled soil-structure models are presented in Figure 3.19 using Bouc-Wen hysteresis. Once the pulse excitation is over, the hysteretic energy no longer changes. It can be seen that the energy response becomes more stable with less fluctuation around the mean response as the frequency of the pulse excitation increases. The plots also show that the structure absorbs a larger amount of energy through its nonlinear response as the frequency content of the pulse excitation decreases. This can be explained by the fact that the energy content of the pulse excitation increases when its frequency decreases. Thus, a greater amount of input energy will be transferred to the structure and consequently the absorbed energy will also grow. However, the different models do not absorb the same amount of energy although they are all subjected to excitations with the same characteristics. It can be seen that the two simpler coupled models, i.e., the Wolf and Gazetas models, produce a lower energy response in comparison to the remaining three models.

3.6 Summary

Energy measures are introduced in this chapter as a general indicator of elastic and inelastic structural responses. The different terms of energy imparted to a structure are computed using the energy approach, which is based on a physically clear concept. A forced dynamic analysis of a structure is performed using two basic types of base motion, i.e., sinusoidal and pulse ground excitations. The results show that the constructed energy response time histories provide valuable information about the dynamic behavior of structure since dynamic SSI effects can be identified and quantified for the different models implemented.. In addition to the structural top displacement, the resulting structural energies and the hysteretic energy, in particular, express the effects of SSI on the structural response. The more complex models lead to more flexible models and thus to less dissipated hysteretic energy in the structure, as well as a reduced top displacement response in comparison to the simpler models implemented.

A good correlation is observed between the computed Park-Ang damage index and the hysteretic energy dissipated in the structure for those models producing the upper and lower margins of damage grades. This applies to both types of the hysteretic rules used to describe the inelastic

structural behavior. However, the damage grades assigned cannot identify the best model quality since the latter does not necessarily correspond to a conservative structural design, which leads to the lowest damage grade. An evaluation methodology is proposed in the next chapter to assess model quality based on different response indicators.

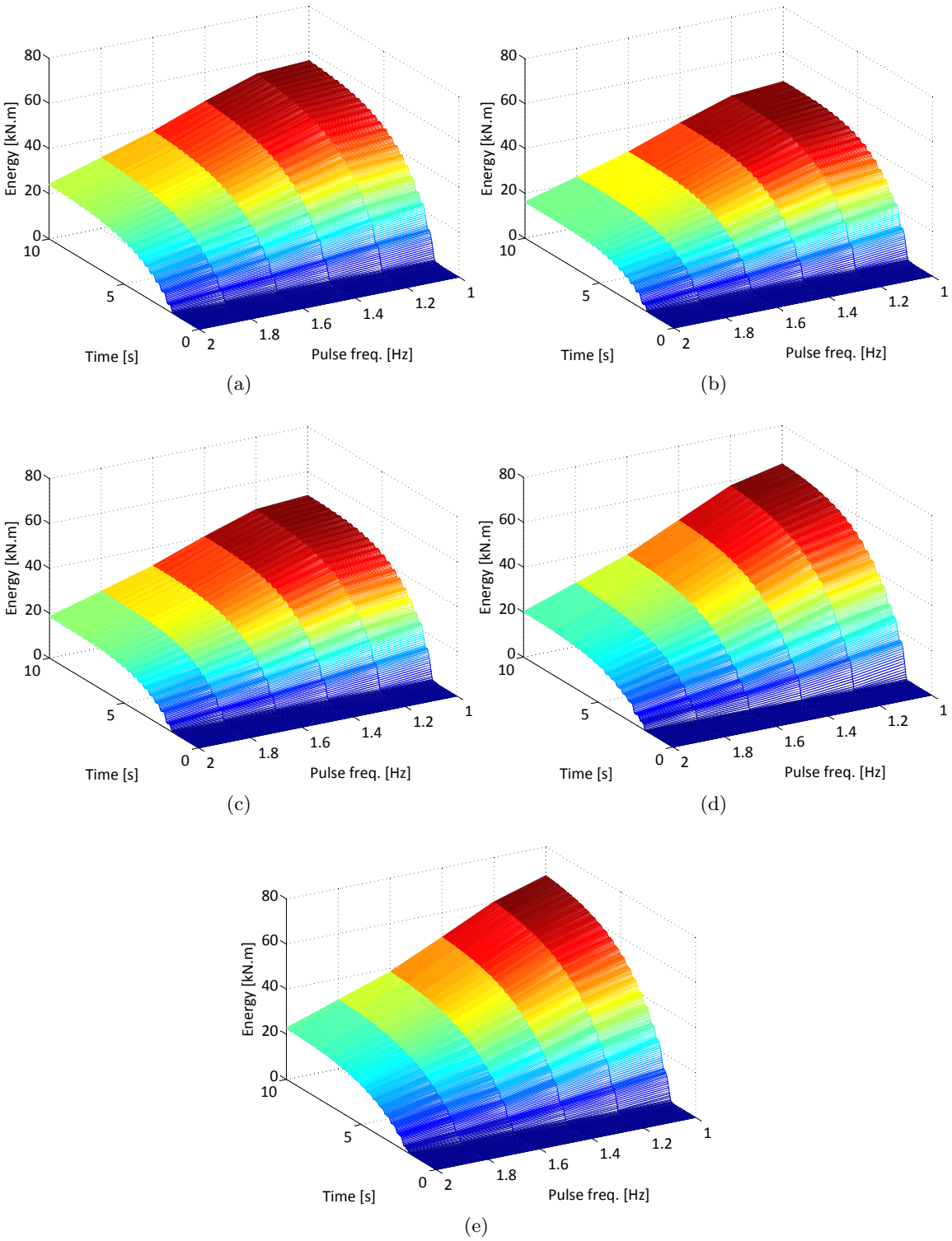

Figure 3.19: Hysteretic energy time histories for the structure with Bouc-Wen hysteresis subjected to a pulse ground excitation of different frequencies: (a) Fixed-base structure, (b) Wolf lumped parameter model, (c) Gazetas dynamic springs, (d) Two-dimensional FE soil model, (e) Three-dimensional FE soil model

Chapter 4

MODEL QUALITY ASSESSMENT

4.1 Introduction

Structural engineers are often faced with the task of selecting an appropriate model for the problem at hand. For a set of several models of varying complexity, the quality of a model can be assessed by quantifying underlying the uncertainty in one model compared to the rest of the adopted models. This uncertainty is defined in terms of the error of the model output. Often, more complex models provide a more detailed representation of the real system since they use fewer idealizations. The focus in this work is on the "computational models"described in EPA (2009). Computational models are based on mathematical relationships and use measurable inputs to produce quantitative outputs. According to the definition introduced in EPA (2009), a model is:

> *A simplification of reality that is constructed to gain insights into select attributes of a particular physical, biological, economic, or social system.*

A model is explained by means of a proper mathematical description of the underlying system or hypothesis. This includes its concepts, assumptions and idealizations. We define the description above for addressing the problem at hand as a "model framework".

In general, engineering systems involve complex influencing factors that also interact with each other. This is why it is difficult to describe the real system mathematically in a way that takes

all the relevant inherent mechanisms into account in order to predict its behavior in the real world. Nevertheless, engineering solutions are necessary, therefore models are constructed and used as an approximation of the reality. Since we are approximating the reality, a great deal of care should be given to selecting the most appropriate model from the set of models available by taking the different types of uncertainty underlying the model into account. In subsection 4.5.1, uncertainty is classified as aleatory (stochastic) and epistemic (related to lack of knowledge) uncertainty. This plays an essential role in the application of the theoretical formulations as shown in subsection 4.5.3.

Model evaluation serves as an aid in the selection of appropriate models, despite the uncertainties associated with them. However, perfect models that consider all aspects do not exist (Penrose, 2004), therefore it should be emphasized that there will always be a lack of knowledge, assumptions and idealizations with regard to models. In view of that, models cannot be a substitute for reality. At best, models can inform decisions. However, an evaluation of models can be useful within a specific scope of application. A preliminary engineering judgment is required for this propose. Such a judgment is usually based on the inherent built-in assumptions of the model and the study, as well as the type of results and conclusions needed.

A sensitivity analysis is considered to be a commonly used tool for determining the important parameters for a model in relation to the set of input parameters involved. While a model parameter uncertainty analysis investigates the type of uncertainty directly related to the values of the parameters as a whole, a sensitivity analysis helps in determining the set of parameters from the total number of parameters that have the most significant effect on model response. A sensitivity analysis is a quantitative measure of how sensitive the model output could be to the variation of the model input. Consequently, reducing the number of input parameters investigated to those that are significant generally leads to a simpler model and the model complexity can be limited by accounting for the significant parameters only and eliminating the rest.

With regard to the SSI models evaluated in this work, all of the input parameters involved are taken into account in the analysis and the model quality assessment is based on the uncertainty introduced in subsection 4.5.1. The uncertainty of the input parameters is taken into account

by means of a sampling strategy. The Monte Carlo analysis described in subsection 4.4.1 is a simple tool, which can be used for this goal. However, the plain Monte Carlo simulation requires a large number of random realizations to provide a satisfactory estimation of the statistical characteristics of a model. The Latin hypercube procedure described in subsection 4.4.2 is an efficient sampling tool since it requires a small number of random realizations compared to the plain method for generating representative statistical characteristics.

Section 4.5 represents the evaluation methodology used to assess the dynamic SSI models introduced in Chapter 2 based on the energy measures presented in Chapter 3. Random variables and vectors and the used statistical distribution are introduced in section 4.3. Sampling techniques are described in section 4.4 and applied in subsection 4.6.2 in order to determine the total model uncertainty of SSI models.

4.2 Previous Studies

Pearl (1978) noted that simpler models are preferred and implemented in many cases since they are often considered to be more plausible and testable. This is also supported by Beck (1987). He pointed out that models of different constructions serve different functions in the field of environmental simulation and that the degree of difficulty in validating models is in proportion to their complexity, whereas Oreskes et al. (1994) argue that it is not proven that accurate results are more likely to be obtained from simpler models compared to more complex models.

In the literature, a distinction is made between the evaluation and validation of models. Suter (1993) refers to two ways of validating models: The first is done by an exact matching to real observations and the second involves reproducing the model's output by means of experimental tests. However, the idealizations and assumptions with respect to the models cannot assure perfect results, which conform to observations or experimental tests that are supposed to represent the reality. Furthermore, Beck (2006) showed that validated models also do not automatically produce precise results for different application scopes compared to what could actually happen in reality. Oreskes et al. (1994) distinguished between the verification and validation of numerical models. Verification examines if a model's numerical solution is close enough to the

analytical solution. They showed that the terms of verification and validation are often used conterminously, which is incorrect. Snowling and Kramer (2001) pointed out that these terms are often used incorrectly to imply that a given model is a precise representation of physical reality. They point out that the unquestionable belief in the accuracy of a model's simulations under any conditions can lead to poor judgment in the selection of an appropriate model for the problem at hand. Konikow and Bredehoeft (1992) noted that the terms of verification and validation are often incorrectly taken by users to mean that the models they have implemented are accurate.

The different types of uncertainty are investigated in the literature using different aspects. Park et al. (2010) and Snowling and Kramer (2001) proposed an empirical estimation of model uncertainty based on the set of appropriate models available. If we already have the measurement data, Bayesian methods could be used to pick the model that best represents the data (Beck and Yuen, 2004; MacKay, 1992). Some literatures refer to model framework uncertainty as model error or model uncertainty (EPA, 1997; Luis and McLaughlin, 1992). This is the type of uncertainty investigated in this study. In contrast, Beck (1987) used structural error to express this type of uncertainty, which is associated with the phase of creating algorithms that describe models. Konikow and Bredehoeft (1992) refer to model framework uncertainty in terms of conceptual error. It stands for the uncertainty in transforming reality into equations that represent and govern the system's behavior.

4.3 Some Concepts in Probability and Statistics

4.3.1 Random variables and random vectors

Concepts of random vectors and their used distribution are reviewed in this subsection and the following one (Fang et al., 2006).

Let X be a random variable with a value, where the function expressed by

$$F(x) = P(X \leq x) \tag{4.1}$$

called the *cumulative distribution function* (cdf) is defined by the probability P, such that the random variable X is equal to or smaller than a deterministic value x. We write $X \sim F(x)$.

A vector $\mathbf{x} = (X_1, , X_p)'$ is called a random vector if all its components $X_1, , X_p$ are random variables. If $p(x_1, \cdots, x_p)$ is a non-negative and integrable function such that

$$F(x_1, \cdots, x_p) = \int_{-\infty}^{x_1} \cdots \int_{-\infty}^{x_p} p(y_1, \cdots, y_p) dy_1 \cdots dy_p, \tag{4.2}$$

the function p is called the *probability density function* (pdf) of $\mathbf{x}$.

Let X and Y be two random variables. If their joint distribution function $F(x, y)$ satisfies

$$F(x, y) = F_x(x) F_y(y) \tag{4.3}$$

for any x and y in R, where $F_x(\cdot)$ and $F_y(\cdot)$ are distributions of X and Y, respectively, we call X and Y statistically independent.

Similarly, let $\mathbf{x} = (X1, \cdots, Xp)$ and $\mathbf{y} = (Y_1, \cdots, Y_q)$ be two random vectors. We call $\mathbf{x}$ and $\mathbf{y}$ statistically independent if their joint distribution function F satisfies

$$F(\mathbf{x}_1, \cdots \mathbf{x}_p, \mathbf{y}_1, \cdots, \mathbf{y}_q) = F_x(\mathbf{x}_1, \cdots \mathbf{x}_p) F_y(\mathbf{y}_1, \cdots, \mathbf{y}_q) \tag{4.4}$$

for any $\mathbf{x} \in R^p$ and $\mathbf{y} \in R^q$, where F_x and F_y are the distribution functions of $\mathbf{x}$ and of $\mathbf{y}$, respectively.

The expected value of a discrete random variable X with $p_i = P(X = x_i), i = 1, 2, \cdots$, is defined as

$$E(X) = \sum x_i p_i \tag{4.5}$$

where the summation is taken over all possible values of X.

The expected value of a continuous random variable X with the density $p(x)$ is defined as

$$E(X) = \int x p(x) dx \tag{4.6}$$

where the integral is taken over the range of X.

The covariance of two random variables X and Y with a pdf $p(x, y)$ is defined by

$$\text{Cov}(X, Y) = \int_{-\infty}^{\infty} \int_{-\infty}^{\infty} (x - E(X))(y - E(Y))p(x, y)dxdy \tag{4.7}$$

or we write

$$\text{Cov}(X, Y) = E(X - E(X))(Y - E(Y)) \tag{4.8}$$

The covariance has the property $\text{Cov}(X, X) = \text{Var}(X)$. The random variables X and Y are called *uncorrelated* if $\text{Cov}(X, Y) = 0$.

The correlation coefficient between two random variables X and Y is defined by

$$\text{Corr}(X, Y) = \rho(X, Y) = \frac{\text{Cov}(X, Y)}{\sqrt{\text{Var}(X)\text{Var}(Y)}} \tag{4.9}$$

Let a random vector $\mathbf{x} = (X_1, \cdots, X_p)'$ have the probability density function $p(x_1, \cdots, x_p)$. The *mean vector* of $\mathbf{x}$ is defined by

$$E(\mathbf{x}) = \begin{bmatrix} E(X_1) \\ \vdots \\ E(X_p) \end{bmatrix} \tag{4.10}$$

Let $\sigma_{ij} = \text{Cov}(X_i, X_j)$ for $i, j = 1, \cdots, p$. We have $\sigma_{ii} = \text{Cov}(X_i, X_i) = \text{Var}(X_i)$. We call the matrix

$$\mathbf{\Sigma_x} = \text{Cov}(\mathbf{x}) = \begin{bmatrix} \sigma_{11} & \cdots & \sigma_{1p} \\ \vdots & & \vdots \\ \sigma_{p1} & \cdots & \sigma_{pp} \end{bmatrix} \tag{4.11}$$

the *covariance matrix* of $\mathbf{x}$ and the matrix

$$\mathbf{R_x} = \text{Corr}(\mathbf{x}) = \begin{bmatrix} \rho_{11} & \cdots & \rho_{1p} \\ \vdots & & \vdots \\ \rho_{p1} & \cdots & \rho_{pp} \end{bmatrix} \tag{4.12}$$

is called the *correlation matrix* of $\mathbf{x}$, where $\rho_{ij} = \text{Corr}(X_i, X_j)$. We write $\text{Cov}(X_i, X_j) = \sigma_{ij} = \sigma_i\sigma_j\rho_{ij}$, where σ_i the standard deviation of X_i. Let $\mathbf{S}$ be the diagonal matrix with diagonal

elements $\sigma_1, \cdots, \sigma_p$, to give the relation

$$\mathbf{\Sigma_x} = \mathbf{S}\mathbf{R_x}\mathbf{S} \tag{4.13}$$

If the covariance matrix of $\mathbf{x}$ has the form

$$\mathbf{\Sigma}(\mathbf{x}) = \begin{bmatrix} \mathbf{\Sigma}_{11} & 0 \\ 0 & \mathbf{\Sigma}_{22} \end{bmatrix} \tag{4.14}$$

after dividing $\mathbf{x}$ into $\mathrm{x} = (\mathrm{x}_1', \mathrm{x}_2')'$, then $\mathbf{x}_1$ and $\mathbf{x}_2$ are uncorrelated, where $\mathbf{\Sigma}_{11} = \mathrm{Cov}(\mathbf{x}_1)$ and $\mathbf{\Sigma}_{22} = \mathrm{Cov}(\mathbf{x}_2)$.

4.3.2 Log-normal statistical distribution

If X is a random positive variable and has a density

$$p(x) = \frac{1}{x\zeta\sqrt{2\pi}} \exp\left\{ -\frac{1}{2}\left(\frac{\ln(x-\lambda)}{\zeta} \right)^2 \right\} \tag{4.15}$$

then X is a log-normal random variable denoted by $X \sim \ln N(\lambda, \zeta^2)$, with the mean and variance

$$\mu = \exp\left(\lambda + \zeta^2/2\right); \quad \sigma = \left[\exp\left(\zeta^2\right) - 1\right] \exp\left(2\lambda + \zeta^2\right)$$

Equivalently, parameters λ and ζ can be obtained if the mean value and variance are known

$$\lambda = \ln \frac{\mu^2}{\sqrt{\sigma + \mu^2}}; \quad \zeta = \sqrt{\ln\left(\frac{\sigma}{\mu^2} + 1 \right)} \tag{4.16}$$

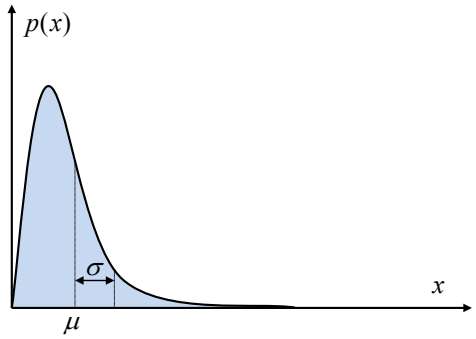

Figure 4.1: Probability density function for log-normal distribution

4.4 Sampling Techniques

4.4.1 Monte Carlo analysis

Let x_i be a sample element of size N generated in consistency with the distribution function of a random vector $\mathbf{x}$ which has the size K

$$\mathrm{x}_i = [x_{i1}, x_{i2}, ..., x_{i,\mathrm{K}}]\,; \quad i = 1, 2, ...,N \tag{4.17}$$

In sampling procedures, statistical quantities such as expected values and variances are obtained from sample elements combined with weights w_i with $i = 1, 2, ..., N$. For random sampling and also Latin hypercube sampling $w_i = 1/N$. The expected value $E(\mathrm{y})$ of $y = f(x)$ can then be approximated using the mean value of sampling results

$$E(\mathrm{y}) \doteq \hat{E}(\mathrm{y}) = \sum_{i=1}^{N} \mathrm{y}_i w_i \tag{4.18}$$

and the variance of y

$$V(\mathrm{y}) \doteq \hat{V}(\mathrm{y}) = \sum_{i=1}^{N} \left[\hat{E}(\mathrm{y}) - \mathrm{y}_i\right]^2 w_i \tag{4.19}$$

4.4.2 Latin hypercube sampling

In order to generate the samples in Eq. 4.17, some type of sampling technique has to be used in the Monte Carlo analysis. The plain Monte Carlo simulation requires a large number of random realizations to provide a satisfactory estimation of the statistical characteristics of a model. The Latin hypercube procedure is considered to be an efficient sampling tool since it requires a small number of random realizations compared to the plain method for generating representative statistical characteristics. Latin hypercube uses the weight $w_i = 1/N$ in combination with sampling elements to calculate the statistical quantities in Eqs. 4.18 and 4.19. The weight $w_i = 1/N$ corresponds to the uniform probability

$$P(\mathbf{x}_i \in D_j) = \frac{1}{N}; \quad i = 1, 2, ..., K; \quad j = 1, 2, ..., N \tag{4.20}$$

where K and N are the size of the base random vector $\mathbf{x}$ and the size of the sample element generated by the Latin hypercube procedure, respectively. Latin hypercube sampling operates in the following manner: A $(N \times K)$ matrix $\mathbf{R}$ is built from the base random vector $\mathbf{x}$. Then a matrix $\mathbf{S}$ with the dimensions $(N \times K)$ is generated for independent uniformly distributed parameters with random values between zero and one. In the next step, the matrix $\mathbf{T}$ is obtained as follows

$$\mathbf{T} = \frac{1}{N}(\mathbf{R} - \mathbf{S}) \tag{4.21}$$

Each variable in the sample element is then generated by mapping the elements of $\mathbf{T}$

$$x_{ij} = F_{x_j}^{-1}(t_{ij}) \tag{4.22}$$

to obtain the sample element generated by the Latin hypercube procedure

$$\mathrm{x}_i = [x_{i1}, x_{i2}, ..., x_{i,\mathrm{K}}]; \quad i = 1, 2, ...,N \tag{4.23}$$

4.5 Evaluation Methodology

The established evaluation methodology is presented in this section based on the energy measures introduced in Chapter 3. The main objective is to suggest a methodology for the assessment of the utility of SSI models. In order to achieve this goal, the modeling uncertainty is characterized as an attribute of model complexity (Most, 2011). The established evaluation methodology allows for a practical quantitative estimate of SSI in the presence of seismic loads and point to whether or not a full-scale nonlinear analysis will be required. Given the degree of uncertainty in the input parameters, users can make an informed decision when choosing one particular SSI model over another. Accordingly, a user can decide on the degree of uncertainty encountered in the implementation of a model.

4.5.1 Classification of uncertainty

Uncertainties are associated with every modeling process. They are inherent and usually cannot be reduced. However, it is critical that the different types of uncertainty are identified in order to select the appropriate model. This identification may take a quantitative or qualitative form depending on the characteristics of the uncertainty concerned.

Following EPA (2009), uncertainty refers to incomplete knowledge about specific factors, parameters (inputs), or models. The evaluation is based on the consideration of two primary types of uncertainty regarding the models of interest, namely the uncertainty in the framework and input parameters of a model.

- **Model framework uncertainty:** This type of uncertainty is produced by the lack of knowledge regarding the theoretical background of the modeled system, i.e., the insufficiency of assigning the factors involved, which influence the real behavior of the system concerned and the possible idealizations and simplifications of the real system.
- **Model input uncertainty:** This type of uncertainty is produced by data measurement errors, an inadequate amount of sample input data and stochastic characteristics of the parameters resulting from the model's natural variability and inherent randomness.

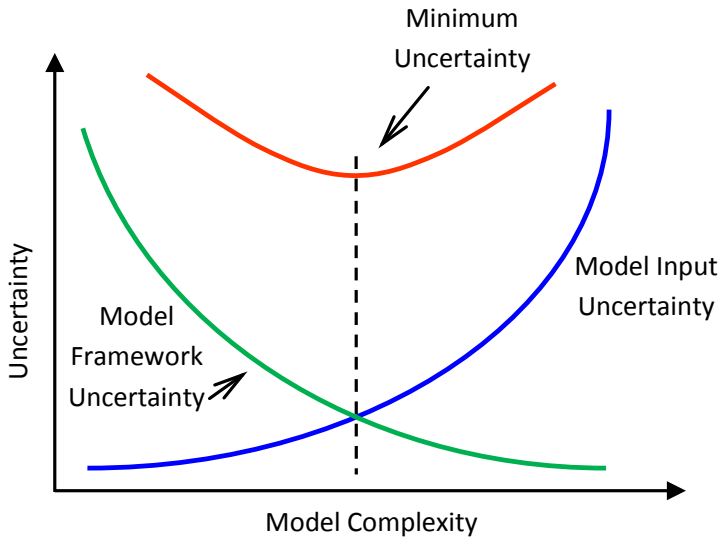

Figure 4.2: Relationship between model framework uncertainty and input parameters uncertainty and the resulted total model uncertainty adapted after (EPA, 2009)

4.5.2 Model complexity

The interest of how engineering systems would behave under certain or in most cases several scenarios explains the importance of using a model as a common tool in structural engineering. There are many models that deal with the SSI problem. However, the main concern that usually arises is how to adopt the best model from the set of those available.

Model complexity is considered to be a major parameter, which influences the quality of a model. Increased model complexity usually means that more parameters are required. Consequently, more input data will be needed. This data either has to be obtained through field measurements or it has to be estimated empirically. Input parameters require initial conditions that are defined by the underlying modeling assumptions. Figure 4.2 illustrates the relationship between the different types of uncertainty. The degree of complexity is associated with the total model uncertainty. A simple model incorporates more idealizations than a sophisticated one and consequently has a smaller number of parameters, but increasing uncertainty in its framework. On the other hand, there are more input parameters involved in the complex model in order to consider more physical aspects. As a result, it has increasing data uncertainty. In this study, model quality is assessed by investigating the model framework uncertainty for each model

adopted, based first on the reference model selected and once again on the averaged model response as introduced in the following subsections. The effect that the uncertainty in model input parameters has on the model response is also investigated. Combining the information gathered from the two types of uncertainty investigated helps in selecting the most suitable model associated with the minimum total uncertainty.

4.5.3 The adjustment factor approach

Following Most (2011) and Park et al. (2010), the adjustment factor approach is used to predict a system response from a set of models as represented in Eq. 4.24

$$Y_{pred} = y^* + E_a^* \tag{4.24}$$

where y^* represents the prediction of the response elicited by the reference model. The latter is first adopted as a more complex model, which provides a more detailed representation of the real system since it uses fewer idealizations, and once again as the averaged model response and E_a^* represents an additive adjustment factor. The mean and variance are computed by

$$E(Y_{pred}) = y^* + E(E_a^*) = y^* + \sum_{i=1}^{k} P_{\mathcal{M}_i}(y^{\mathcal{M}_i} - y^*) \tag{4.25}$$

$$V(Y_{pred}) = V(E_a^*) = \sum_{i=1}^{k} P_{\mathcal{M}_i}(y^{\mathcal{M}_i} - E(Y_{pred}))^2 \tag{4.26}$$

where $y^{\mathcal{M}_i}$ represents the deterministic prediction of the response by model $\mathcal{M}_i$ since the uncertainty in the input parameters is excluded at this stage. $P_{\mathcal{M}_i}$ represents the probability of the model $\mathcal{M}_i$, and k is the number of available models. The model probability $P_{\mathcal{M}_i}$ can be assumed to be equal to $1/k$ considering the model as a uniformly distributed discrete variable. Otherwise, $P_{\mathcal{M}_i}$ can be considered as a weighting factor with different values adding up to one. The mean and variance of E_a^* given in Eq. 4.25 are the averaged mean and variance of the differences between the prediction of the reference model response and the other models considered. The model probabilities in $P_{\mathcal{M}_i}$ are used as weights. The sum of probabilities is

equal to one, so that

$$E(Y_{pred}) = \sum_{i=1}^{k} P_{\mathcal{M}_i} y^{\mathcal{M}_i} = \bar{Y}^{\mathcal{M}} \tag{4.27}$$

$$V(Y_{pred}) = \sum_{i=1}^{k} P_{\mathcal{M}_i} (y^{\mathcal{M}_i} - E(Y_{pred}))^2 = V(Y^{\mathcal{M}}) \tag{4.28}$$

Eq. 4.27 and Eq. 4.28 represent the prediction for the averaged response of the adopted models without consideration of the reference model and only taking the uncertainty in the model framework into account. Including the uncertainty of model parameter gives

$$Y_{pred} = Y^{\mathcal{M}} = \sum_{i=1}^{k} P_{\mathcal{M}_i} Y^{\mathcal{M}_i} \tag{4.29}$$

The mean and variance are given as

$$E(Y_{pred}) = \bar{Y}^{\mathcal{M}} = \sum_{i=1}^{k} P_{\mathcal{M}_i} E(Y^{\mathcal{M}_i}) \tag{4.30}$$

$$V(Y_{pred}) = V(Y^{\mathcal{M}}) = \sum_{i=1}^{k} P_{\mathcal{M}_i} E(Y^{\mathcal{M}_i} - \bar{Y}^{\mathcal{M}})^2 \tag{4.31}$$

The total variance is related to the variance of each of the models considered and is written as

$$\begin{aligned} V_{\mathcal{M}_i}(Y_{pred}) &= E(Y^{\mathcal{M}_i} - \bar{Y}^{\mathcal{M}})^2 \\ &= E(Y^{\mathcal{M}_i})^2 + E(-2Y^{\mathcal{M}_i}\bar{Y}^{\mathcal{M}} + (\bar{Y}^{\mathcal{M}})^2) \\ &= V(Y^{\mathcal{M}_i}) + (\bar{Y}^{\mathcal{M}_i})^2 - 2\bar{Y}^{\mathcal{M}_i}\bar{Y}^{\mathcal{M}} + (\bar{Y}^{\mathcal{M}})^2 \\ &= V(Y^{\mathcal{M}_i}) + (\bar{Y}^{\mathcal{M}_i} - \bar{Y}^{\mathcal{M}})^2 \end{aligned} \tag{4.32}$$

The first part of Eq. 4.32 represents the uncertainty of input parameter associated with each model considered, and the second part introduces the uncertainty in the model framework which

is obtained as the difference between the averaged model response and the mean of the model considered.

The modified model response introduced by Most (2011) for a considered model is based on an adopted reference response with additive model errors, which is represented as follows

$$Y^{\mathcal{M}_i^*} \approx Y^{\mathcal{M}_i} + \epsilon_{\triangle}^{\mathcal{M}_i} + \epsilon^{\mathcal{M}_{ref}} \tag{4.33}$$

where $\epsilon_{\triangle}^{\mathcal{M}_i}$ represents the model framework uncertainty as an additive error to the reference model response, and $\epsilon^{\mathcal{M}_{ref}}$ is the error associated with the reference model response itself. The standard deviation of $\epsilon_{\triangle}^{\mathcal{M}_i}$ is then approximated as

$$V(\epsilon_{\triangle}^{\mathcal{M}_i}) \approx b^2(\bar{Y}^{\mathcal{M}_i} - \bar{Y}^{\mathcal{M}_{ref}})^2 \tag{4.34}$$

where $\bar{Y}^{\mathcal{M}_{ref}}$ is the reference response, b is a constant which can be chosen to be equal to 0.608, which corresponds to a 95% one-sided quantile. Considering Eq. 4.32 b can be chosen to be equal to 1. The total variance of a considered model can be written as

$$V(Y^{\mathcal{M}_i^*}) \approx V(Y^{\mathcal{M}_i}) + b^2(\bar{Y}^{\mathcal{M}_i} - \bar{Y}^{\mathcal{M}_{ref}})^2 + V(\epsilon^{\mathcal{M}_{ref}}) \tag{4.35}$$

Eq. 4.35 deems that the best model from a set of considered models is the one with minimum total variance, i.e., the smallest sum of model input uncertainty and model framework uncertainty.

4.6 Numerical Application

In this section, the established evaluation methodology is introduced through a numerical application. The soil media and the effects of dynamic SSI are taken into account accordingly by implementing four different soil models coupled with the structural model as introduced in Chapter 2. The uncertainty associated with the SSI models is quantitatively assessed within the framework presented in subsection 4.5.3. Furthermore, the uncertainty in model input parameters is also estimated in subsection 4.6.2.

Four structural response indicators are used to estimate the uncertainty of the models investigated, namely the maximum top displacement of the structure d_{max}, the ratio of total structural hysteretic energy to total structural input energy E_h/E_i (see section 3.3.2), the Park-Ang damage index DI_{PA} described in section 3.2 and the averaged structural top displacement d along a determined time window truncated from the entire response time history. This time window is determined in such a way that it covers all of the maximum top displacements for the different models.

4.6.1 Uncertainty in model framework

In this subsection, uncertainty in the model framework is investigated for the adopted models as described in subsection 4.5.3. The effects due to uncertainty in the input parameters are ignored in the analysis in this subsection. Two types of hysteretic rules are used in the nonlinear analysis as introduced in subsection 2.7.2 and the models are subjected to different types of excitation as presented in section 3.5.

As introduced in subsection 4.5.3 the uncertainty in the model framework for each model is estimated based on a reference response. In general, this response can be obtained through measurements, experiments, or from the solutions of other analytical or numerical models. The reference response adopted in this numerical application is the averaged model response derived from the responses of the models implemented. Different probabilities (weights) are assumed for the models, which have different abstraction levels. Besides the fixed-base model, the Gazetas and Wolf models are considered to be simpler models since the soil medium in these models

Table 4.1: Natural periods and predictions of the structure coupled to the soil models

Model	Natural period[s]	Model probability $P_{\mathcal{M}_i}$
Fixed-base	0.5	1/9
Wolf	0.622	1/9
Gazetas	0.588	1/9
2D-FE	0.8	3/9
3D-FE	0.765	3/9

is replaced with a spring-dashpot system. Each of these three models has a weighted model prediction equal to one, which corresponds to a probability that is equal to 1/9 related to the sum of all model probabilities. The two remaining FE models are considered as more complex models, which are more representative of the real system than the simpler models. Therefore, each of them is given a larger weighted prediction, which is equal to three. That corresponds to a probability that is equal to 3/9 related to the sum of all model probabilities. The probabilities shown in Table 4.1 are applied as weights ($P_{\mathcal{M}_i}$) in Eqs. 4.25 through 4.31 and can be updated subjectively.

Figures 4.3 and 4.4 show the deterministic predictions of the four SSI models assessed in addition to the fixed-base model. An overview of the estimation results is introduced in Table 4.2 provide perspective. The results represent model-to-model uncertainty. In general, the response indicators lead to a smaller model error when using the Takeda hysteresis model in comparison to the Bouc-Wen hysteresis model. The results show that the hypothesis of decreasing model error with increasing model complexity ignoring the uncertainty of input parameters only holds when the quality assessment is based on the energy ratio E_h/E_i as a response indicator. The estimation of model uncertainty based on E_h/E_i and on the damage index DI_{PA} leads to models with the same order with regard to their quality as shown in Figure 4.3. This also holds in Figure 4.4, but only based on the energy ratio as a response indicator. The results apply for both of the hysteretic models used and show that the more complex three-dimensional FE model has the best quality of the models investigated, whereas the Wolf model produces the lowest model uncertainty of the three simpler models and therefore has the best model quality compared to the other two models. The fixed-base model produces the highest estimated uncertainty and consequently the worst quality of all the models investigated. This once again

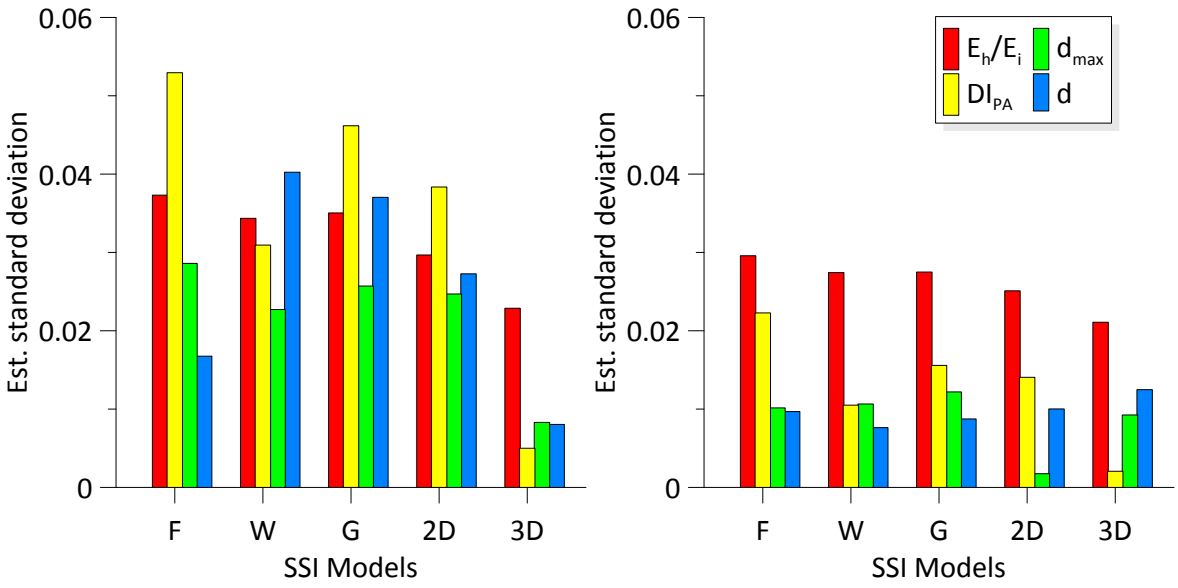

Figure 4.3: Estimated model framework uncertainty for the models subjected to harmonic ground excitation ($f = 2Hz$) based on averaged response as a reference and using: (a) Bouc-Wen hysteresis, (b) Takeda hysteresis. F = Fixed-base; W = Wolf model; G = Gazetas model; 2D = two-dimensional FE model; 3D = three-dimensional FE model; E_h/E_i = ratio of total hysteretic energy to total input energy; DI_{PA} = Park-Ang damage index; d_{max} = maximum top displacement; d = averaged top displacement

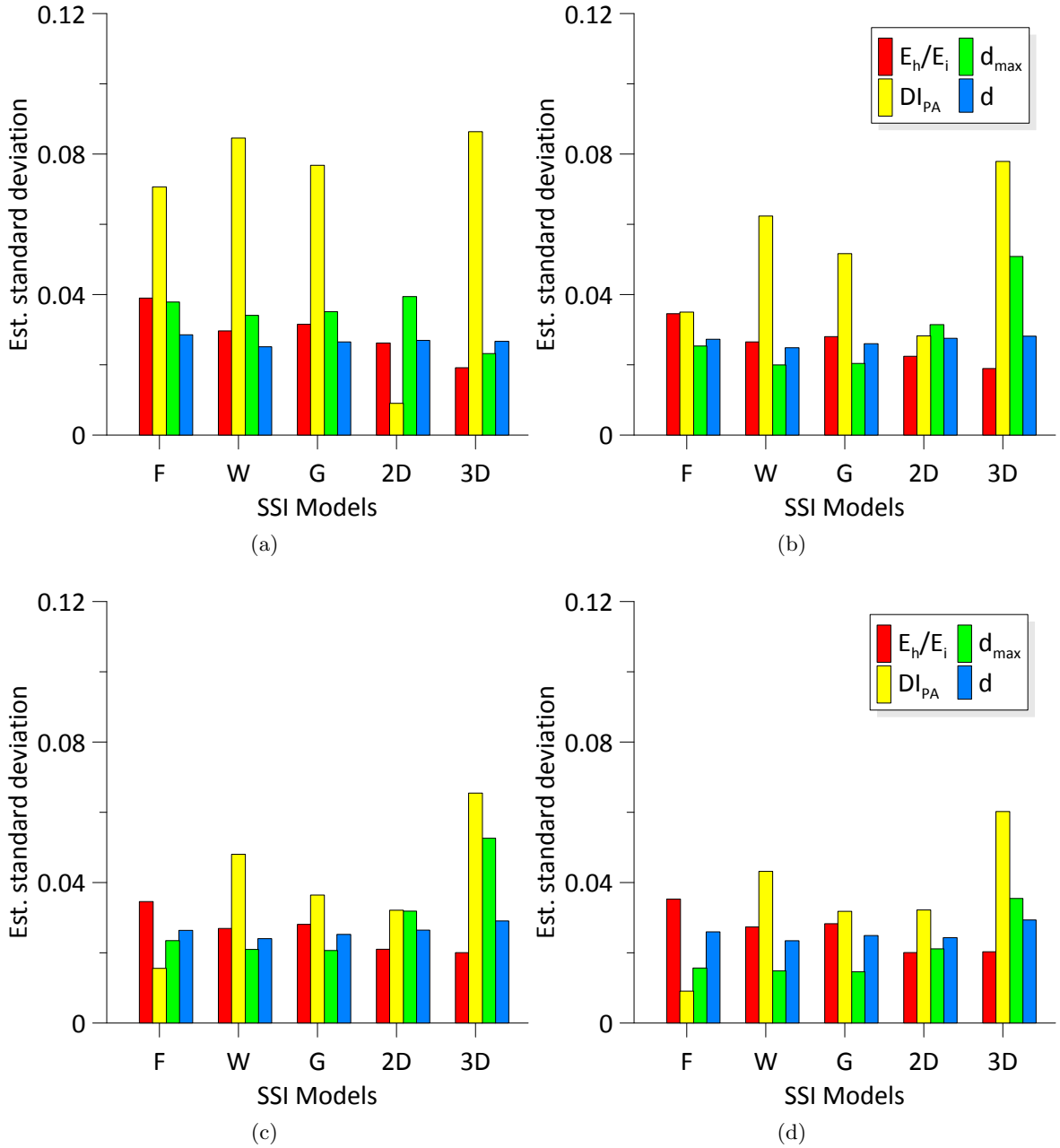

Figure 4.4: Estimated model framework uncertainty for the models based on averaged response as a reference using Bouc-Wen hysteresis and subjected to pulse ground excitation: (a) $f = 1.0Hz$, (b) $f = 1.2Hz$, (c) $f = 1.4Hz$, (d) $f = 1.6Hz$ F = Fixed-base; W = Wolf model; G = Gazetas model; 2D = two-dimensional FE model; 3D = three-dimensional FE model; E_h/E_i = ratio of total hysteretic energy to total input energy; DI_{PA} = Park-Ang damage index; d_{max} = maximum top displacement; d = averaged top displacement

Table 4.2: Model quality predictions corresponding to the model framework uncertainty illustrated in Figure 4.4. A = best quality; E = worst quality

indicator	freq. [Hz]	**fixed-base**	**Wolf**	**Gazetas**	**2D FE**	**3D FE**
E_h/E_i	1.0	E	C	D	B	A
	1.2	E	C	D	B	A
	1.4	E	C	D	B	A
	1.6	E	C	D	B	A
DI_{PA}	1.0	B	D	C	A	E
	1.2	B	D	C	A	E
	1.4	A	D	C	B	E
	1.6	A	D	B	C	E
d_{max}	1.0	D	B	C	E	A
	1.2	C	A	B	D	E
	1.4	C	B	A	D	E
	1.6	C	B	A	D	E
d	1.0	E	A	B	D	C
	1.2	D	A	B	C	E
	1.4	D	A	B	C	E
	1.6	D	A	C	B	E

confirms the hypothesis of increasing model error with decreasing complexity only when the assessment is based on the energy ratio as a response indicator. The results in Figure 4.4 show that, in general, the estimated model framework uncertainty is interrelated with the excitation frequency. However, the estimation based on E_h/E_i is independent from these frequencies. It has also been observed that the energy ratio E_h/E_i leads to a less sensitive estimation of model quality.

4.6.2 Total model uncertainty

In addition to the uncertainty in the model framework, the uncertainty in model input parameters is also estimated in this subsection. The results are presented as a total model uncertainty as described in subsection 4.5.3. Uncertainty in model parameters is investigated by means of the Latin hypercube sampling method introduced in subsection 4.4.2. The sampling is performed from independent log-normal distributions with values of mean μ and a coefficient of variation cv as illustrated in Table 4.3. Three parameters are considered in the analysis, namely shear wave velocity in soil c_s, structural strength ratio η and the modulus of elasticity for the

Table 4.3: Stochastic parameters of soil and structure variables according to the log-normal distribution

c_s [m/s]		η		E_f [N/m^2]	
μ	cv	μ	cv	μ	cv
175	0.4	1.5	0.15	29.9×10^9	0.03

foundation E_f. Eight samples are randomly generated for the soil and structure variables. The main objective of sampling is to investigate and measure the relative effect of an uncertain input parameter on the total uncertainty of a model if this input parameter is not involved in the other models.

Besides the averaged model response used in subsection 4.6.1, the response of the two-dimensional FE model is also used as a reference model response in this subsection. Again, the results represent model-to-model uncertainty. The two-dimensional FE model is adopted as a reference since it is considered to be the best approximation of the real system of the models investigated. The soil medium in this model has a width of $4km$, which is large enough to prevent the reflection of the waves propagating from the model's boundaries. The time of the excitation and the speed of the waves transmitting through soil require this dimension of soil model at least. Thus, there is no need for implementing artificial absorbing boundaries in this model.

Accounting for the uncertainty in the in the parameters in the quality estimation of the models updates the order of models regarding their total uncertainty. A fixed-base model, which only has the structural strength ratio η as a stochastic input parameter has the lowest total error as shown in Figure 4.5. The results show quantitatively how the uncertain input parameters affect the total estimated uncertainty. The differences in the estimated uncertainties become smaller between the simpler models and the more complex models after including the uncertainty in the parameters. The three simpler models have fewer input parameters and are therefore less sensitive to the uncertainty associated with the parameters, while the two more complex FE models produce a significantly increased total error after including the uncertainty of their input parameters. The FE models use more parameters, and consequently produce a higher total uncertainty than the three simpler models.

Figures 4.6 to 4.9 show the estimation results for the models subjected to pulses with varied

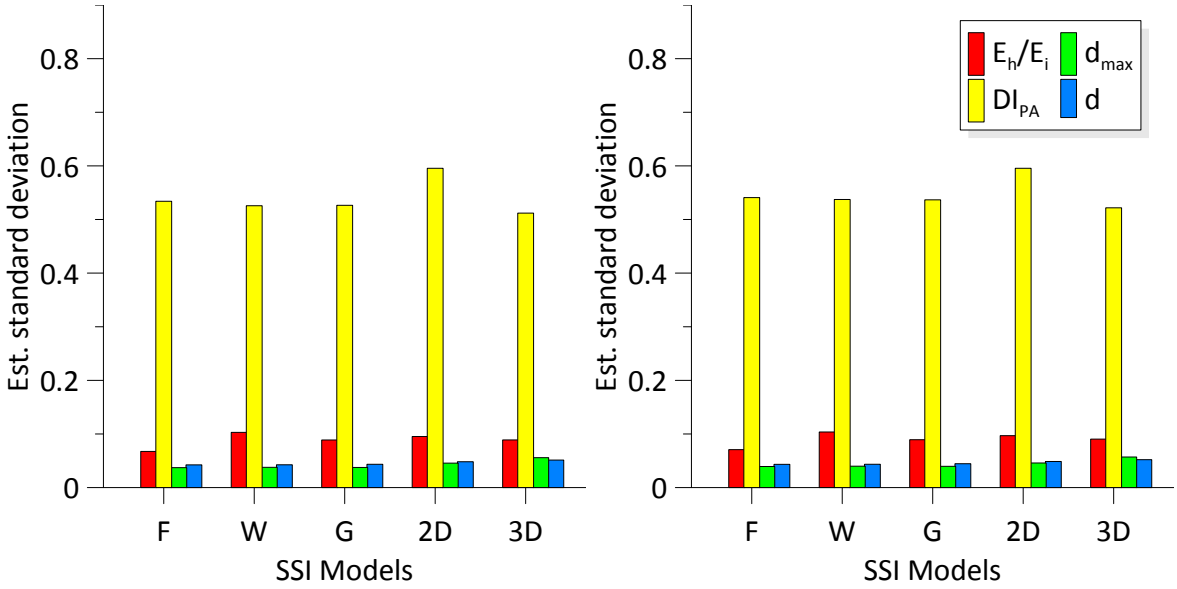

Figure 4.5: Estimated total model uncertainty for the models with Bouc-Wen hysteresis subjected to harmonic ground excitation ($f = 2Hz$): (a) Two-dimensional model as a reference, (b) Averaged model response as a reference. F = Fixed-base; W = Wolf model; G = Gazetas model; 2D = two-dimensional FE model; 3D = three-dimensional FE model; E_h/E_i = ratio of total hysteretic energy to total input energy; DI_{PA} = Park-Ang damage index; d_{max} = maximum top displacement; d = averaged top displacement

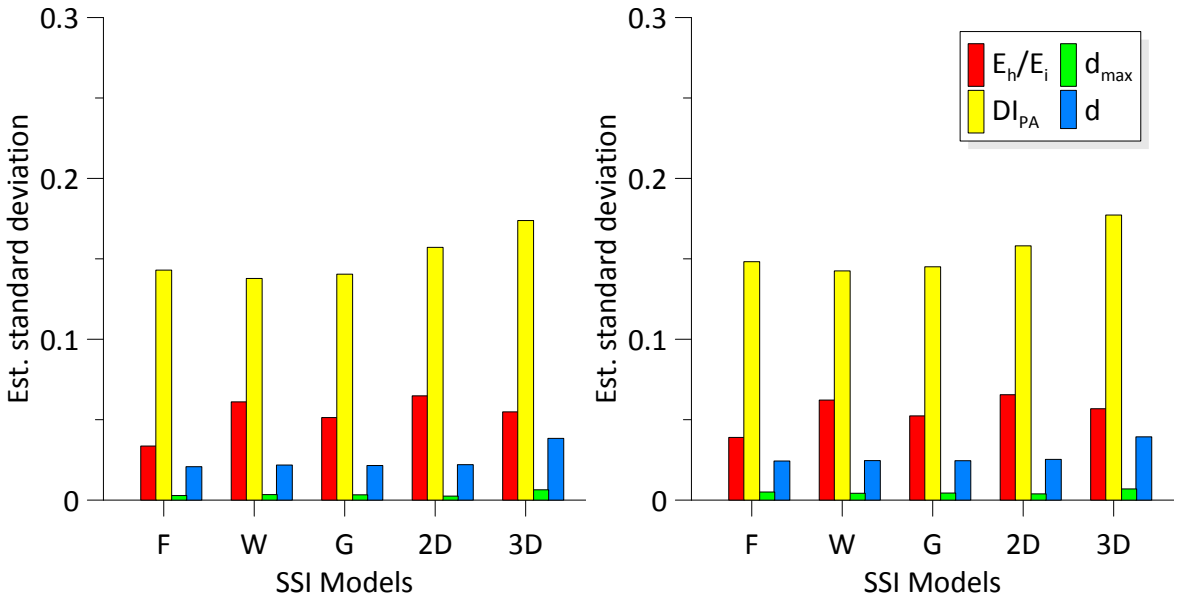

Figure 4.6: Estimated total model uncertainty for the models with Bouc-Wen hysteresis subjected to pulse ground excitation ($f = 1Hz$): (a) Two-dimensional model as a reference, (b) Averaged model response as a reference. F = Fixed-base; W = Wolf model; G = Gazetas model; 2D = two-dimensional FE model; 3D = three-dimensional FE model; E_h/E_i = ratio of total hysteretic energy to total input energy; DI_{PA} = Park-Ang damage index; d_{max} = maximum top displacement; d = averaged top displacement

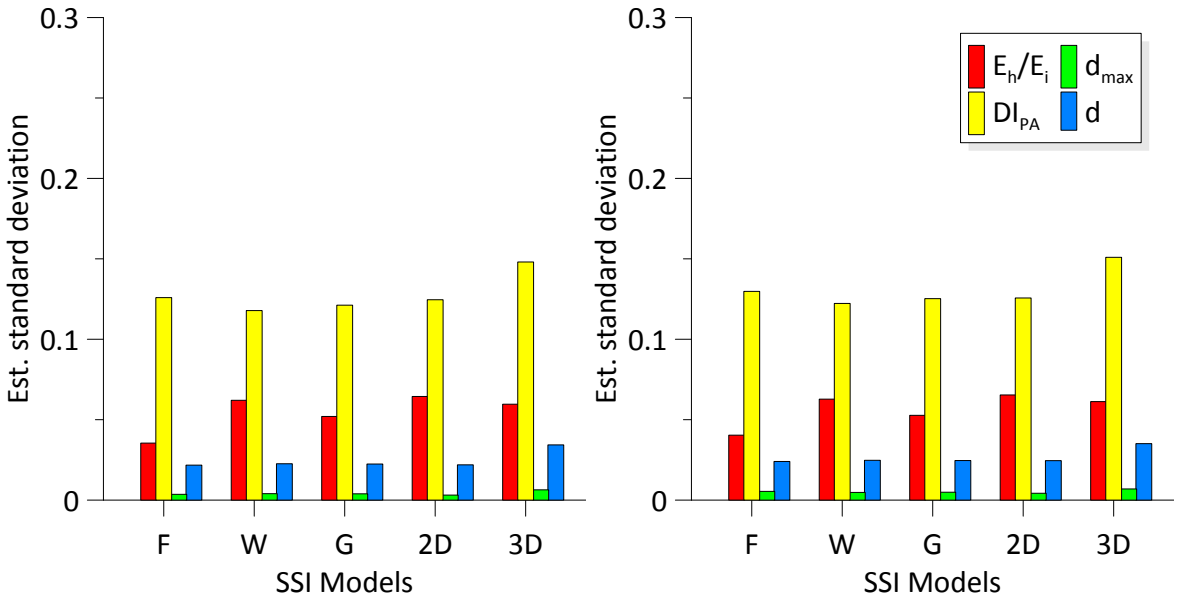

Figure 4.7: Estimated total model uncertainty for the models with Bouc-Wen hysteresis subjected to pulse ground excitation ($f = 1.2Hz$): (a) Two-dimensional model as a reference, (b) Averaged model response as a reference. F = Fixed-base; W = Wolf model; G = Gazetas model; 2D = two-dimensional FE model; 3D = three-dimensional FE model; E_h/E_i = ratio of total hysteretic energy to total input energy; DI_{PA} = Park-Ang damage index; d_{max} = maximum top displacement; d = averaged top displacement

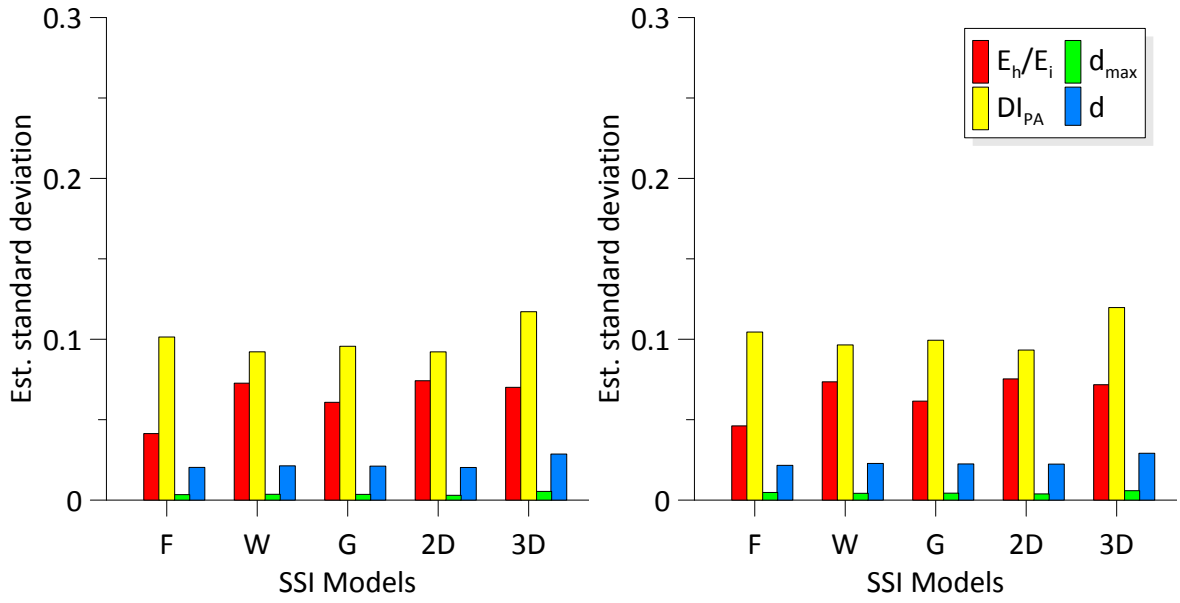

Figure 4.8: Estimated total model uncertainty for the models with Bouc-Wen hysteresis subjected to pulse ground excitation ($f = 1.4Hz$): (a) Two-dimensional model as a reference, (b) Averaged model response as a reference. F = Fixed-base; W = Wolf model; G = Gazetas model; 2D = two-dimensional FE model; 3D = three-dimensional FE model; E_h/E_i = ratio of total hysteretic energy to total input energy; DI_{PA} = Park-Ang damage index; d_{max} = maximum top displacement; d = averaged top displacement

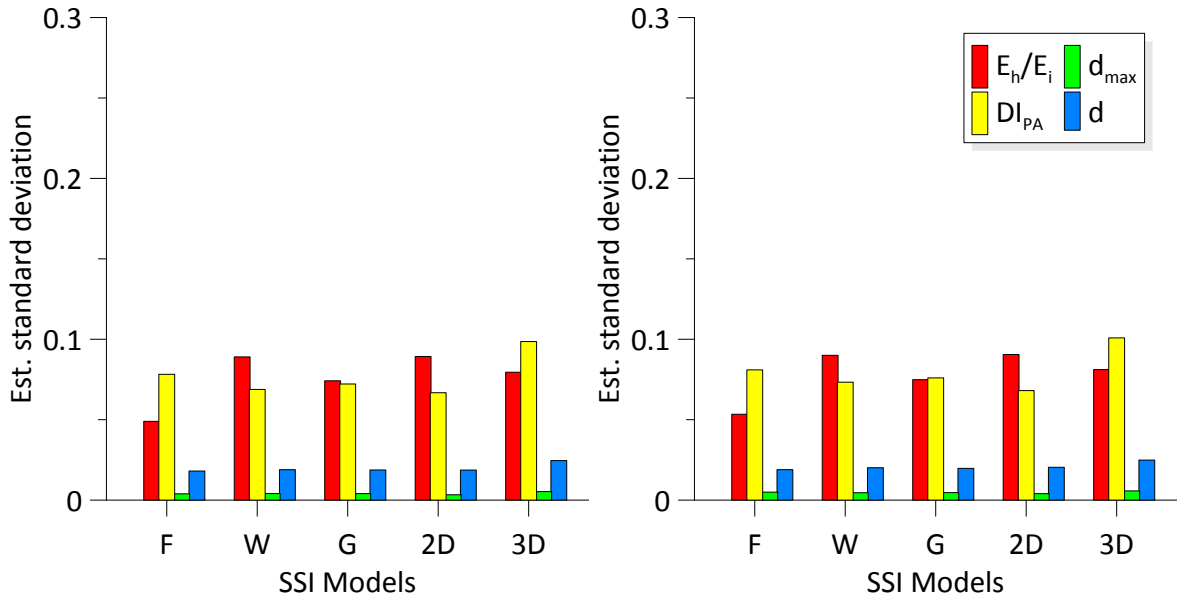

Figure 4.9: Estimated total model uncertainty for the models with Bouc-Wen hysteresis subjected to pulse ground excitation ($f = 1.6Hz$): (a) Two-dimensional model as a reference, (b) Averaged model response as a reference. F = Fixed-base; W = Wolf model; G = Gazetas model; 2D = two-dimensional FE model; 3D = three-dimensional FE model; E_h/E_i = ratio of total hysteretic energy to total input energy; DI_{PA} = Park-Ang damage index; d_{max} = maximum top displacement; d = averaged top displacement

Table 4.4: Model quality predictions corresponding to the total model uncertainty illustrated in Figures 4.6 (a) to 4.9 (a). A = best quality; E = worst quality

indicator	freq. [Hz]	**fixed-base**	**Wolf**	**Gazetas**	**2D FE**	**3D FE**
E_h/E_i	1.0	A	D	B	E	C
	1.2	A	D	B	E	C
	1.4	A	D	B	E	C
	1.6	A	D	B	E	C
DI_{PA}	1.0	C	A	B	D	E
	1.2	D	A	B	C	E
	1.4	D	A	C	B	E
	1.6	D	B	C	A	E
d_{max}	1.0	B	D	C	A	E
	1.2	B	D	C	A	E
	1.4	B	D	C	A	E
	1.6	B	C	D	A	E
d	1.0	A	C	B	D	E
	1.2	A	D	C	B	E
	1.4	B	D	C	A	E
	1.6	A	D	B	C	E

Table 4.5: Model quality predictions corresponding to the total model uncertainty illustrated in Figures 4.6 (b) to 4.9 (b). A = best quality; E = worst quality

indicator	freq. [Hz]	**fixed-base**	**Wolf**	**Gazetas**	**2D FE**	**3D FE**
E_h/E_i	1.0	A	D	B	E	C
	1.2	A	D	B	E	C
	1.4	A	D	B	E	C
	1.6	A	D	B	E	C
DI_{PA}	1.0	C	A	B	D	E
	1.2	D	A	B	C	E
	1.4	D	B	C	A	E
	1.6	D	B	C	A	E
d_{max}	1.0	D	B	C	A	E
	1.2	D	C	B	A	E
	1.4	D	B	C	A	E
	1.6	D	B	C	A	E
d	1.0	A	C	B	D	E
	1.2	A	D	C	B	E
	1.4	A	D	B	C	E
	1.6	A	C	B	D	E

frequencies, and Tables 4.4 and 4.5 provide an overview of the estimation results. We can once again observe that the estimation based on the energy ratio E_h/E_i as a response indicator leads

to the same order of models regarding their quality. This also holds for the estimation based on both types of reference response shown in (a) and (b) in Figures 4.6 to 4.9. This observation does not apply for the other response indicators.

4.7 Summary

An evaluation methodology is introduced in this chapter for assessing the utility of SSI models. The established evaluation methodology allows for a practical quantitative estimate of SSI in the presence of dynamic loads and points to whether or not a full-scale nonlinear analysis will be required. In the evaluation process, energy measures are used within the framework of the adjustment factor approach in order to quantitatively assess the uncertainty associated with SSI models. Two primary types of uncertainty are considered, namely the uncertainty in the model framework and the uncertainty in the model input parameters. The uncertainty associated with each model is first investigated based on a selected reference model and then again on the averaged model response.

The analysis has been performed using two types of hysteretic rules for coupled soil-structure systems subjected to different types of excitation. Four structural response indicators are used to estimate the uncertainty of the models investigated. For all of the analysis scenarios, the estimation of model uncertainty based on the energy ratio leads to a same order of the SSI models with regard to their quality. The results show that the more complex three-dimensional FE model has the best quality of the models investigated, whereas the Wolf model produces the lowest model uncertainty of the three simpler models and thus has the best model quality compared to the other two models. The fixed-base model produces the highest estimated uncertainty and accordingly the worst quality of all the models investigated. These results confirm the hypothesis of increasing model uncertainty with decreasing complexity only when the assessment is based on the energy ratio as a response indicator. It has also been observed that E_h/E_i leads to less sensitive results regarding model quality.

Accounting for the uncertainty in the parameters in the quality estimation of the models updates the order of models regarding their total uncertainty. In addition, the differences in

the estimated uncertainties become smaller between the simpler models and the more complex models after including the uncertainty in the parameters. The three simpler models have fewer input parameters and are therefore less sensitive to the uncertainty associated with the parameters, while the two more complex FE models produce a significantly increased total error after including the uncertainty of their input parameters. The FE models use more parameters, and consequently produce a higher total uncertainty than the three simpler models.

Chapter 5

CONCLUSIONS AND FUTURE DEVELOPMENTS

A methodology for evaluating the quality of dynamic SSI models is introduced in this research work. The proposed evaluation methodology using energy measures is based on a physically clear concept. It provides a tool that helps structural engineers in selecting appropriate SSI models, despite the uncertainties associated with them. The theoretical approach employed for the treatment of model uncertainty is considered to be a useful tool within the framework of the proposed evaluation methodology. This tool provides insights into a model's attributes by distinguishing between aleatory and epistemic uncertainty. The uncertainty in modeling is characterized as an attribute of model complexity. It is defined in terms of error in the model output and can be assessed quantitatively this way. For the set of adopted models for SSI with different levels of complexity, the quality of a model is assessed by quantifying the underlying uncertainty in one model compared to the remaining models. Accordingly, the results represent model-to-model uncertainty. Two scenarios are investigated in the proposed methodology. The first scenario considers the response of the most sophisticated model as a reference solution, whereas the second one uses the average response from all models.

The energy dissipated by MDOF systems can be estimated using equivalent SDOF systems (McKevitt et al., 1980), and input and hysteretic energies are approximately the same regard-

less of whether the system plan is symmetric or asymmetric (Goel, 1997). Thus, more emphasis has been given to the soil model. The established evaluation methodology in this work allows for a practical quantitative estimate of SSI in the presence of dynamic loads and points to whether or not a nonlinear structural analysis will be required by using a more complex soil model. Combining the information gathered from both types of uncertainty investigated, helps in selecting the most suitable model associated with minimum total uncertainty. The assessment results show the degree of independence from the frequency content of the applied base excitation and from the choice of hysteretic rules as well. In view of this, the results from the investigations on model framework uncertainty can be generally applied. Given the degree of uncertainty in the input parameters, users can make an informed decision on the selection of one particular SSI model over another. Accordingly, a user can decide on the amount of uncertainty in a modeling implementation. This can help to reduce the numerical simulation effort and unnecessary costs created by more complex models, since the case study shows that more complex models do not necessarily have a better quality.

The conclusions of this study are drawn from the results of the sensitivity of the calculated response to the complexity of the analysis and to the uncertainty in the input parameters. Dynamic SSI effects are investigated using models with different abstraction levels. Different coupling scenarios are investigated for soil and structure models, in which the quality of the coupling is implicitly investigated. In addition to the fixed-base model, the proposed methodology is demonstrated using the dynamic SSI models adopted, which represent simplified and more complex alternative models. The forced dynamic analysis of soil-structure system has been performed using two types of hysteretic rules. Subsequently, energy response time histories were constructed for sinusoidal and pulse excitations.

The significant influence of SSI can be observed for the structural response when using more complex partial models of soil. This can be explained by the ability of these models to incorporate more influencing factors, such as kinematic SSI and foundation flexibility, in addition to the more realistic representation of the soil medium and its stress-strain relationship. The results show that the constructed energy response time histories provide valuable information about the dynamic behavior of the structure since the dynamic SSI effects can be identified and

quantified for the different models implemented. The coupled soil-structure models generally produce a decreased energy response. However, the energy response of the structure coupled to the three-dimensional FE soil model seems to be relatively high in comparison to the other coupled models. This can be a sign of propagated waves reflecting from the model's boundaries to the structure.

Energy measures provide a convincing indicator for the quality assessment of SSI models. The ratio of structural hysteretic energy to input energy E_h/E_i produces steady predictions for evaluating the quality of SSI models in comparison to those predictions based on the maximum displacement response. The resulting energies exhibit the relation expected between the structural response and frequency content of signals applied. This relation is clearly demonstrated by using a specific frequency content of pulse-type wavelets. However, contrary to the other response indicators, the predictions based on the energy ratio E_h/E_i show the independence of using different hysteretic rules, as well as varied excitation frequencies. In other words, the estimation of model uncertainty based on the energy ratio E_h/E_i in all the analysis scenarios leads to the same order of the SSI models regarding their quality.

Investigations on model framework uncertainty show that the more complex three-dimensional FE model has the best quality of the models investigated, whereas the Wolf SSI model produces the lowest model uncertainty of the three simpler models and thus has the best model quality relative to the other two models. The fixed-base model produces the highest estimated uncertainty and accordingly the worst quality of all models investigated. These results confirm the hypothesis of increasing model uncertainty with decreasing complexity only when the assessment is based on the energy ratio E_h/E_i as a response indicator, which leads to less sensitive results regarding model quality as well.

Despite the good correlation between the Park-Ang damage index and the hysteretic energy dissipated in the structure for those models producing the upper and lower bounds of damage grades, it can be seen that the best model quality does not necessarily correspond to a conservative structural design resulting in the lowest damage grade. Accounting for the uncertainty in the input parameters in the quality estimation of the models, updates the order of models regarding their total uncertainty. Also, the differences in the estimated uncertainties

become smaller between the simpler models and the more complex models after including the uncertainty in the input parameters. The simpler models have fewer input parameters and are therefore less sensitive to their uncertainty, while the more complex models produce an increase in total error after including the uncertainty of their input parameters.

The computed uncertainty in model response is directly related to the model predictions used, which are considered as weights within the framework of the *adjustment factor* approach. Thus, misrepresented model predictions might affect the resulting uncertainty considerably. Investigations to incorporate the uncertainty in model predictions into the evaluation process should be made in future research.

The introduced evaluation method using energy measures can be extended to solve other assessment problems in structural engineering, such as the efficiency of different isolation techniques for vibrating systems.

REFERENCES

Akiyama, H. (1985). *Earthquake-resistant Limit-state Design for Buildings*. Tokyo: University of Tokyo Press.

Atanakovic, T. M. and D. T. Spasic (2004). On viscoelastic compliant contact-impact models. *Journal of Applied Mechanics of ASME 71*, 134–139.

Baber, T. T. and Y. K. Wen (1979). Stochastic equivalent linearization for hysteretic, degrading, multistory structures. Technical Report UILU-ENG-80-2001, University of Illinois, Urbana, Illinois.

Banon, H. and D. Veneziano (1982). Seismic safety of reinforced concrete members and structures. *Earthquake Engineering & Structural Dynamics 10*(2), 179–193.

Bathe, K.-J. and E. L. Wilson (1976). *Numerical Methods in Finite Element Analysis*. Prentice Hall Inc.

Beck, B. (2006). *Model evaluation and performance*. John Wiley & Sons, Ltd.

Beck, J. L. and K. V. Yuen (2004). Model selection using response measurements: Bayesian probabilistic approach. *Journal of Engineering Mechanics 130*, 192.

Beck, M. B. (1987). Water quality modeling: a review of the analysis of uncertainty. *Water Resources Research 23*, 1393–1442.

Bettess, P. (1977). Infinite elements. *International Journal for Numerical Methods in Engineering 11*(1), 53–64.

Bettess, P. (1980). More on infinite elements. *International Journal for Numerical Methods in Engineering 15*(11), 1613–1626.

Bielak, J., K. Loukakis, Y. Hisada, and C. Yoshimura (2003). Domain reduction method for threedimensional earthquake modeling in localized regions. Part I: Theory. *Bulletin of the Seismological Society of America 93*(2), 817824.

Bouc, R. (1967). Forced vibrations of mechanical systems with hysteresis. In *Proc. 4th Conf. on Non-Linear Oscillation*.

Bradford, S. C., J. F. Clinton, J. Favela, and T. H. Heaton (2004). Results of Millikan Library forced vibration testing. Technical Report EERL-2004-03, California Institute of Technology, Pasadena, California.

Bruneau, M. and N. Wang (1996). Some aspects of energy methods for the inelastic seismic response of ductile SDOF structures. *Engineering Structures 18*(1), 1–12.

Chai, Y. H., K. M. Romstad, and S. M. Bird (1995). Energy-based linear damage model for high-intensity seismic loading. *Journal of Structural Engineering 121*(5), 857–864.

Chopra, A. K. (2007). *Dynamics of Structures, 3rd edition*. Upper Saddle River, New Jersey: Pearson Prentice Hall.

Chuhan, Z., C. Xinfeng, and W. Guanglun (1999). A coupling model of FE-BE-IE-IBE for non-linear layered soil-structure interactions. *Earthquake Engineering & Structural Dynamics 28*(4), 421–441.

Cosenza, E., G. Manfredi, and R. Ramasco (1993). The use of damage functionals in earthquake engineering: a comparison between different methods. *Earthquake Engineering & Structural Dynamics 22*(10), 855–868.

Crocker, M. J. (Ed.) (2007). *Handbook of Noise and Vibration Control*. John Wiley & Sons, Inc.

Crouse, C. B., B. Hushmand, J. E. Luco, and H. L. Wong (1990). Foundation impedance functions: Theory versus experiment. *Journal of Geotechnical Engineering 116*, 432–449.

Deeks, A. J. and J. P. Wolf (2002). An h-hierarchical adaptive procedure for the scaled boundary finite-element method. *International Journal for Numerical Methods in Engineering 54*(4), 585–605.

Dobry, R. and G. Gazetas (1986). Dynamic response of arbitrarily shaped foundations. *Journal of Geotechnical Engineering 112*.

Dobry, R., G. Gazetas, and K. H. Stokoe (1986). Dynamic response of arbitrarily shaped foundations: Experimental verification. *Journal of Geotechnical Engineering 112*.

Dutta, S. C. and R. Roy (2002). A critical review on idealization and modeling for interaction among soil-foundation-structure system. *Computers & Structures 80*, 1579–1594.

Elgamal, A., Z. Yang, E. Parra, and A. Ragheb (2010). Cyclic 1D - Internet-based computer simulation of site earthquake response and liquefaction. UCSD.

EPA (1997). *Guiding Principles for Monte Carlo Analysis*, Number EPA-630-R-97-001, Washington, D.C., U.S. Environmental Protection Agency. EPA.

EPA (2009, March). *Guidance on the development, evaluation, and application of environmental models*, Number EPA/100/K-09/003, Office of the Science Advisor, Washington, D.C., U.S. Environmental Protection Agency. EPA.

Fang, K. T., R. Li, and A. Sudjianto (2006). *Design and Modeling for Computer Experiments*. Chapman & Hall/CRC.

Favela, J. (2004). *Energy radiation from a multi-story building*. Ph. D. thesis, California Institute of Technology.

FEMA (2005). *Improvement of nonlinear static seismic analysis procedures*, Number 440, Washington, D.C., Federal Emergency Management Agency. FEMA.

Foutch, D. A. (1976). *A study of the vibrational characteristics of two multistory buildings*. Ph. D. thesis, California Institute of Technology.

Gazetas, G. (1991). Formulas and charts for impedances of surface and embedded foundations. *Journal of Geotechnical Engineering 117*(9), 1363–1381.

Goel, R. K. (1997). Seismic response of asymmetric systems: Energy-based approach. *Journal of Structural Engineering 123*(11), 1444–1453.

Graff, K. F. (1973). *Wave Motion in Elastic Solids*. Columbus, Ohio: Ohio State University Press.

Housner, G. W. (1956). Limit design of structures to resist earthquakes. In *Proceedings of the 1st World Conference on Earthquake Engineering*, California. Earthquake Engineering Research Institute.

Hsieh, T. K. (1962). Foundation vibrations. *ICE Proceedings 22*, 211–226.

Jeremić, B. (2010). Lecture notes on computational geomechanics: Inelastic finite elements for pressure sensitive materials.

Johnson, J. J. (1981). Soil Structure Interaction (SSI): The status of current analysis methods and research. Technical Report UCRL-53011. NUREGICR-1780, Lawrence Livermore National Laboratory (LLNL), Washington (DC): US Nuclear Regulatory Commission.

Kausel, E. (1988). Local transmitting boundaries. *Journal of Engineering Mechanics 114*(6), 1011–1027.

Khashaee, P. (2004). *Energy-based seismic design and damage assessment for structures*. Ph. D. thesis, School of Engineering Southern Methodist University.

Khashaee, P., B. Mohraz, F. Sadek, H. S. Lew, and J. L. Gross (2003). Distribution of earthquake input energy in structures. Technical Report NISTIR 6903, National Institute of Standards and Technology.

Konikow, L. F. and J. D. Bredehoeft (1992). Ground-water models cannot be validated. *Advances in Water Resources 15*, 75–83.

Kramer, S. L. (1996). *Geotechnical Earthquake Engineering*. Prentice Hall, Inc.

Krawinkler, H. and M. Zohrei (1983). Cumulative damage in steel structures subjected to earthquake ground motions. *Computers & Structures 16*, 531–541.

Kunnath, S. K., A. M. Reinhorn, and Y. J. Park (1990). Analytical modeling of inelastic seismic response of R/C structures. *Journal of Structural Engineering 116*(4), 996–1017.

Liao, Z. P. and H. L. Wong (1984). A transmitting boundary for the numerical simulation of elastic wave propagation. *International Journal of Soil Dynamics and Earthquake Engineering 3*(4), 174–183.

Luchko, Y. F., H. Martinez, and J. J. Trujillo (2008). Fractional Fourier transform and some of its applications. *Fractional Calculus and Applied Analysis 11*, 457–470.

Luco, J. E., H. L. Wong, and M. D. Trifunac (1986). Soil-structure interaction effects on forced vibration tests. Technical report, Dept. of Civil Engineering, University of Southern California Los Angeles.

Luis, S. J. and D. McLaughlin (1992). A stochastic approach to model validation. *Advances in Water Resources 15*, 15–32.

Lysmer, J. (1965). *Vertical motion of rigid footings*. Ph. D. thesis, University of Michigan.

Lysmer, J. and R. Kuhlemeyer (1969). Finite dynamic model for infinite media. *Journal of the Engineering Mechanics Division 95*, 859–875.

Lysmer, J., F. Ostadan, and C. C. Chin (1999, November). *SASSI2000- A system for analysis of soil-structure interaction*. Geotechnical Engineering Division, Civil Engineering Department, University of California, Berkeley.

Lysmer, J., T. Udaka, H. B. Seed, and R. Hwang (1974). LUSH - A computer program for complex response analysis of soil-structure systems. Technical Report EERC 74-4, Earthquake Engineering Research Center, University of California, Berkeley.

Lysmer, J., T. Udaka, C.-F. Tsai, and H. B. Seed (1975). FLUSH - A computer program for approximate 3-D analysis of soil structure interaction problems. Technical Report EERC-75/30, Earthquake Engineering Research Center, University of California, Berkeley.

MacKay, D. J. C. (1992). Bayesian interpolation. *Neural Computation 4*, 415–447.

Mahin, S. A. and J. Lin (1983). Construction of inelastic response spectra for single-degree-of-freedom systems. Technical Report EERC-83/17, University of California, Berkeley, CA.

Manfredi, G. (2001). Evaluation of seismic energy demand. *Earthquake Engineering & Structural Dynamics 30*(4), 485–499.

Manolis, G. D., A. Markou, and M. Nasser (2011). Base isolation for buildings in the presence of soil-structure interaction: The basic model. abstract (1 page) and paper (10 pages) in cd congress proceedings. In A. G. Boudouvis and G. E. Stavroulakis (Eds.), *Seventh Greek Association of Computational Mechanics (7th GRACM) International Congress on Computational Mechanics*, Greece, Athens. 30 June–2 July 2011.

McKenna, F. and G. L. Fenves (2001). *The OpenSees command language manual, version 1.2*. Earthquake Engineering Research Center, University of California, Berkeley.

McKevitt, W. E., D. L. Anderson, and S. Cherry (1980). Hysteretic energy spectra in seismic design. In *Proceeding of the Seventh World Conference on Earthquake Engineering*, pp. 487–494.

Medina, F. and J. Penzien (1982). Infinite elements for elastodynamics. *Earthquake Engineering & Structural Dynamics 10*(5), 699–709.

Most, T. (2011). Assessment of structural simulation models by estimating uncertainties due to model selection and model simplification. *Computers & Structures 89*(17–18), 1664 – 1672.

Mylonakis, G., S. Nikolaou, and G. Gazetas (2006). Footings under seismic loading: Analysis and design issues with emphasis on bridge foundations. *Soil Dynamics and Earthquake Engineering 26*, 824–853.

Naiem, F. (2001). *The Seismic Design Handbook. 2nd edition*. Kluwer Academic Publications, Dordrecht.

Nasser, M. and G. Manolis (2011). Soil-structure interaction Validation study using energy measures. *Technical Note, Bautechnik Sonderheft 88*(6), 35–38.

Nasser, M., M. Schwedler, F. Wuttke, and C. Könke (2010). Seismic analysis of structural response using simplified soil-structure interaction models. *D-A-CH-Mitteilungsblatt 85*, 10–16.

Nova, R. and C. Di Prisco (2003). The macro-element concept and its application in geotechnical engineering. In J.-P. Magnan and N. Droniuc (Eds.), *International symposium on shallow foundations*, pp. 389–396. Presse ENPC, Paris.

Nova, R. and L. Montrasio (1991). Settlements of shallow foundations on sand. *Géotechnique 41*(2), 243–256.

Oreskes, N., K. Shrader-Frechette, and K. Belitz (1994). Verification, validation, and confirmation of numerical models in the earth sciences. *Science 263 (5147)*, 641–646.

Papakonstantinou, K. G., P. C. Dimizas, and V. K. Koumousis (2008). An inelastic beam element with hysteretic damping. *Shock and Vibration Journal 15*, 273–290.

Park, I., H. K. Amarchinta, and R. V. Grandhi (2010). A Bayesian approach for quantification of model uncertainty. *Reliability Engineering & System Safety 95*, 777–785.

Park, Y. J. and A. H.-S. Ang (1985). Mechanistic seismic damage model for reinforced concrete. *Journal of Structural Engineering 111*, 722–739.

Pearl, J. (1978). On the connection between the complexity and credibility of inferred models. *International Journal of General Systems 4*, 255–264.

Penrose, R. (2004). *The Road to Reality, a complete guide to the laws of the universe.* Jonathan Cape.

Prager, W. (1955). The theory of plasticity: A survey of recent achievements. *Proceedings of the Institution of Mechanical Engineers 169*, 41–57.

Rahnama, M. and L. Manuel (1996). The effect of strong motion duration on seismic demands. In *Proceedings of the 11th World Conference on Earthquake Engineering*, Number 108.

Richart, F. E., J. R. Hall, and R. D. Woods (1970). *Vibrations of Soils and Foundations.* Prentice-hall, Inc.

Richart, F. E. and R. V. Whitman (1967). Comparison of footing vibration tests with theory. *ASCE Journal of Soil Mechanics & Foundations Div 93*, 143–168.

Ryan, H. (1994). Ricker, Ormsby; Klander, Butterworth-a choice of wavelets. *CSEG Recorder*, 8–9.

Schanz, T., Z. Bonev, F. Wuttke, R. Iankov, and V. Georgiev (2008). Design seismic performance of RC frame structures taking into account foundation flexibility. In *NATO advanced research workshop*, Borovets, Bulgaria.

Snowling, S. D. and J. R. Kramer (2001). Evaluating modelling uncertainty for model selection. *Ecological Modelling 138*, 17–30.

Stewart, J. P., R. B. Seed, and G. L. Fenves (1998). Empirical evaluation of inertial soil-structure interaction effects. Technical Report PEER-98/07, Pacific Earthquake Engineering Research Center University of California, Berkeley.

Suter, G. W. I. (1993). Ecological risk assessment. *Lewis, Boca Raton*.

Takeda, T., M. A. Sozen, and N. N. Nielsen (1970). Reinforced concrete response to simulated earthquakes. *Journal of the Structural Division 96*(12), 2557–2573.

Tassoulas, J. L. and E. Kausel (1984). On the dynamic stiffness of circular ring footings on an elastic stratum. *Int. J. Numer. Anal. Meth. Geomech. 8*, 411–426.

Uang, C. M. and V. V. Bertero (1988). Use of energy as a design criterion in earthquake-resistant design. Technical Report EERC-88/18, Earthquake Engineering Research Centre, University of California, Berkeley, CA.

Uang, C. M. and V. V. Bertero (1990). Evaluation of seismic energy in structures. *Earthquake Engineering & Structural Dynamics 19*, 77–90.

Ungless, R. F. (1973). An infinite finite element. Master's thesis, The University of British Columbia.

Veletsos, A. S. (1974). Basic response functions for elastic foundations. *Journal of the Engineering Mechanics 100*, 189–202.

Veletsos, A. S. and Y. Tang (1987). Vertical vibration of ring foundations. *Earthquake Engng. Struct. Dyn. 15*, 1–21.

Wen, Y.-K. (1976). Method for random vibration of hysteretic systems. *Journal of the Engineering Mechanics Division 102*, 249–263.

Wolf, J. P. (1985). *Dynamic Soil-Structure-Interaction*. Prentice-Hall, Englewood Cliffs (NJ).

Wolf, J. P. (1988). *Soil-Structure-Interaction Analysis in Time Domain*. Prentice Hall (Englewood Cliffs, N.J.).

Wolf, J. P. (1994). *Foundation Vibration Analysis using Simple Physical Models*. Prentice-Hall, Englewood Cliffs (NJ).

Wolf, J. P. and A. J. Deeks (2004). *Foundation Vibration Analysis: A Strength-of-materials Approach*. Butterworth-Heinemann.

Wolf, J. P. and M. Schanz (2004). The scaled boundary finite element method. *Computational Mechanics 33*(4).

Wolf, J. P. and C. Song (2002). Some cornerstones of dynamic soil-structure interaction. *Engineering Structures 24*, 13–28.

Wong, H. and J. Luco (1985). Tables of impedance functions for square foundations on layered media. *International Journal of Soil Dynamics and Earthquake Engineering 4*, 64–81.

Yoshimura, C., J. Bielak, and Y. Hisada (2003). Domain reduction method for threedimensional

earthquake modeling in localized regions. Part II: Verification and examples. *Bulletin of the Seismological Society of America 93*(2), 825840.

Zahrah, T. F. and W. J. Hall (1984). Earthquake energy absorption in SDOF structures. *Journal of Structural Engineering 110*(8), 1757–1772.

Zhao, C. and S. Valliappan (1993). A dynamic infinite element for three-dimensional infinite-domain wave problems. *International Journal for Numerical Methods in Engineering 36*(15), 2567–2580.

SOLEMN DECLARATION

I do solemnly declare that I have made this work without undue assistance from third parties and without the use of other than the referenced sources. From other sources directly or indirectly acquired data and concepts are identified by referencing the source.

Other people were not involved in the development of content and material of the present work. In particular, I have not used any paid help of mediation or counseling services (promotion consultants or other persons). No one has received directly or indirect monetary benefits from me for any work in connection with the content of the submitted dissertation.

The work has been neither submitted to any other Examining Authority in Germany nor abroad in the same or similar style. I certify on my honor that I have said the whole truth and that I concealed nothing.

Weimar, June 2012 Mourad Nasser